

2013

Synthesis Of Substituted Pyrrolo[2,3-D]Pyrimidines As Microtubule- Binding Agents and HSP90 Inhibitors

Lu Lin

Follow this and additional works at: <https://dsc.duq.edu/etd>

Recommended Citation

Lin, L. (2013). Synthesis Of Substituted Pyrrolo[2,3-D]Pyrimidines As Microtubule-Binding Agents and HSP90 Inhibitors (Doctoral dissertation, Duquesne University). Retrieved from <https://dsc.duq.edu/etd/826>

This Immediate Access is brought to you for free and open access by Duquesne Scholarship Collection. It has been accepted for inclusion in Electronic Theses and Dissertations by an authorized administrator of Duquesne Scholarship Collection. For more information, please contact phillips@duq.edu.

SYNTHESIS OF SUBSTITUTED PYRROLO[2,3-*d*]PYRIMIDINES
AS MICROTUBULE-BINDING AGENTS AND HSP90 INHIBITORS

A Dissertation

The Graduate School of Pharmaceutical Sciences

Mylan School of Pharmacy

Duquesne University

In partial fulfillment of the requirements for
the degree of Doctor of Philosophy

By

Lu Lin

May 2013

Copyright by

Lu Lin

2013

SYNTHESIS OF SUBSTITUTED PYRROLO[2,3-*d*]PYRIMIDINES
AS MICROTUBULE-BINDING AGENTS AND HSP90 INHIBITORS

By

Lu Lin

Approved February 20, 2013

Aleem Gangjee, Ph. D.
Distinguished Professor of Medicinal
Chemistry
(Committee Chair)

Marc W. Harrold, Ph. D.
Professor of Medicinal Chemistry
(Committee Member)

Patrick T. Flaherty, Ph. D.
Associate Professor of Medicinal
Chemistry
(Committee Member)

David J. Lapinsky, Ph. D.
Assistant Professor of Medicinal
Chemistry
(Committee Member)

Lawrence H. Block, Ph. D.
Professor of Pharmaceutics
(Committee Member)

J. Douglas Bricker, Ph. D.
Dean, Mylan School of Pharmacy
Professor of Pharmacology-Toxicology

James K. Drennen, Ph.D.
Associate Dean, Research and Graduate
Programs, Mylan School of Pharmacy
Associate Professor of Pharmaceutical
Sciences

ABSTRACT

SYNTHESIS OF SUBSTITUTED PYRROLO[2,3-*d*]PYRIMIDINES AS MICROTUBULE-BINDING AGENTS AND HSP90 INHIBITORS

By

Lu Lin

May 2013

Dissertation supervised by Professor Aleem Gangjee, Ph.D.

An introduction, background and recent advances in the areas of microtubule-binding agents and heat shock protein 90 (HSP90) inhibitors as anticancer agents are briefly reviewed. The work in this dissertation is centered on the synthesis of substituted pyrrolo[2,3-*d*]pyrimidines as potential anticancer agents that act via microtubule inhibition or HSP90 inhibition.

Microtubule-binding agents are effective against a broad range of tumors and lymphomas and have been common components of combination cancer-chemotherapy in the clinic. Despite the unparalleled success, drawbacks among microtubule-binding agents such as multi-drug resistance, dose-limiting toxicity, poor pharmacokinetic profile and high cost have supported the sustaining momentum in searching for novel agents of this class.

The research on microtubule-binding agents in this dissertation was initiated by an unexpected discovery. The lead compound, a 4-*N*-methyl-4'-methoxyaniline-substituted pyrrolo[2,3-*d*]pyrimidine, was found to inhibit the majority cancer cell lines in the NCI-60 panel at sub-micromolar concentration. The COMPARE analysis based on the activity profile indicated microtubule inhibition as the main mechanism of action of this compound, and was later confirmed through multiple assays. Further, the lead compound displaced 70% of [³H]colchicine from tubulin at a concentration of 5 μM, and was identified as a colchicine-site binder. The compound has also shown unabated or even increased activities against several drug-resistant cancer cell lines, especially the cell lines overexpressing P-glycoprotein or βIII-tubulin. In addition, the compound has favorable physicochemical properties such as high water solubility as its hydrochloride salt.

Based on the preliminary data and molecular modeling, a hypothesis on the relationship between binding affinity and the lowest-energy conformation of pyrrolo[2,3-*d*]pyrimidines was proposed. To test the hypothesis and search for compounds with improved potency, 38 pyrrolo[2,3-*d*]pyrimidine analogs in six series were designed and synthesized. The biological evaluations of these compounds are currently in progress at the time this dissertation is submitted.

HSP90 is one the molecular chaperones that assist the proper folding of the newly synthesized polypeptides and proteins. The majority of its client proteins are signal transducers with unstable conformations, which play critical roles in growth control, cell survival and development. The expressions of these proteins in normal cells were much less than cancer cell, making HSP90 a viable target for cancer chemotherapy. As of 2012,

there are 16 HSP90 inhibitors in clinical trial, among which four are based on the purine-scaffold. All the compounds in clinical trials bind to or overlap with the ATP site on the N-terminal of HSP90.

The pyrrolo[2,3-*d*]pyrimidine scaffold is structurally close to purines. In the design of receptor tyrosine kinase (RTK) inhibitors, Gangjee et al. have shown that properly functionalized pyrrolo[2,3-*d*]pyrimidines bind to the ATP site and achieve high degrees of selectivity. This was partly attributed to the incorporation of substitution patterns that are impossible on the purine scaffold. Based on these previous findings and the established SAR of the two purine derivatives in clinical trials (**PU-H71** and **BIIB021**), 18 substituted pyrrolo[2,3-*d*]pyrimidines in three series (in connection with this dissertation) were designed and synthesized. The biological evaluations of these compounds are currently in progress.

TABLE OF CONTENTS

	Page
ABSTRACT	iii
LIST OF TABLES	vii
LIST OF FIGURES	viii
LIST OF SCHEMES	x
I. BIOLOGICAL REVIEW	1
II. CHEMICAL REVIEW	25
III. STATEMENT OF THE PROBLEM	35
IV. CHEMICAL DISCUSSION	61
V. EXPERIMENTAL	91
VI. SUMMARY	143
BIBLIOGRAPHY	147

LIST OF TABLES

	Page
Table 1	HSP90 inhibitors in clinical trials 20
Table 2	HSP90 inhibitors based on 8-arylsulfanyl-adenine with alkyne chain 53
Table 3	HSP90 inhibitors based on 8-arylsulfanyl-adenine with amine chain 53
Table 4	BIIB021 and its activities (μM) 57
Table 5	Conditions attempted for de-methylation of the phenyl ether 64
Table 6	Experimented conditions for the reaction of 153 and 181 70
Table 7	Experimented hydrogenation conditions 73
Table 8	Experimented conditions for the removal of N-tosyl 76

LIST OF FIGURES

	Page
Figure 1	Schematic representation of microtubules 1
Figure 2	3D reconstruction of microtubule through cryoelectron microscopy 2
Figure 3	Polymerization dynamics and the GTP cap 3
Figure 4	Dynamic instabilities of the microtubules 4
Figure 5	Treadmilling of the microtubules 5
Figure 6	Microtubules changes during cell cycle 5
Figure 7	Structures of vinca alkaloids and their binding site on the microtubule 6
Figure 8	Structures of taxanes , epothilones and illustration of their binding site 8
Figure 9	Structures of the colchicine-site binding agents and their binding site 10
Figure 10	Examples of microtubule-binding agents with novel binding sites 12
Figure 11	Orthogonal views of HSP90 monomer 17
Figure 12	The middle segment before (left) and after (right) ATP binding 18
Figure 13	The HSP90 chaperone cycle 19
Figure 14	Structures of eribulin and vinflunine 35
Figure 15	Lead compounds 90 and 91 38
Figure 16	The lowest-energy conformation of 90 , 91 and energy plot 41
Figure 17	¹ HNMR chemical shift of the 5-H proton in 90 and 91 41
Figure 18	Superimposition of docked conformation of 2-mercapto-colchicine 43
Figure 19	Lowest-energy conformation of 91 from the docked results 44
Figure 20	Overlap of 90 and 2-mercapto-colchicine at colchicine-binding site 45
Figure 21	Interaction plots of 91 and 2-mercapto-colchicine at binding site 46
Figure 22	Series I 48
Figure 23	Series II 48
Figure 24	Series III 49
Figure 25	Series IV 49
Figure 26	Series V 50

Figure 27	The lowest-energy conformation of 117 and energy plot	51
Figure 28	Series VI	51
Figure 29	Crystal structure of PU-H71 and interaction plot	54
Figure 30	Series VII	56
Figure 31	Superimposition BIIB021 and PU24FCI ; interaction plot of BIIB021	58
Figure 32	Series VIII	59
Figure 33	Series IX	59

LIST OF SCHEMES

		Page
Scheme 1	Synthesis of 2-amino-pyrrolo[2,3- <i>d</i>]pyrimidines	25
Scheme 2	Synthesis of 2-oxo or 2-thieno pyrrolo[2,3- <i>d</i>]pyrimidines	26
Scheme 3	Synthesis of the 2-methyl-4-oxo-pyrrolo[2,3- <i>d</i>]pyrimidine	26
Scheme 4	Synthesis of the 6-substituted pyrrolo[2,3- <i>d</i>]pyrimidine	27
Scheme 5	Pd coupling followed by the 5- <i>endo</i> -dig cyclization	27
Scheme 6	Synthesis of the 5-methyl-pyrrolo[2,3- <i>d</i>]pyrimidine	28
Scheme 7	Cyclization of the appropriate pyrrole	28
Scheme 8	The Fischer Indole synthesis of 5,6-disubstituted pyrrolo[2,3- <i>d</i>]pyrimidine	29
Scheme 9	6,7-dihydro-pyrrolo[2,3- <i>d</i>]pyrimidine as the intermediate	30
Scheme 10	Synthesis of 4-chloro-6,7-dihydro-pyrrolo[2,3- <i>d</i>]pyrimidine	30
Scheme 11	Reductive hydrogenation of pyrrolo[2,3- <i>d</i>]pyrimidines	31
Scheme 12	Direct cyclization to the furo[2,3- <i>d</i>]pyrimidines	32
Scheme 13	Competition between the formation of furo- and pyrrolo[2,3- <i>d</i>]pyrimidine	32
Scheme 14	Synthesis of 2-substituted furo[2,3- <i>d</i>]pyrimidines	33
Scheme 15	Cyclization from furan	33
Scheme 16	Cyclization from substituted furans	34
Scheme 17	Synthesis of 2-methyl-3 <i>H</i> -pyrrolo[2,3- <i>d</i>]pyrimidin-4(7 <i>H</i>)-one (15)	61
Scheme 18	Proposed mechanism for cyclization leading to 15	62
Scheme 19	Synthesis of target compounds 90 – 98	62
Scheme 20	Synthesis of target compound 99	63
Scheme 21	Synthesis of <i>N</i> -methylnaphthalen-2-amine (159)	64
Scheme 22	Synthesis of target compounds 100 and 101	65
Scheme 23	Synthesis of target compounds 102 and 103	66
Scheme 24	One-pot synthesis of 165 via 4-bromo-pyrrolo[2,3- <i>d</i>]pyrimidine	67
Scheme 25	Synthesis of target compounds 104 – 109	68
Scheme 26	Synthesis of target compounds 110 – 113	69

Scheme 27	Synthesis of target compounds 114 – 116	71
Scheme 28	The strategy toward the target compound 118	72
Scheme 29	Hydrogenation without N-7 electron-withdrawing group	72
Scheme 30	Hydrogenation in the presence of the 4-methoxy- <i>N</i> -methylaniline	73
Scheme 31	Synthesis of N-7-tosylated pyrrolo[2,3- <i>d</i>]pyrimidines 189	74
Scheme 32	Reactions on <i>N,O</i> -distosyl-pyrrolo[2,3- <i>d</i>]pyrimidine 188	75
Scheme 33	Synthesis of 5,6-dihydropyrrolo[2,3- <i>d</i>]pyrimidine 193	75
Scheme 34	Removal of the tosyl group from nitrogen	76
Scheme 35	Alternative synthetic sequence for the target compound 118	77
Scheme 36	Attempted reduction of 102 by triethylsilane	78
Scheme 37	Alternative strategy toward the 5,6-dihydropyrrolo[2,3- <i>d</i>]pyrimidine	78
Scheme 38	Synthesis from functionalized pyrimidines	79
Scheme 39	Direct hydrogenation with the 4-position substituted	80
Scheme 40	Synthesis of the target compound 117	80
Scheme 41	Attempted synthesis of 1-(4-methoxyphenyl)ethyl Grignard reagent	81
Scheme 42	Alkylation of the pyrrolopyrimidine through a free radical reaction	81
Scheme 43	S _N Ar displacement with a strong carbon nucleophile	82
Scheme 44	Choice of protecting groups at the N7 position	83
Scheme 45	Conversion of the nitrile to a methyl	83
Scheme 46	Synthesis of target compounds 120 – 122 and 124	84
Scheme 47	Synthesis of the target compound 123 via Buchwald-Hartwig reaction	85
Scheme 48	Synthesis of 5-methyl-7 <i>H</i> -pyrrolo[2,3- <i>d</i>]pyrimidine-2,4-diamine (38)	86
Scheme 49	Synthesis of 5-methyl-7 <i>H</i> -pyrrolo[2,3- <i>d</i>]pyrimidin-4-amine (43)	87
Scheme 50	Synthesis of target compounds 130 – 145	88
Scheme 51	Synthesis of target compounds 136 – 141	89
Scheme 52	Synthesis of target compounds 144 – 149	90

I. BIOLOGICAL REVIEW

1) Microtubule-binding agents as anticancer drugs

1.1) Structures of microtubules

Microtubules are components of the cell skeleton.¹ In addition to mechanical support, microtubules play critical roles in numerous vital cellular events such as cell division, trafficking, signaling and migration.^{1, 2} The proper functioning of the microtubules, particularly during mitosis, depends on exquisite dynamics that are highly sensitive to chemical intervention.² For this reason, microtubule-binding agents such as vinca alkaloids and taxanes possess potent inhibitory activities against a broad range of cancers. Drugs targeting microtubules are highly successful in clinic and have been integrated into the therapeutic regimens against both solid tumors (breast, ovarian, non-small-cell lung cancer and Kaposi's sarcoma) and hematological malignancies (non-Hodgkin's lymphomas).^{1, 2}

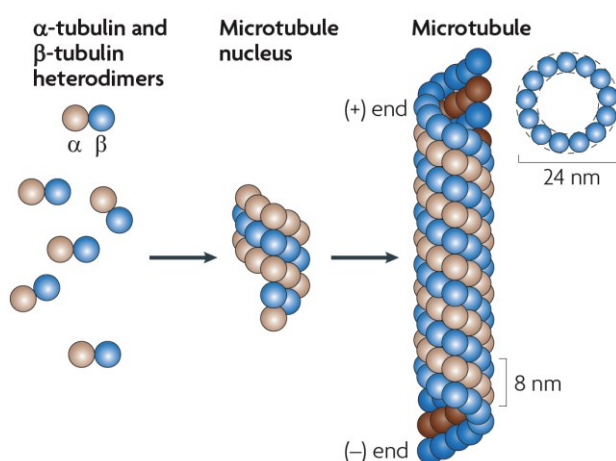


Figure 1 Schematic representation of microtubules²

Microtubules are tube like protein filaments assembled from individual tubulin dimers. The dimer, present in cytoplasm in soluble form, consists of one α - and one β -tubulin peptide (**Figure 1**).² Each tubulin has a molecular weight of 55 kDa.¹ The tubulin dimers polymerize “head-to-tail” between the α - and β -tubulin into the protofilaments, forming the wall of the tube like structure. The resulting microtubule “tube” consists of 13 protofilaments laterally and has an outer diameter of 24 nm. The length of certain microtubules can extend up to 25 μm .

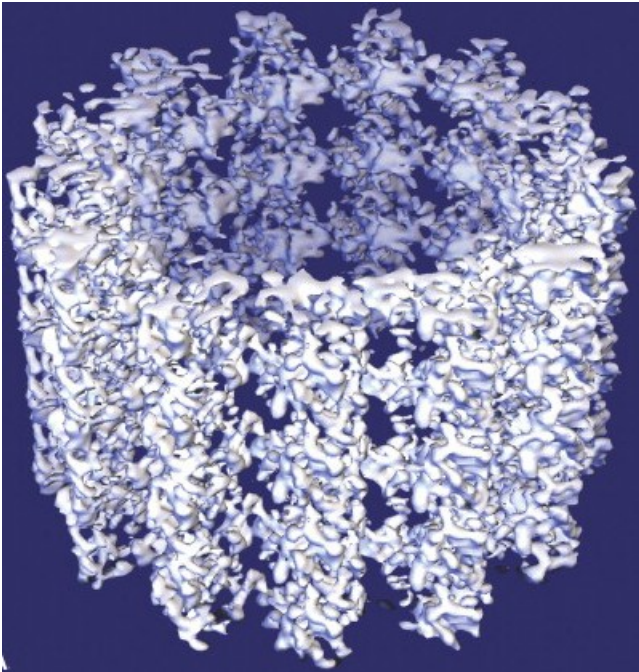


Figure 2 3D reconstruction of microtubule through cryoelectron microscopy³

The structural details of the microtubule are directly observable through the reconstructed cryoelectron microscopy (**Figure 2**).³ Small nano-size pores exist on the microtubule “walls” between the interfaces of α - and β -tubulins.

1.2) Dynamics of microtubules

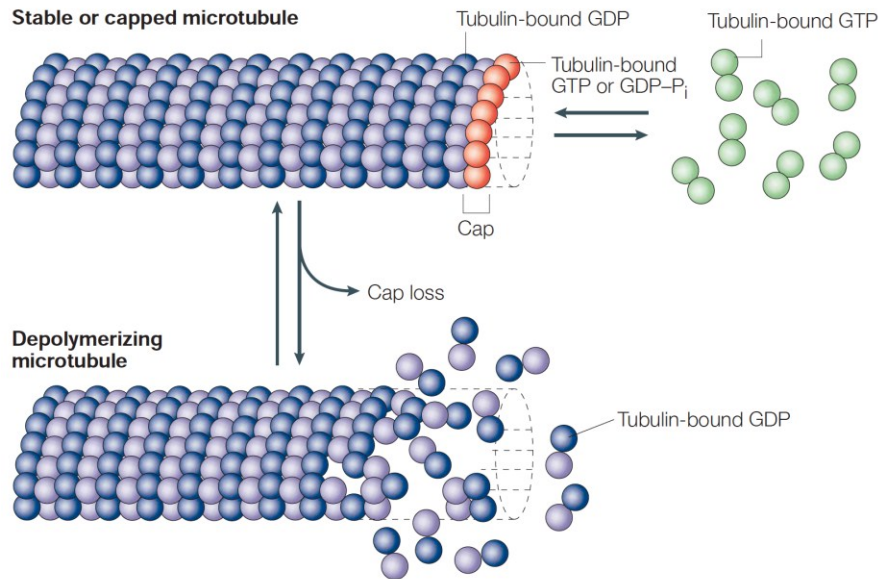


Figure 3 Polymerization dynamics and the GTP cap¹

The polymerization of tubulins follows a nucleation-elongation mechanism.¹ In this process, a short microtubule nucleus is formed slowly, followed by the rapid elongation through the reversible, non-covalent addition of the soluble tubulin dimers. The polymerization is driven by the hydrolysis of GTP upon the attachment of the GTP-bound tubulin dimer to the ends of the microtubule (**Figure 3**). Prior to attachment, GTP binds to the β -tubulin and the dimer switches to a straight conformation that promotes the polymerization.^{4, 5} Delayed hydrolysis of the GTP results in the formation of a “GTP-cap”, which contains GTP or GDP with unreleased phosphate (GDP-P_i). The GTP-cap stabilizes the open-sheet conformation of the growing microtubule end ((+)-end) and prevents microtubule shrinkage and catastrophe.^{6, 7} The size of the cap depends on the polymerization rate but in most cases it is no longer than a single layer of tubulin.^{1, 8} The hydrolysis of GTP occurs after the tubulin dimer is integrated into the microtubule. At the

final stage of the polymerization, the cap dissociates and leaves a microtubule core of β -tubulin bound with GDP. However, if the GTP-cap is not formed, the relatively unstable core of the microtubule is exposed and depolymerization proceeds rapidly.^{1,8} Controlling the accessibility and conformation of tubulin dimers is the most direct way to regulate the dynamics of microtubules.⁸

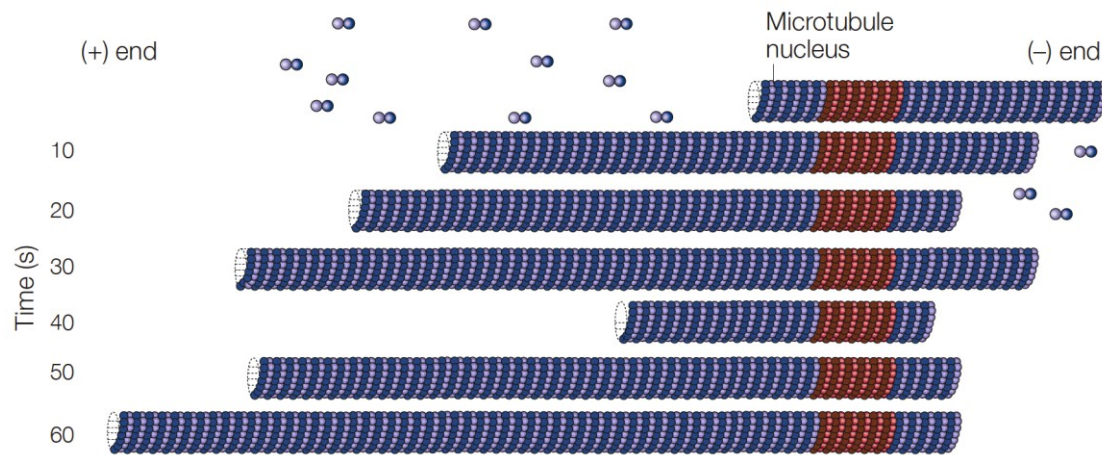


Figure 4 Dynamic instabilities of the microtubules¹

Microtubules are highly dynamic structures.^{1,8} The force generated through elongation and shrinkage is the energy source for the microtubules to carry out its functions. Microtubules display two major types of non-equilibrium dynamics *in vitro* and in cells.¹ The first type is called “dynamic instabilities” (**Figure 4**). This process is defined by four main factors: 1) the rate of growing; 2) the rate of shrinking; 3) the frequency of the “catastrophe” event (transition from the growing or paused state to shrinking) and 4) the frequency of the “rescue” event (transition from shrinking to growing or pause. The β -tubulin-exposed (+)-end has a higher rate of polymerization than the α -tubulin-exposed (-)-end.

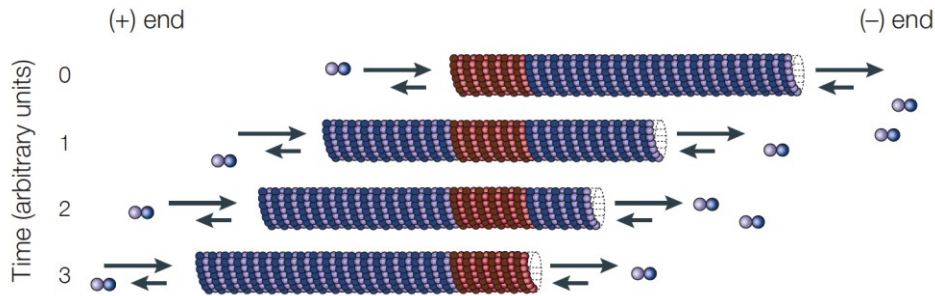


Figure 5 Treadmilling of the microtubules¹

The second type of the non-equilibrium dynamics is called “treadmilling”. During treadmilling, the plus-end of the microtubule extends and minus-end shrinks in equivalent amount (**Figure 5**). The effect of this dynamics is a net flow of the tubulins from the (-)-end to the (+)-end.

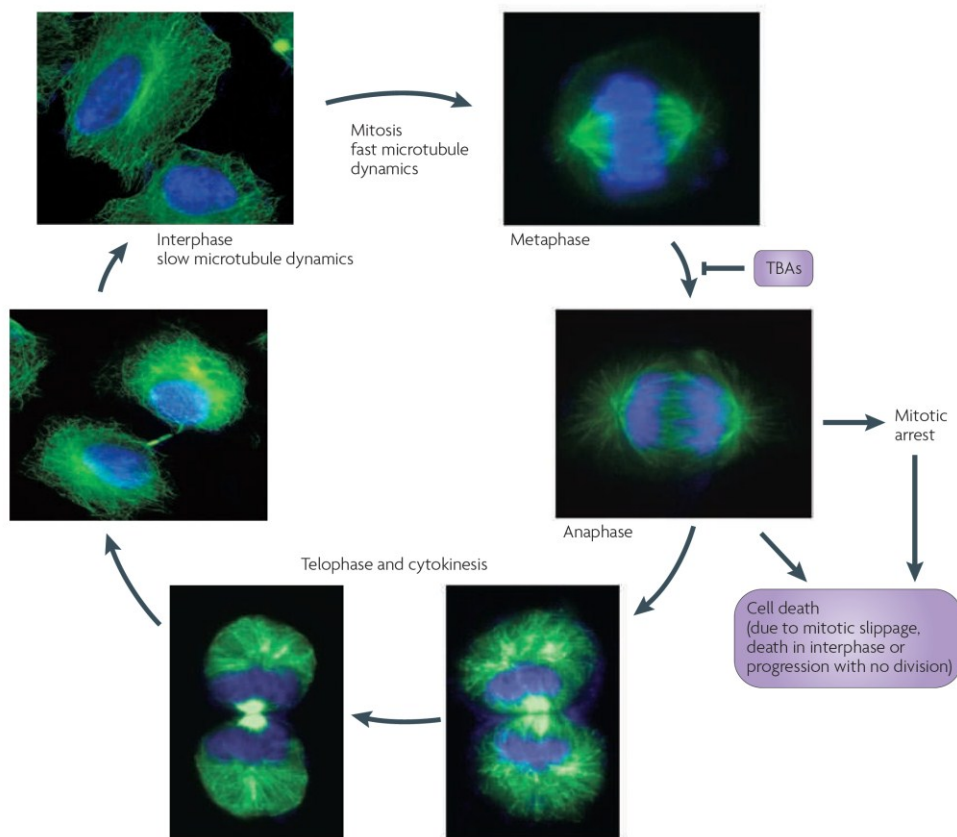


Figure 6 Microtubules changes during cell cycle;⁹ microtubule shown in green and DNA shown in blue

The rate of microtubule dynamics changes throughout the cell cycle (**Figure 6**).⁹ The interphase cells have the slowest dynamics. The rate accelerates when the cells enter the metaphase, during which the formation of the microtubule spindles drives the dynamic 4- to 100-times faster. The microtubule dynamics at this stage is highly delicate and extremely sensitive to chemical interventions. Microtubule-binding agents or tubulin-binding agents (TBAs) disrupt the microtubule dynamics and lead to mitotic arrest at the anaphase, eventually resulting in cell death.^{2,9}

1.3) Three major classes of microtubule-binding agents

One notably feature of the microtubule-binding agents is their vastly diverse structures.² Most of these compounds are natural products, which plants or animals use to wage “chemical warfare” against the competitors and predators. In cancer chemotherapy, microtubule-binding agents are mainly antimetabolic agents. They inhibit malignant cell proliferation by interrupting the microtubule dynamics at the mitotic stage of the cell cycle.²

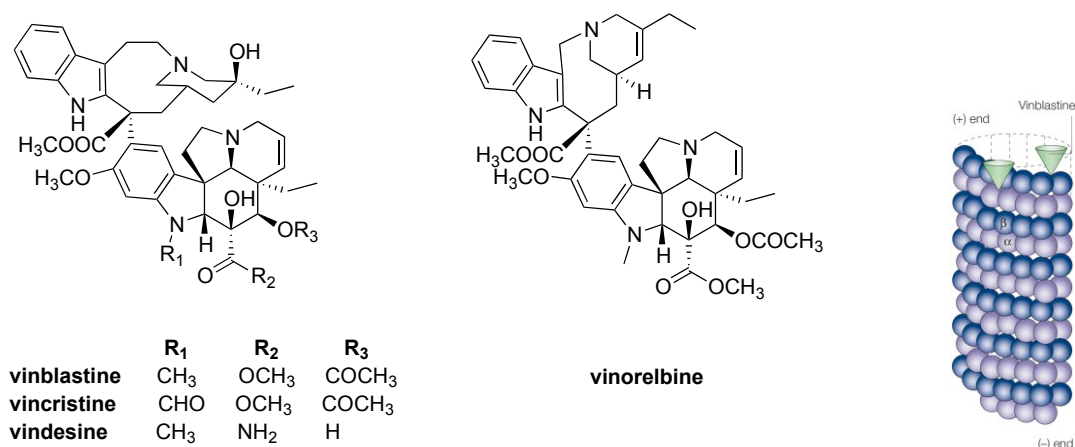


Figure 7 Structures of vinca alkaloids and their binding site on the microtubule¹

Most of the known microtubule-binding agents bind to three major sites on tubulin and accordingly they are divided into three major classes.^{1, 2} The first class is the vinca alkaloid, including vinblastine, vincristine, vindesine, and vinorelbine (**Figure 7**).^{1, 2} The naturally occurring vinblastine and vincristine were isolated from the leaves of periwinkle plant *Catharanthus roseus* in the 1950s. They are also the first microtubule-binding agents discovered. For over four decades, drugs of this class have been widely used in clinic for cancers like leukemia, lymphomas and non-small-cell lung cancer.

The binding site of the vinca alkaloids (“vinca domain”) is located at the β -tubulin. Vinca alkaloids could bind to both soluble tubulin dimer and the microtubule (at the (+)-end).^{10, 11} The binding between vinblastine and the soluble tubulin dimer is rapid and reversible.^{10, 12} The binding incurs a conformational change that promotes self-association of the tubulin and prevents the integration of the dimer into the microtubule.¹³ When vinblastine binds directly to the microtubule, the outcome is dependent on the concentration of the drug. At high concentrations (e.g. 10 – 100 nM in HeLa cells), vinblastine effectively depolymerizes microtubules and destroys the mitotic spindles.¹⁴ At low but clinically relevant concentrations (e.g. around 1 nM HeLa cells), mitosis is still blocked but without depolymerizing the spindle microtubules.¹² The blocking effect under low concentrations is solely due to the suppression of microtubule dynamics.¹² Remarkably, the binding of one or two molecules of vinblastine is sufficient to reduce the rate of the dynamic instability and treadmilling in a single microtubule by 50%. This dynamic suppression also leads to the disruption of the normal assembly of the mitotic spindle and eventually cell death through apoptosis.

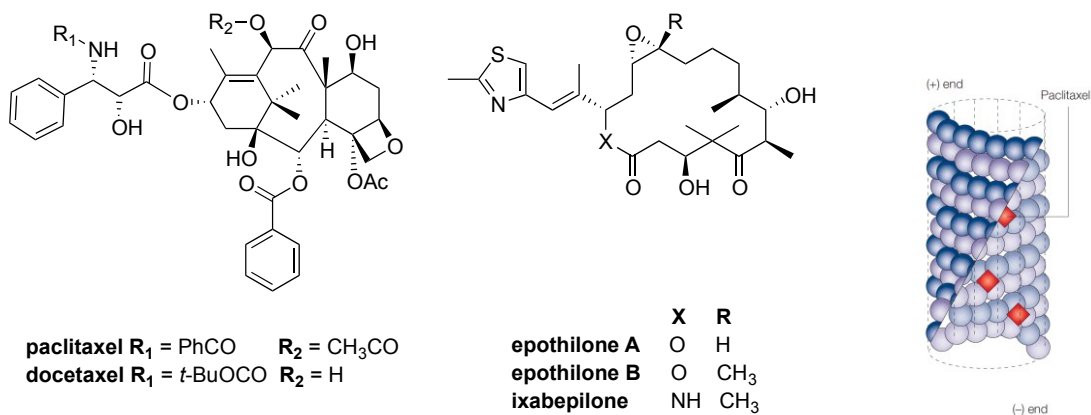


Figure 8 Structures of taxanes, epothilones and illustration of their binding site¹

The second class of microtubule-binding agents includes the taxanes and epothilones (**Figure 8**).^{1, 2} Paclitaxel, a prominent member of the taxane family, is one of the most important discoveries in the field of cancer chemotherapy in the twentieth century. It was first isolated from the bark of the pacific yew tree *Taxus brevifolia* in 1967.¹⁵ The initial development was slow due to the limited quantity of the compound. In 1979, it was revealed that unlike vinblastine, paclitaxel functions by promoting the polymerization of the microtubule.¹⁶ This surprising finding spurred pharmaceutical interest in paclitaxel. The scarcity of the natural source prompted synthetic chemists to develop effective process for large-scale production.¹⁷ In 1995, after three decades of development, paclitaxel was finally approved for clinical use. It is now a common component of the regimens for treating breast, ovarian, non-small-cell lung cancer and the Kaposi's sarcoma.¹

Paclitaxel has low affinity to the soluble tubulin dimers but binds strongly to the microtubules. The binding site of the taxanes is also on the β -tubulin but locates in the interior lumen of the microtubule (**Figure 8**).¹⁸ Paclitaxel reaches the binding site by

diffusing through the nano-size “pores” on the surface of the microtubule (as shown in **Figure 2**).¹⁹ The binding of paclitaxel introduces a conformational change on the β -tubulin that increases the affinity between adjacent tubulins.¹⁹

The stoichiometry to promote the polymerization of microtubules is approximately 1:1 between paclitaxel and the tubulin dimer.²⁰ That is to say if a certain microtubule contains 20,000 tubulin units, the number of paclitaxel molecules needed to promote the polymerization is 10,000. This corresponds to a rather high concentration of paclitaxel. However, under concentrations ten times lower, paclitaxel can effectively stabilize the dynamics of the microtubules without promoting microtubule polymerization.²⁰ Similar to vinblastine, disruption of microtubule dynamics by paclitaxel under low concentrations leads to mitotic block without changing the mass of the microtubules.²¹ For example, in HeLa cells the IC_{50} for paclitaxel to block mitosis is 8 nM and no increase in microtubule mass was observed with concentrations below 10 nM.²² On the other hand, the concentration of paclitaxel to increase the microtubule mass in HeLa cells by 50% is 80 nM.²²

Epothilones, originally identified as metabolites produced by the soil-dwelling myxobacterium *Sorangium cellulosum*, act in a similar mechanism as the taxanes.²³ Their binding sites are overlapped but non-identical.²⁴ Ixabepilone (**Figure 8**) was approved for the treatment of drug-refractory metastatic breast cancer in 2007. Epothilone B and ixabepilone have also shown activities against taxane-resistant metastatic breast cancer and non-small-cell lung cancer in clinical trials, alone or in combination with other drugs.^{25, 26} In some types of cancer, epothilones are preferred over taxanes to overcome drug resistance.²⁷

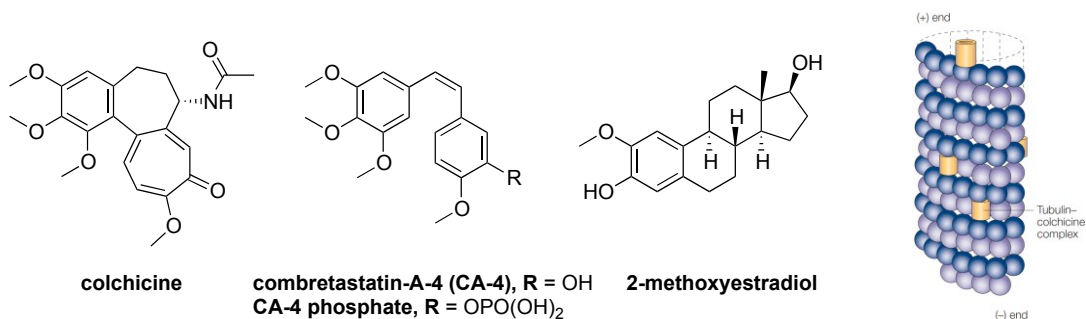


Figure 9 Structures of the colchicine-site binding agents and their binding site¹

The third class of the microtubule-binding agents, represented by colchicine, is a collection of structurally diverse compounds (**Figure 9**).^{1,2} Colchicine is a toxic natural product extracted from the plants of the *Colchicum* genus. For three thousand years, it has been used for the treatment of rheumatism and swelling in some parts of the world.²⁸ Colchicine is mainly used for treating gout and familial Mediterranean fever today.

The compounds in this class share a common “colchicine site” site on β -tubulin at the interface between the α - and β - tubulins.²⁹ Similar to vinca alkaloids, colchicine-site-binding agents depolymerizes the microtubules at high concentrations and disrupts microtubule dynamics at low concentrations.²⁹ However, the way in which colchicine binds to the microtubule is different from vinblastine. Colchicine binds to the soluble tubulin dimer, incurs a conformational change and forms the colchicine-tubulin complex. The complex is then integrated into the microtubule ends.³⁰ The ends with the complex are still able to grow, but their dynamics are greatly suppressed.

In addition to the antimitotic effect, some colchicine-site-binding agents are also potent vasculature-disrupting agents (VDA). Tumor vasculature is essential for tumor growth and is readily accessible to drugs in blood circulation. Antiangiogenic mechanism

is an established approach to target the tumor vasculature.³¹ Antiangiogenic drugs are mainly receptor tyrosine kinase (RTK) inhibitors and are widely used in the clinic as antitumor agents for the past decade.³¹ Another way to target the tumor vasculature is to destroy the existing blood vessel through VDA. Combretastatin A-4 phosphate (CA-4-P) rapidly depolymerizes the microtubules of endothelial cells *in vitro* at a concentration of 0.1 – 1 μ M and leads to cell detachment within minutes.³² The cells show no signs of apoptosis. In studies on rodents, CA-4-P reduces 95% of the blood flow to the tumor within one hour, along with increased vascular permeability and hemorrhage of peripheral vessels.³³ Based on this property of some of the colchicine-binding agents, both combretastatin A-4 (CA-4) and CA-4-P have been developed as anti-vascular agents and are in clinical trials.^{34,35} One encouraging finding from these clinical trials is that the VDA showed fairly high selectivity for tumor vasculature over normal blood vessels.³⁶ The source of this selectivity was suggested to lie in the differences between the mature vasculature of normal tissues and the immature or forming vasculature of tumors.³³ The actin cytoskeleton in endothelial cells of immature vasculature is underdeveloped, which is likely to make the cells more susceptible to anti-microtubule intervention.³⁷ In addition, the differences in the endothelial cell proliferation rate may also be contributing factor to the observed selectivity.³³

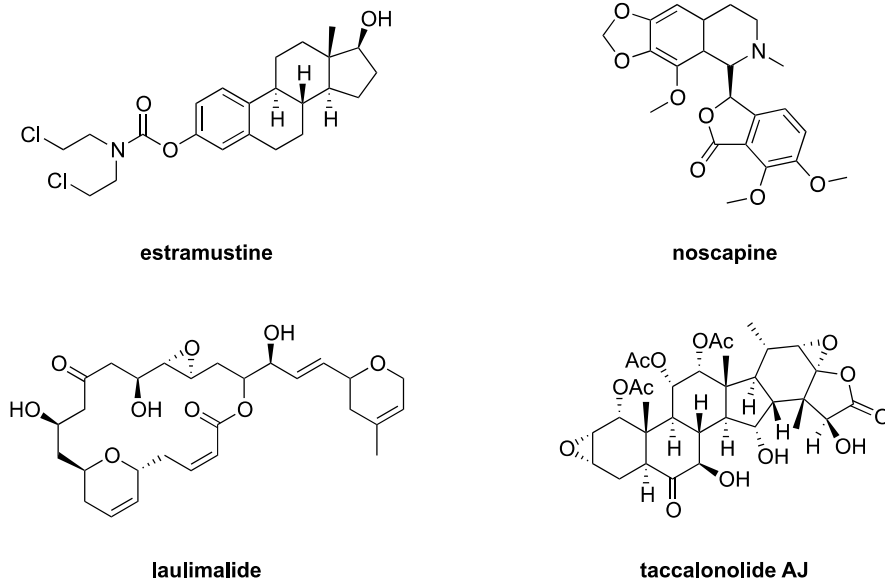


Figure 10 Examples of microtubule-binding agents with novel binding sites

In addition to the three major classes described above, there are microtubule-binding agents that do not bind to or overlap with any of the three sites.^{1, 2} Examples of such compounds include estramustine, noscapine, laulimalide and the taccalonolides (**Figure 10**). Estramustine and noscapine are microtubule-depolymerizing agents like vinca alkaloids and colchicine-site binders while laulimalide and taccalonolides promote microtubule polymerization in a similar way to taxanes and epothilones.³⁸⁻⁴¹ Noscapine is in phase II clinical trial for the treatment of multiple myeloma (ClinicalTrials.gov identifier: NCT00912899). A number of clinical trials for the combination of estramustine with vinca alkaloids, taxanes and epothilones are currently in progress (reports available at ClinicalTrials.gov).⁴²

Surprisingly, synergistic effects were observed in the combinations of estramustine with vinblastine or paclitaxel.^{42, 43} Extensive cell assays and in some cases clinical trials indicated that the synergy among the microtubule-binding agents is pervasive: they could

act synergistically in suppressing microtubule dynamics.¹ Although the cause for the synergy is not well understood, its therapeutic value is being actively explored in multiple clinical trials (reports available at ClinicalTrials.gov).

1.4) Toxicities of microtubule-binding agents

Several highly potent microtubule-binding agents have failed in the early stages of clinical trials due to toxicities. Recent examples include discodermolides and cryptophycin 52 (LY355703).^{44, 45} Neurological toxicity is the most prominent dose-limiting side effect shared by all microtubule-binding agents.² This potentially severe and dose-accumulative side effect usually appears as a painful peripheral axonal neuropathy.⁴⁶ The impact of this can persist for several years after the end of treatment. The reasons for this nervous-system-preferred toxicity are uncertain. However, the relative abundance and sensitivity of the neuronal microtubules could be the cause.²

Other common toxicities of microtubule-binding agents include myelosuppression and neutropenia. The myeloid toxicity, which is usually reversible, is seen in vinca alkaloids and taxanes.^{47, 48} Neutropenia was observed in several combination chemotherapy clinical trials with other drugs and was mostly manageable.⁴⁹⁻⁵¹

1.5) Resistances to microtubule-binding agents

Multiple-drug resistance (MDR) is a common cause in cancer chemotherapy failures.⁵² The microtubule-binding agents are no exception.^{2, 9} The main resistance mechanisms

among this category of drugs are drug efflux by ATP binding cassette (ABC) proteins and the alterations of the microtubules.

Membrane efflux by ABC proteins such as P-glycoprotein (Pgp) was identified as the primary mechanism of resistance against vinca alkaloids and taxanes *in vitro*.⁵³ For example, the potency of paclitaxel was reduced over 800 times against Pgp-overexpressing SK-OV-3 MDR-1-6/6 cell lines than the parental cell lines.⁵⁴ The expression of the ABC pumps is frequently correlated with lower responses to microtubule-binding agents. Intriguingly, the combination of Pgp inhibitors with the microtubule-binding agents failed to reverse the resistance in clinical trials.⁵⁵ The clinical relevance of this resistance mechanism is still under debate due to the limited data on the ABC pumps in cancer patients.⁵⁶

The alterations of the microtubules include changes in the microtubule-associated proteins (MAP) or the expression of certain isotypes of tubulin in the cells. The binding of MAPs stabilizes the microtubules. Depending on the type of the microtubule-binding agent, varying levels in the expression of the MAPs such as tau, MAP2 and MAP4 could result in resistance or increased activity.⁹ For example, the down-regulation of the MAP4 led to resistance against paclitaxel but increased response to vinblastine.^{57, 58} Up-regulation of MAP4 did the reverse.

More than 13 different isotypes of tubulins are known to be involved in the assembly of the microtubules. Among them, increased levels of class III β -tubulin (β III-tubulin) is of paramount concern since it is closely associated with resistance against taxanes in lung, breast and ovarian cancers.^{59, 60} In HeLa cell lines, the activity of paclitaxel decreased

five times when the cells were modified to express β III-tubulin.⁶¹ It was hypothesized that resistance of taxanes was due to loss of a key Ser275 on the β III-tubulin, which facilitates the diffusion of paclitaxel across the pores.⁶² However, this theory could not explain the β III-tubulin-mediated resistance in vinca alkaloids.⁶⁰ In addition, β III-tubulin was shown to mediate the resistance against a broad range of drugs with different action mechanisms of action.⁶³ Several studies confirmed the essential role played by β III-tubulin in protecting cells from the drug-induced genotoxic stresses.⁶⁴⁻⁶⁶ It is conceivable that the role of β III-tubulin in cancer may extend beyond drug resistance and it will continue to be an active area of research.

2) Heat shock protein 90 (HSP90) inhibitors as anticancer agents

Molecular chaperones are proteins that assist the proper folding of the newly synthesized polypeptides and proteins.⁶⁷ They also minimize the risk of the protein aggregation inside the cell. Many chaperone proteins are termed heat shock proteins (HSP).⁶⁸ The “heat shock” in the name is a broad indication of environmental stresses. When the cell is challenged with stresses like elevated temperature, the expression of HSP is dramatically increased to restore the normal protein-folding environment.⁶⁸ HSPs are named according to their molecular weights, e.g. HSP90 is the 90 kDa HSP. Following the discovery of the heat-shock response in the 1960s, major families of HSPs such as HSP33, HSP60, HSP70, HSP90 and HSP100 have been identified.⁶⁹ The “heat shock” name does not preclude their expression under normal conditions. HSP90 accounts for 1 to 2% of the total cell protein content even under normal conditions.⁶⁸

HSP90 is ubiquitous and vital for all eukaryotes tested. It is also unique in the sense that it is rarely involved in the biogenesis of most polypeptides.⁷⁰ Instead, the majority of its client proteins are signal transducers with unstable conformations, which play critical roles in growth control, cell survival and development.⁷¹ Some of these proteins are known to have direct involvement in cancer. Examples are receptor tyrosine kinases, serine/threonine kinases and steroid hormone receptors in uncontrolled proliferation, immortalization telomerase, AKT in impaired apoptosis, matrix metalloproteinase in metastasis. Elevated cellular levels of HSP90 and/or HSP70 are common in both solid tumor and hematological malignancies.⁷²⁻⁸⁰

2.1) Structure and functions of the heat shock protein 90

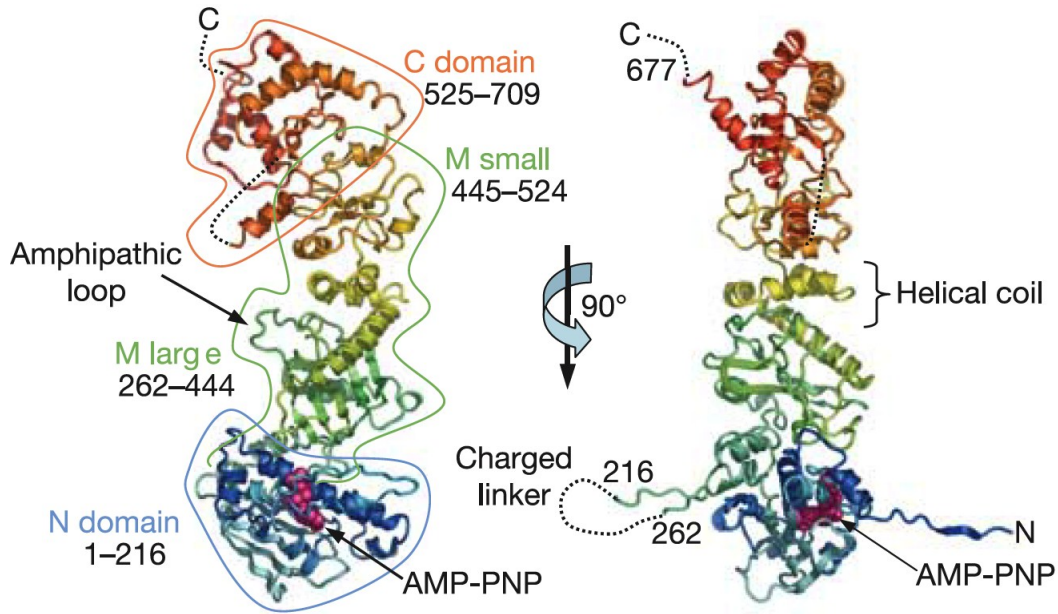


Figure 11 Orthogonal views of HSP90 monomer⁸¹

HSP90s exist predominantly in homodimers. Each monomer consists of three domains (**Figure 11**). The N-domain (residues 1 – 216) is formed by a twisted β -sheet and a cluster of α -helices, with the ATP-binding site and co-chaperon-interacting motifs in between. The middle segment contains a large three-layer α - β - α domain (residues 262 – 444) and a small α - β - α domain (445 – 524). The amphipathic loop (residues 329 – 339) of the middle segment interacts with the client protein during the chaperoning process. The C-domain (residues 525 – 709) is involved in the dimerization of the monomers.

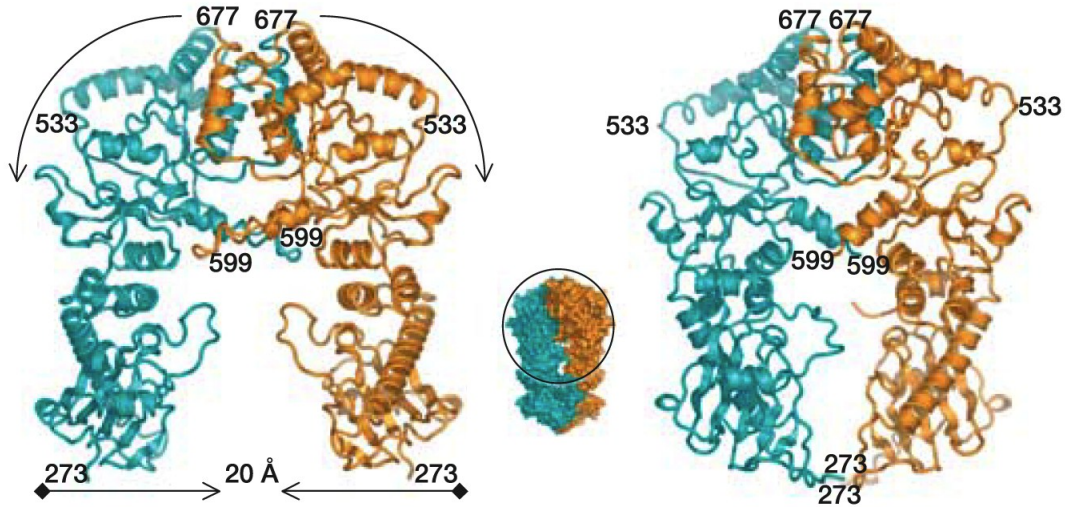


Figure 12 The middle segment before (left) and after (right) ATP binding⁸¹

The operation of the Hsp90 dimer follows a “molecular clamp” mechanism coupled with the ATPase cycle.⁸² The binding of ATP restructures the N-domain and leads to the closure of the “lid” segment (residues 94 – 125). This movement exposes a hydrophobic patch centered on Leu15 and Leu18. The exposed hydrophobic patch on each monomer directly contacts each other and the resulting burial of the patches stabilizes the transient dimerization of the N-domains.⁸² This dimerization of the N-domains draws the middle segment of each monomer 20 Å closer, but do not contact (**Figure 12**).⁸¹ Instead, each middle segment interacts with the N-domain of the other monomer. The γ -phosphate of ATP is cradled in a glycine-rich loop at the end of the lid segment, making a single contact outside the N-domain with Arg380, which is brought to place through the movement of the middle segment. The ATPase is also activated through this series of arrangement, as a water molecule activated by Glu30, is ready to attack the Arg380-polarized γ - β phosphodiester bond.⁸¹

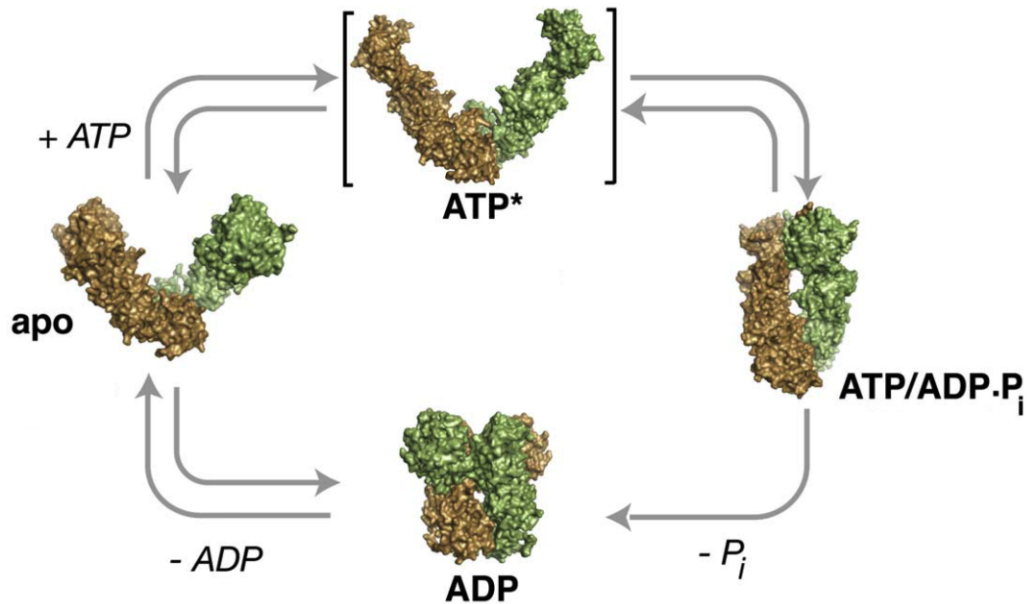


Figure 13 The HSP90 chaperone cycle⁸³

The large-scale conformational changes (ATP* to ATP/ADP-P_i in **Figure 13**) experienced by HSP90 are not the sole result of ATP binding, but is also driven by client association.⁸⁴ The hydrolysis of ATP causes all of the once-exposed hydrophobic motifs to be covered and leads to a very compact ADP-bound state.⁸³ The release of the client proteins and co-chaperones occurs and completes the chaperon cycle.

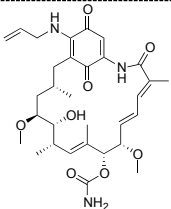
HSP90 has over 200 client proteins.⁶⁷ To achieve the optimal chaperoning condition for each client, HSP90 recruits HSP70 and a variety of co-chaperones.^{67, 68} Phosphorylation at certain serine residues has been linked in regulating the conformational switching of the chaperone complex in recent studies.⁸⁵

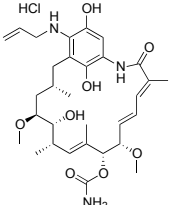
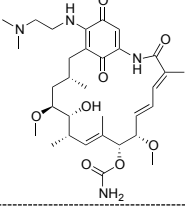
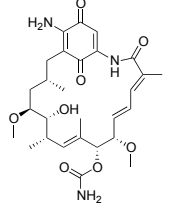
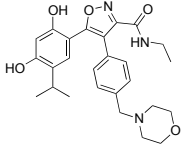
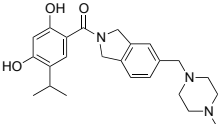
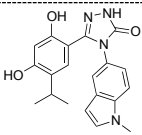
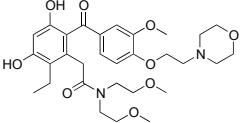
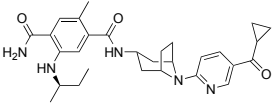
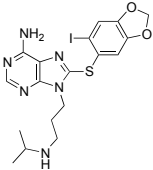
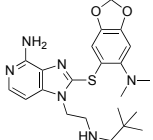
2.2) HSP90 inhibitors

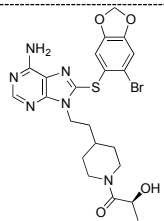
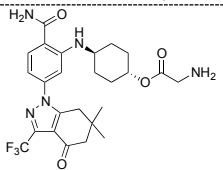
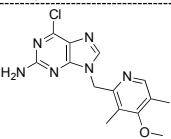
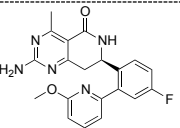
Some of the HSP90 client proteins are particularly sensitive to HSP90 inhibition. Even low concentrations of the inhibitors could drive them into rapid degradation. These client proteins are usually involved in growth signaling, which are pivotal to the proliferation of cancer cells. In addition, mutated proteins like mutant p53 or imatinib-resistant Bcr-Abl are particularly dependent on HSP90.⁸⁶ HER2 (human epidermal growth factor receptor 2) seems to be the most sensitive to HSP90 inhibition among those cancer-related client proteins.⁸⁷ Other common cancer-related client proteins in decreasing sensitivities are mutant EGFR (epidermal growth factor receptor), c-Raf, Akt (Protein Kinase B), mutant BRAF and wild-type EGFR.⁸⁷

The ability to cause degradation in proteins vital to cancer proliferation has made HSP90 an attractive target for cancer chemotherapy. Inhibition of HSP90 results in the simultaneous attack on several key players in cancer progression, thus reducing the chance of developing resistance. In addition, HSP90 inhibitors are found to preferentially accumulate in cancer cells and the sensitivity of HSP90 to inhibitors in cancer cells is fundamentally different than in normal cells.⁸⁸⁻⁹⁰

Table 1 HSP90 inhibitors in clinical trials

Structure	Name	Phase	Route	Sponsors
	Tanespimycin (17-AAG)	III	Intravenous	Cancer Research UK, Kosan-BMS

Structure	Name	Phase	Route	Sponsors
	Retaspimycin (17-AAG hydroquinone)	III	Intravenous	Infinity
	Alveospimycin (17-DMAG)	I	Intravenous	NCI, Kosan-BMS
	IPI-493 (17-AG)	I	Oral	Infinity
	NVP-AUY922	II	Intravenous	Novartis
	AT13387	II	Intravenous	Astex
	STA-9090 (ganetispib)	II	Intravenous	Synta
	KW-2478	I/II	Intravenous	Kyowa Hakko Kirin
	XL888	I	Intravenous	Exelixis
	PU-H71	I	Intravenous	Memorial Sloan-Kettering Center
	DEBIO-0932/CUDC-305	I	Oral	Debiopharm, Curis

Structure	Name	Phase	Route	Sponsors
	MPC-3100	I	Oral	Myrexix
	PF-4929113 (SNX-5422)	I	Oral	Pfizer
	BIIB021	II	Oral	Biogen Idec
	NVP-HSP990	I	Oral	Novartis
(undisclosed)	BIIB028	I	Intravenous	Biogen Idec

None of the HSP90 inhibitors has been approved yet. Currently, there are 16 HSP90 inhibitors at various stages of clinical development (**Table 1**).^{67, 91, 92} The first HSP90 inhibitor entered clinical trials was tanespimycin (17-AAG, 17-allylamino-17-desmethoxygeldanamycin), a derivative of the natural product geldanamycin.⁹³ It is given intravenously and has recently advanced to phase III clinical trials. Retaspimycin is the hydroquinone analog of tanespimycin and the ease with which it is converted into the water-soluble hydrochloride salt provides advantages in formulation.⁹⁴ Development of alvespimycin was also aimed at enhancing water solubility, but it resulted in higher toxicity in preclinical studies.⁹⁰ IPI-493 is a metabolite of tanespimycin with significantly enhanced oral bioavailability. It is developed as the only oral drug among geldanamycin derivatives.

The remaining HSP90 inhibitors in clinical trials are synthetic small-molecule compounds developed in recent years. Among them, four intravenously administered compounds share the same 2,4-dihydrobenzene motif: NVP-AUY922, AT13387, STA-9090 (ganetispib) and KW-2478.⁹⁵⁻⁹⁸ Other intravenous drug candidates include a tropane based compound XL888, purine based PU-H71 and an undisclosed structure BIIB028.^{67, 99, 100} Purine or purine analog based compounds have been developed as orally bioavailable HSP90 inhibitors. Examples include DEBIO-0932/CUDC-305, MPC-3100 and BIIB021.¹⁰¹⁻¹⁰³ Other orally active HSP90 inhibitors in clinical trials are NVP-HSP990 and PF-4929113.^{104, 105}

All the HSP90 inhibitors in clinical trials are reported to bind to the N-domain, overlapping entirely or partly with the ATP-binding site. The mechanism for HSP90 inhibitors is not limited to the displacement of ATP and the interruption of the following chaperoning cycle.¹⁰⁶ The inhibitor-bound HSP90 tends to recruit E3 ubiquitin ligases such as CHIP (carboxyl-terminus of HSP70-interacting protein) to the chaperone complex.¹⁰⁷ Under these conditions, the misfolded client proteins are more likely to be degraded by proteasome.¹⁰⁷

One of the challenges in maximizing the therapeutic potential of HSP90 inhibitors is to identify the right cancer types that have the best response to HSP90 inhibition.⁹² It followed logically that the breast cancer, mostly driven by HER-2, became the primary target for HSP90 inhibitors.¹⁰⁸ Non-small-cell lung cancer and multiple myeloma also have high response rates to HSP90 inhibitors, alone or in combination with other drugs.^{109, 110} The efficacy of HSP90 maybe more pronounced in combinations with other

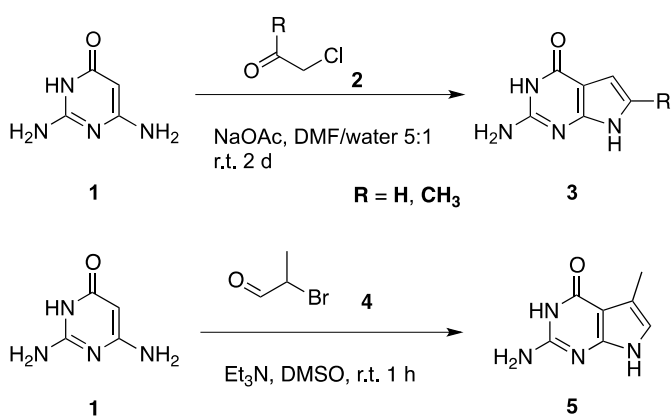
drugs, since the benefits of overcoming resistance, increasing response and reducing dose-related toxicity were frequently observed in such clinical trials.^{67, 91, 108, 111}

II. CHEMICAL REVIEW

1) Synthesis of the pyrrolo[2,3-*d*]pyrimidines

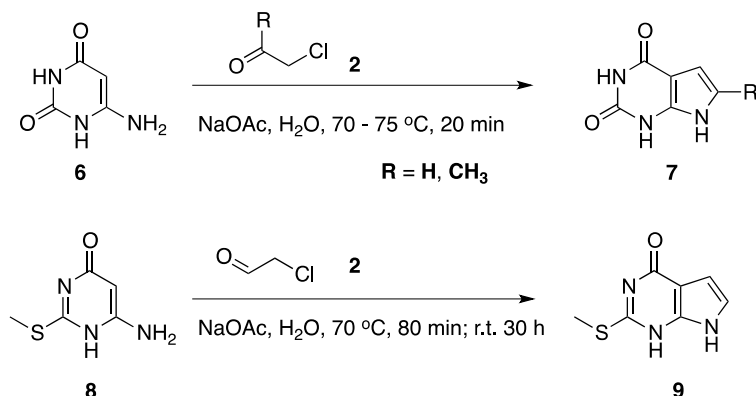
There were relatively abundant reports on the synthesis of pyrrolopyrimidines in literature. A review on the synthesis of pyrrolopyrimidines in general is available.¹¹² This section will focus on the reported methods that directly connected to the structures in this dissertation.

Scheme 1 Synthesis of 2-amino-pyrrolo[2,3-*d*]pyrimidines



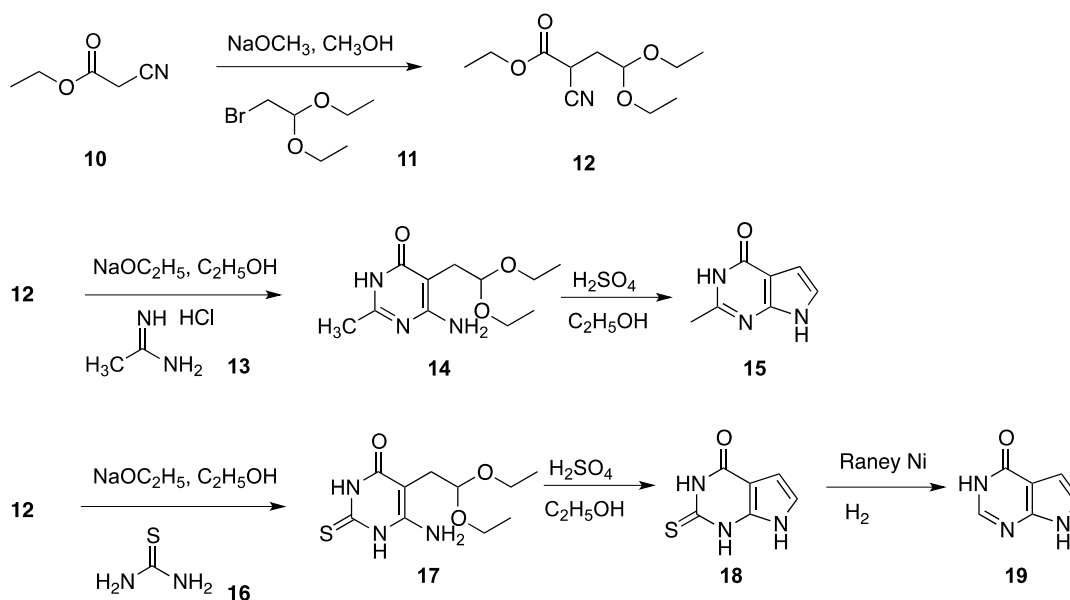
The direct cyclization between the pyrimidine and the α -halogen aldehyde (or ketone) is usually the quickest synthetic route to pyrrolo[2,3-*d*]pyrimidines. Examples of this strategy are reactions between the 2,6-diamino-4-oxo-pyrimidines and α -haloaldehydes or ketones (Scheme 1).¹¹³⁻¹¹⁸ Both 5- and 6-substituted pyrrolo[2,3-*d*]pyrimidines could be obtained in concise sequences.

Scheme 2 Synthesis of 2-oxo or 2-thieno pyrrolo[2,3-*d*]pyrimidines



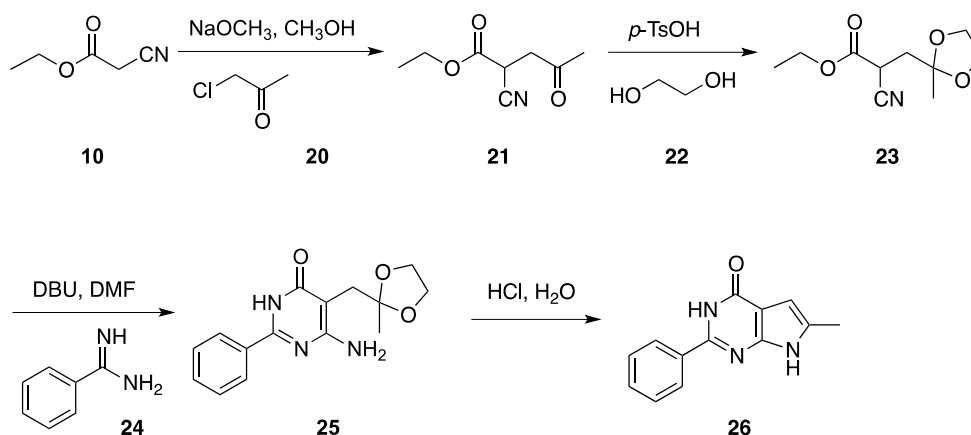
The same synthetic method applies to the 2-oxo-6-amino-pyrimidines (Scheme 2).¹¹⁹ In some patent literature, 2-methylthio-pyrimidine underwent the same reaction under similar conditions.¹²⁰⁻¹²² Reactions with α -haloketones to give the 6-substituted pyrrolo[2,3-*d*]pyrimidines have also been reported.¹²³

Scheme 3 Synthesis of the 2-methyl-4-oxo-pyrrolo[2,3-*d*]pyrimidine



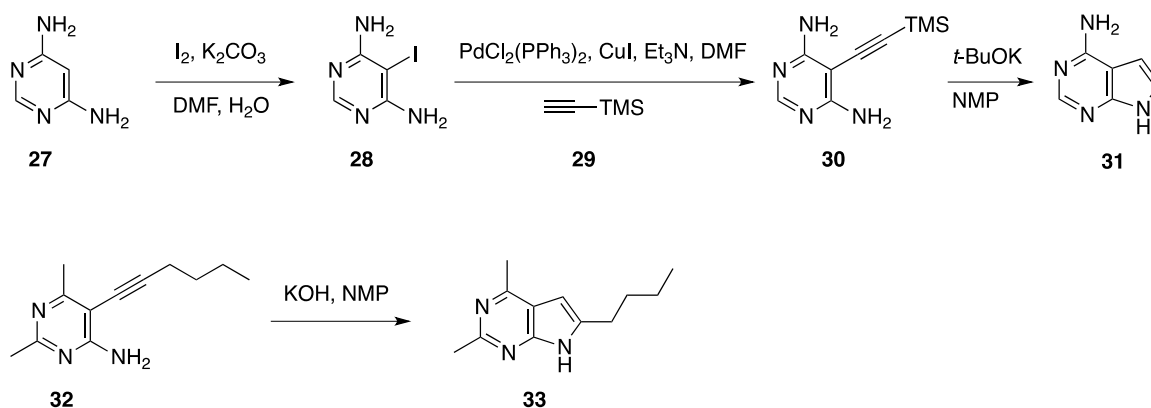
The direct-cyclization strategy is subject to a structural limitation: the 2-position of the pyrimidine must be occupied by a group able to donate a lone pair of electrons. For pyrrolo[2,3-*d*]pyrimidines without an electron-donating group at the 2-position, a *de novo* synthesis of the pyrimidine with a functionalized 5-position is usually chosen (**Scheme 3**). The cyanoethyl acetate **12** cyclizes with amidine **13** or thiourea **16** to afford pyrimidines **14** and **17**, which lead to the desired products **15** and **19**.^{124, 125}

Scheme 4 Synthesis of the 6-substituted pyrrolo[2,3-*d*]pyrimidine



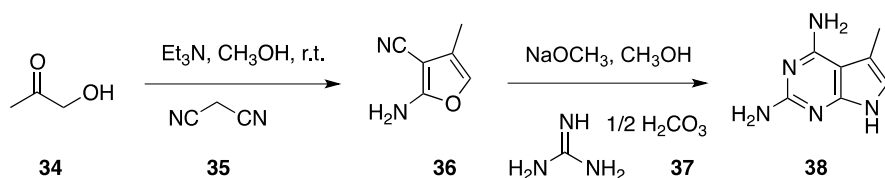
Replacing the acetal **12** with a ketone affords to the 6-substituted analogs of **15** and **19** (**Scheme 4**).¹²⁶

Scheme 5 Pd coupling followed by the 5-*endo*-dig cyclization



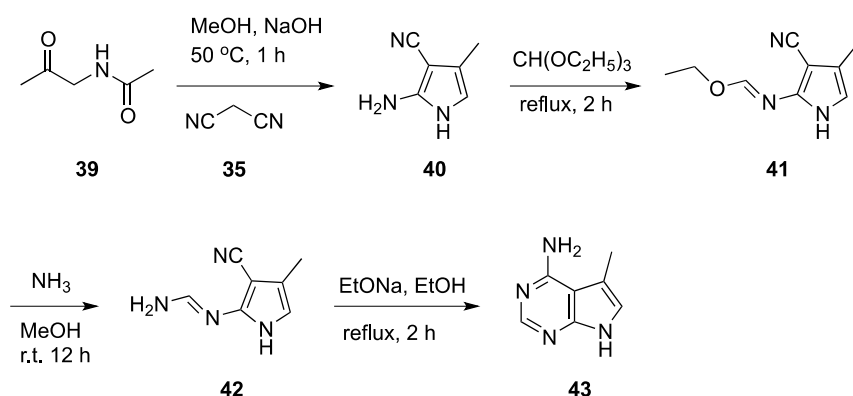
Palladium catalyzed coupling reactions provided direct methods to functionalize the pyrimidine as the precursor for the pyrrolo[2,3-*d*]pyrimidine. A good demonstration of this idea is the concise synthesis of **31** (Scheme 5), which would be otherwise be synthesized through **19**.¹²⁷ Replacing the TMS (Scheme 5) with other groups in the last 5-*endo*-dig cyclization step would give 6-substituted pyrrolo[2,3-*d*]pyrimidines such as **33**.¹²⁸

Scheme 6 Synthesis of the 5-methyl-pyrrolo[2,3-*d*]pyrimidine



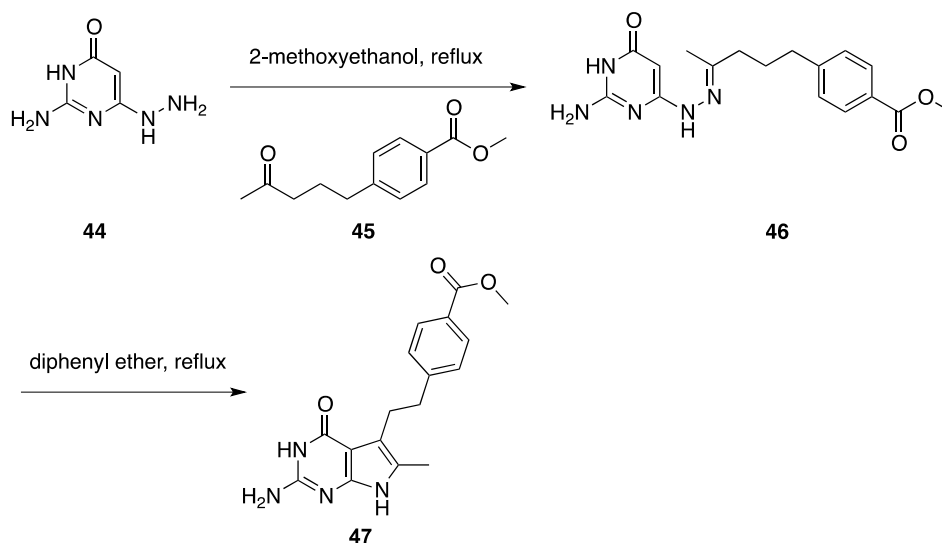
Synthetic approaches other than “cyclization from pyrimidine” have also been applied for shorter reaction schemes. A good example is the synthesis of the 5-methyl-2,4-diamino-pyrrolo[2,3-*d*]pyrimidine **38** (Scheme 6).¹²⁹ In this route, the meta-stable furan **29** ring opened upon the attacking of the guanidine **37**, followed by a rearrangement to afford the pyrrolo[2,3-*d*]pyrimidine **38**. An alternative method would be to obtain the 4-oxo compound **5** first, followed by its conversion to **38** in a two-step amination process.

Scheme 7 Cyclization of the appropriate pyrrole



Cyclization starting with the appropriated pyrrole is another viable option for synthesizing pyrrolo[2,3-*d*]pyrimidines, especially when the desired substituents on the final compounds are easily introduced in the pyrrole ring as illustrated in **Scheme 7**.¹³⁰

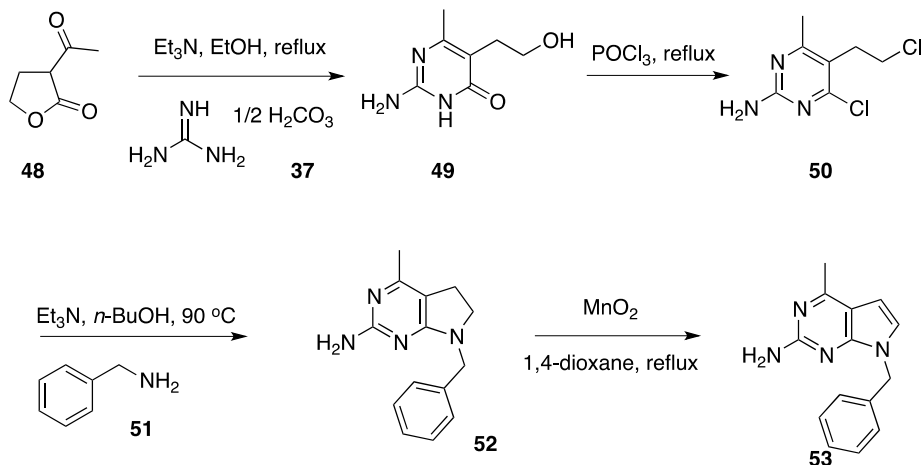
Scheme 8 The Fischer Indole synthesis of the 5,6-disubstituted pyrrolo[2,3-*d*]pyrimidine



The Fischer indole synthesis has also been utilized in the synthesis of pyrrolo[2,3-*d*]pyrimidines. This method is particularly efficient for 5,6-disubstitured systems (**Scheme 8**), using the appropriate pyrimidine hydrazine and a suitable ketone.¹³¹

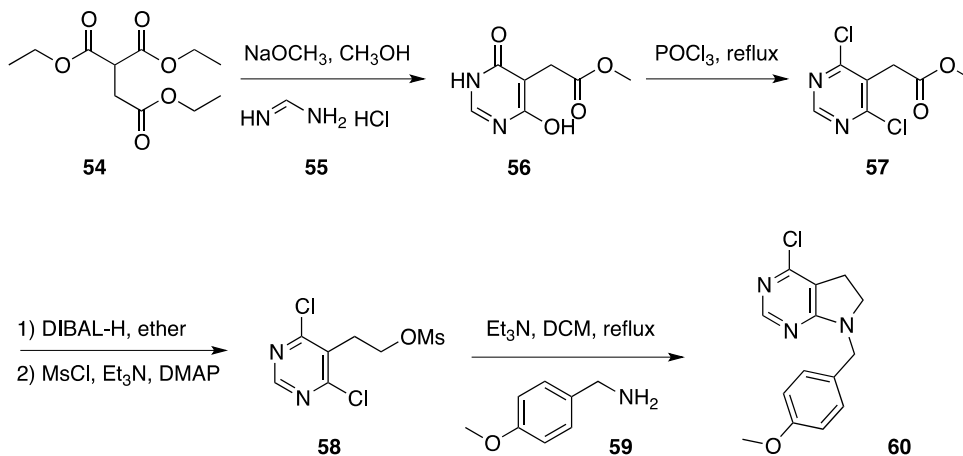
2) Synthesis of the 6,7-dihydro-pyrrolo[2,3-*d*]pyrimidines

Scheme 9 6,7-dihydro-pyrrolo[2,3-*d*]pyrimidine as the intermediate



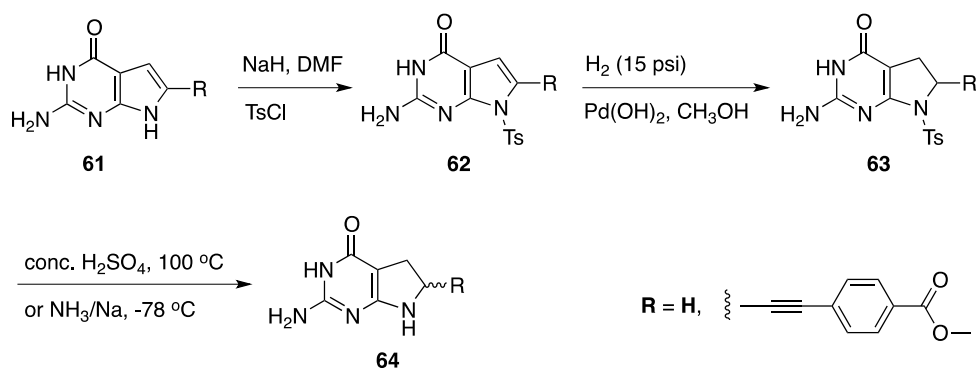
There are reports in the literature for the use of 5,6-dihydro-pyrrolo[2,3-*d*]pyrimidines as the precursor for some synthetically challenging pyrrolo[2,3-*d*]pyrimidines. An application of this strategy is the synthesis of 4-methyl-pyrrolo[2,3-*d*]pyrimidines (Scheme 9), when aromatization of the 5,6-dihydro precursor affords the pyrrolo[2,3-*d*]pyrimidine.¹³¹

Scheme 10 Synthesis of 4-chloro-6,7-dihydro-pyrrolo[2,3-*d*]pyrimidine



The patent literature uses a similar approach (**Scheme 10**), which could be used to functionalize the 4- and 5-positions with appropriate precursors.¹³²

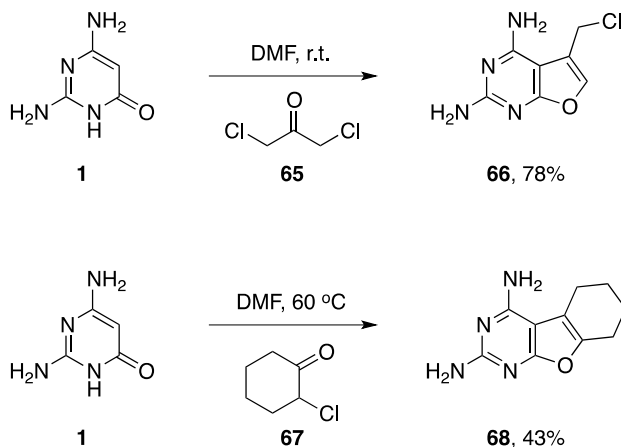
Scheme 11 Reductive hydrogenation of pyrrolo[2,3-*d*]pyrimidines



To synthesize the 5,6-dihydropyrrolo[2,3-*d*]pyrimidines, if the synthesis of the corresponding pyrrolo[2,3-*d*]pyrimidine is easier, a direct reduction of the pyrrole ring would be the optimal choice. However, for the hydrogenation reaction to succeed, it normally requires a strong electron-withdrawing group such as tosyl or acetyl at the N7-position (**Scheme 11**).¹³³

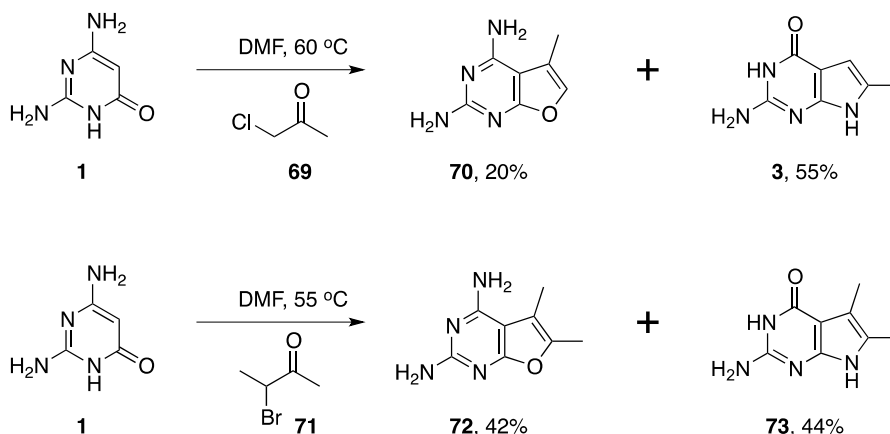
3) Synthesis of furo[2,3-*d*]pyrimidines

Scheme 12 Direct cyclization to the furo[2,3-*d*]pyrimidines



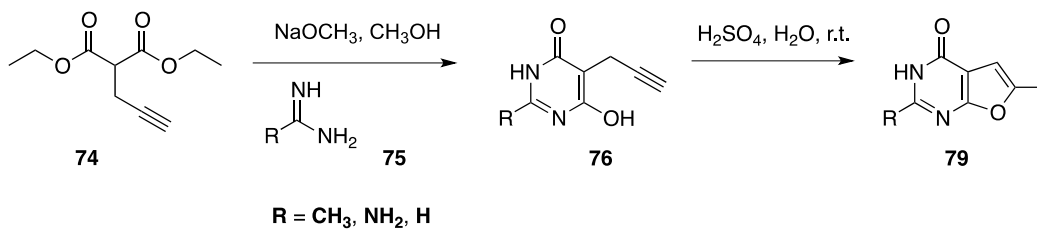
The general strategy for the synthesis of furo[2,3-*d*]pyrimidines share a lot in common with those for the pyrrolo[2,3-*d*]pyrimidine. The bicyclic ring could be built from either substituted pyrimidines or from the furans. The direct cyclization of the 2-amino-6-oxopyrimidines and α -haloketones affords furo[2,3-*d*]pyrimidines exclusively under certain conditions (Scheme 12).¹³⁴

Scheme 13 Competition between the formation of furo- and pyrrolo[2,3-*d*]pyrimidine



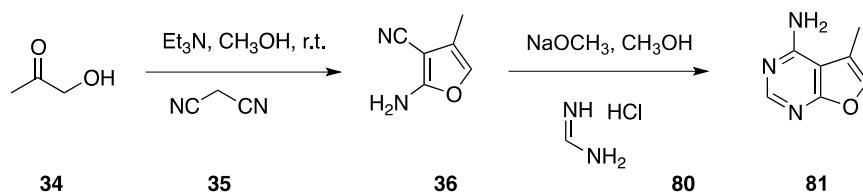
However, this reaction frequently suffers from the competing reaction that leads to the formation of pyrrolo[2,3-*d*]pyrimidines (**Scheme 13**).¹³⁴

Scheme 14 Synthesis of 2-substituted furo[2,3-*d*]pyrimidines



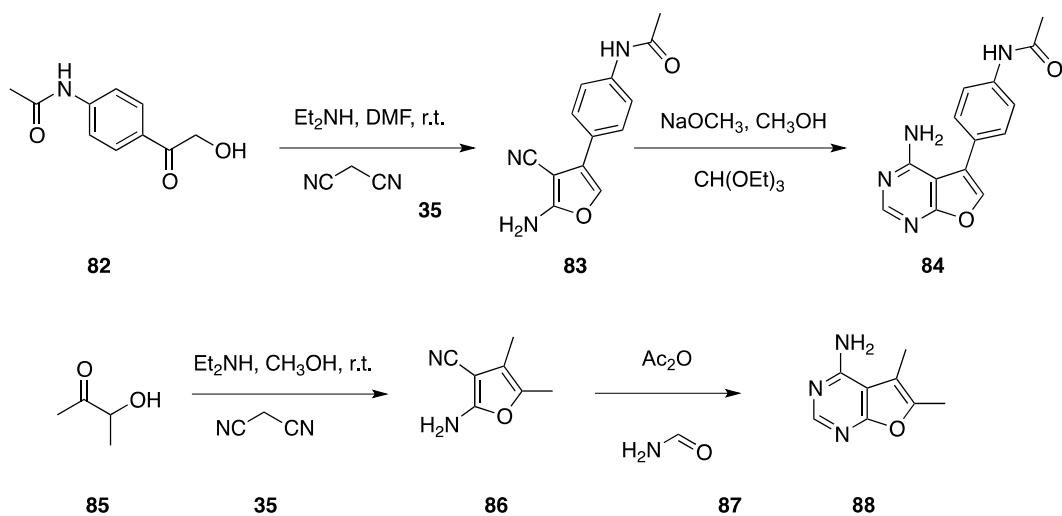
A *de novo* synthesis of the pyrimidine precursors followed by a 5-*endo*-dig cyclization provides access to various 2-substituted furo[2,3-*d*]pyrimidines (**Scheme 14**).¹³⁵

Scheme 15 Cyclization from furan



Cyclization from the furan is also a feasible method for the synthesis of the furo[2,3-*d*]pyrimidines. As mentioned above, the furan ring tends to rearrange and form pyrrolo[2,3-*d*]pyrimidines under certain conditions, as shown in **Scheme 6**. However, careful selection of the cyclization partner leads to furo[2,3-*d*]pyrimidines (**Scheme 15**).¹³⁵

Scheme 16 Cyclization from substituted furans



Phenyl-substituted or tetra-substituted furans tend to be more stable and are more commonly used as precursors for the synthesis of furo[2,3-*d*]pyrimidines (Scheme 16).¹³⁵⁻¹³⁷

III. STATEMENT OF THE PROBLEM

1) Microtubule-binding agents

1.1) Drawbacks of current microtubule-binding agents

The unparalleled broad-range anticancer potency has afforded the microtubule-binding agents unprecedented success among cancer chemotherapeutic drugs. The “anti-microtubule arsenal” is still expanding – the introduction of eribulin and vinflunine (**Figure 14**) in 2010 demonstrates the continuing momentum in the search of new agents this area.¹³⁸

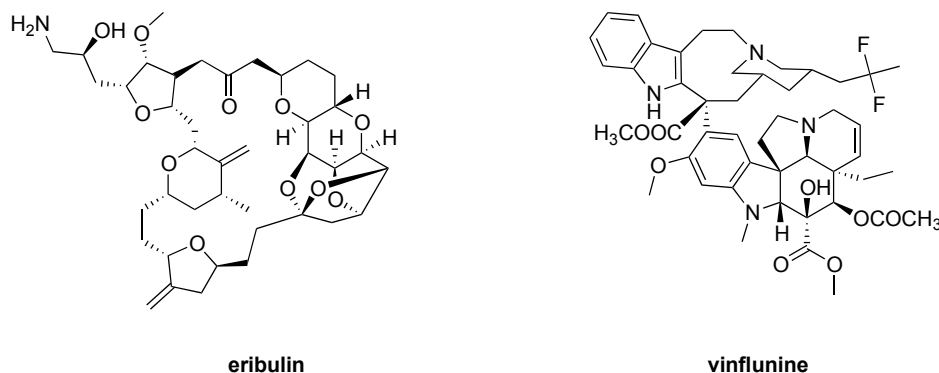


Figure 14 Structures of eribulin and vinflunine

Eribulin, a synthetic analog of the marine natural product halichondrin B, was approved for metastatic breast cancer (MBC) that is resistant to taxanes.¹³⁹ Vinflunine is a semisynthetic vinca alkaloid with higher antitumor activity, lower neurotoxicity and less Pgp-mediated resistance than its vinca predecessors.^{140, 141} It was approved for urothelial tract carcinoma that is resistance to platinum-containing regimen. Both the

recent new approvals and the ongoing clinical trials indicate the momentum for these agents is driven by the drawbacks of current microtubule-binding agents in clinic.

One of the major drawbacks is the development of multidrug resistance (MDR), against which most microtubule-binding agents are ineffective.^{2,9} Overexpression of Pgp has been reported in the clinical setting in a number of cancer types, particularly following chemotherapy.^{142, 143} In addition, Pgp expression has been linked with poor response to chemotherapy and could be a prognostic indicator in certain cancers.^{144, 145} However, combining Pgp inhibitors with chemotherapeutic agents in the clinic has been unsuccessful.⁵⁵ These findings indicate that novel microtubule-binding agents that are not substrates for Pgp would be likely to overcome this type of resistance and are actively sought.

In addition to Pgp, overexpression of the β III-tubulin is another clinically relevant resistance mechanism to the microtubule-binding agents.^{2, 9} The involvement of β III-tubulin in taxane and vinca alkaloid resistances in non-small-cell lung cancer, breast and ovarian cancer is firmly supported by clinical evidences.^{59, 60} However, resistances mediated by the β III-tubulin were not usually seen among the colchicine-site-binding agents.^{2, 9} In cell studies, the potency loss of the colchicine-site-binding agents due to β III-tubulin expression was moderate.⁵⁴ This encouraging finding highlights the critical importance of developing novel colchicine-site-binding agents to overcome β III-tubulin-associated cancer resistances.

The advantages of developing colchicine-site-binding agents such as combretastatin A (CA) are not limited to overcoming β III-tubulin-associated resistances, they are also

unique as potent vascular disrupting agents.³²⁻³⁵ In addition, synergistic effects of microtubule-binding agents that act at different sites on the microtubule are well established *in vitro* and *in vivo* and such combinations are actively undergoing clinical developments.^{25, 42-44} To date, no colchicine-site-binding agent has been approved by FDA as an anticancer agent except for a rare form of thyroid cancer. The benefits of combining combretastatin A-4 phosphate (CA-4-P) and paclitaxel are being evaluated in clinical trials.¹⁴⁶ Additional novel colchicine-site-binding agents are anticipated to open up more opportunities for monotherapy as well as synergistic combination chemotherapy protocols.

All the clinically used microtubule-binding agents are derived from natural products. With very few exceptions, economical synthetic methods for these drugs are still evasive and their production still relies on precursors from natural sources. In one extreme case, the process for the commercial production of eribulin involves 62 steps!¹³⁸ Thus the economic benefit offered by fully synthetic small-molecule microtubule-binding agents is significant.

Another non-trivial problem of the currently used microtubule-binding agents, particularly the taxanes, is their poor physical properties, especially poor water solubility.¹⁴⁷ Special formulations based on cremophor were developed for the administration of paclitaxel and ixabepilone.¹⁴⁷ However, these formulations come with a high risk of hypersensitivity reactions and long administration time. Enormous efforts have been committed in modifying the structures of these large molecules to enhance water solubility. Thus the development of water-soluble microtubule-binding agents is highly desirable.

1.2) Discovery of lead compounds

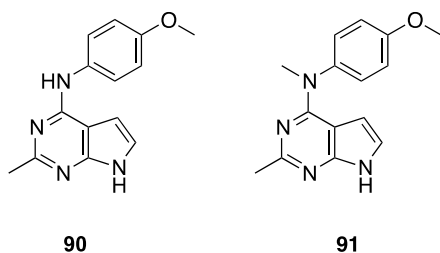


Figure 15 Lead compounds 90 and 91

The discovery of water-soluble small-molecule microtubule-binding agents in the present work was somewhat serendipitous. Compounds **90** and **91** (Figure 15), both readily convertible to the water-soluble hydrochloride salts, were designed as RTK inhibitors to explore the SAR of the pyrrolo[2,3-*d*]pyrimidine scaffold. The biological evaluation of several RTK-overexpressing cancer cell lines showed poor RTK inhibitory activities of the two compounds. Unexpectedly, when **91** was tested in the preclinical screening program of the National Cancer Institute in its 60-cancer-cell-line panel, it was found to inhibit the proliferation of most of the cancer cell lines with a GI₅₀ of less than 500 nM.⁵⁴

To determine the mechanism of action of **91**, a COMPARE analysis based on the 60-cancer-cell-line panel data was performed.^{148, 149} Among compounds with known mechanisms, vincristine sulfate has the closest Pearson's correlation coefficient with **91**. The other compounds in the ranking were vinblastine sulfate and maytansine. All these compounds are microtubule-binding agents, which suggested that **91** would most likely be an antimitotic agent as well.

In order to confirm that **91** was indeed a microtubule binding agent, a series of microtubule related assays were performed.⁵⁴ One of the results showed that **91** caused a dramatic reorganization of the interphase microtubule network, which was similar to the effects of colchicine and CA-4-P. In the cell cycle distribution assays, **91** was observed to effect the same G₂-M phase arrest as the paclitaxel.

The EC₅₀ for **91** in the microtubule depolymerization assay was 5.8 μM and it inhibited the proliferation of MDA-MB-435 cancer cells at an IC₅₀ of 183 nM.⁵⁴ In contrast, **90** failed to show any meaningful activities in any of the assays.

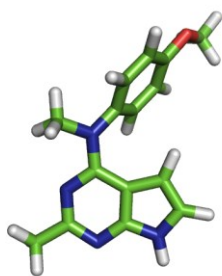
What made **91** an excellent lead compound for further development was its impressive activities against both Pgp- and βIII-tubulin-overexpressing cancer cell lines. Unlike paclitaxel, **91** maintains most of its potency against Pgp-overexpressing cell lines and showed slightly better activities against βIII-tubulin-expressing cancer cell lines.⁵⁴

For analog optimization centered on **91**, it was of paramount importance to determine the binding site of **91** on tubulin. In the competitive binding assay, **91** was observed to displace 70% of the [³H]colchicine at a concentration of 5 μM. In association with other evidences, it was confirmed that **91** was a colchicine-site binding agent

1.3) Hypothesis on the influence of conformation over the biological activities

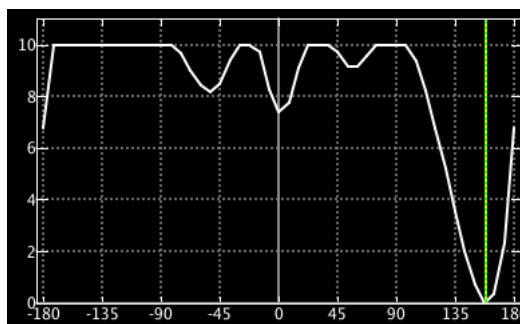
The discovery of **91** was an inspiration to extensively explore the SAR of this class of compounds as microtubule-binding agents. Prior to this work, there was no report on pyrrolo[2,3-*d*]pyrimidine-based colchicine-site binding agents. Co-crystal structure between similar structures and tubulin was also absent. However, the vast differences in activities between **90** and **91** in contrast with their minor structural divergence conveyed important information about the SAR.

A)

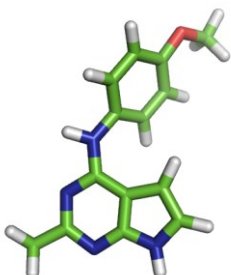


91

B)

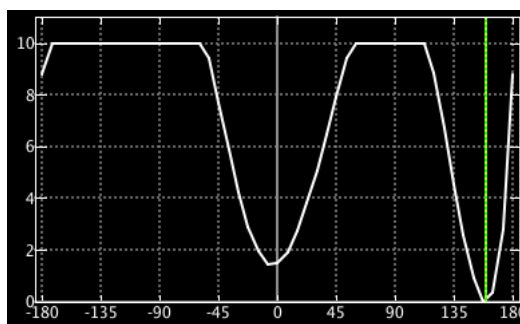


C)

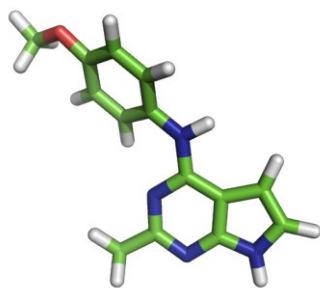


90

D)



E)



90

Figure 16 A) The lowest-energy conformation of **91**; B) plot of energy vs. dihedral angle between pyrrolo[2,3-*d*]pyrimidine and aniline in **91**; C) the lowest-energy conformation of **90**; D) plot of energy vs. dihedral angle between pyrrolo[2,3-*d*]pyrimidine and aniline in **90**; E) next-lowest-energy conformation of **90**. Units: energy in kcal/mol; green line in the plot indicates the current dihedral angle. Plot generated with MOE 2011.10; figure generated with Pymol 1.5.

The lowest-energy conformations of **90** and **91** are very similar, with the dihedral angles between the pyrrolo[2,3-*d*]pyrimidine and aniline of 159.14° and 158.68°, respectively (A – D, **Figure 16**). This conformation is dominant in **91** with a difference of over -7.5 kcal/mol. over the next lowest-energy conformation (B, **Figure 16**). However, preference of the same level is not available in **90** (D, **Figure 16**). In fact, the energy difference between the lowest- and next-lowest-conformations for **90** (E, **Figure 16**) is hardly over 1.5 kcal/mol.

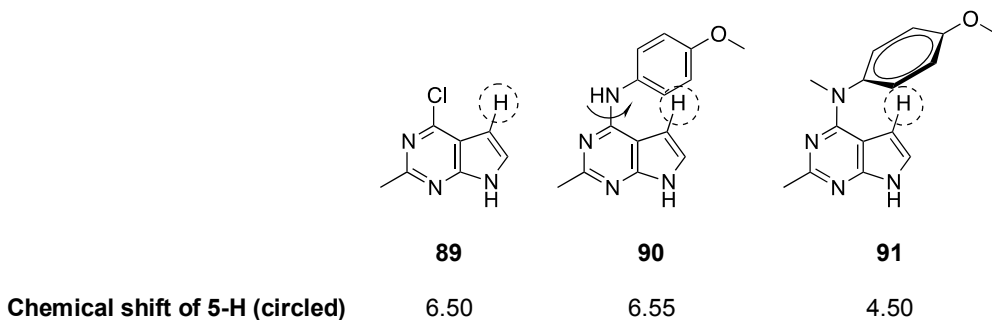


Figure 17 ¹HNMR chemical shift of the 5-H proton in **90** and **91**

This conformational preference was confirmed in ^1H NMR (**Figure 17**). For **90**, the chemical shift of 5-H proton in ^1H NMR was comparable to the 4-chloro-pyrrolo[2,3-*d*]pyrimidine **89**. However, in **91**, the chemical shift for the same proton was considerably lower. This phenomenon was consistent with the existence of the dominant conformation, which covered the 5-H in the shielding cone of the aniline phenyl ring.

The dominance of the lowest-energy conformation in **91** can only be explained with the presence of the *N*-methyl, which is the only difference between the structures of **90** and **91**.

This finding in conjunction with the differences in activities led us to propose a working hypothesis on the conformation and biological activity: the lowest conformation of 91 (and 90) is at least close to the productive binding conformation of the compound at the colchicine-binding site. Under this hypothesis, “locking-in” the productive conformation should enhance the potency.

1.4) Testing of the hypothesis by molecular modeling

This hypothesis was initially tested in docking studies. The program Autodock Vina was selected after a few trials of available docking programs.¹⁵⁰ The 3.58 Å crystal structure of 2-mercapto-colchicine and tubulin (PDB: 1SA0) was used as the macromolecule. Pre-calculation including the addition of partial charges and polar hydrogen were performed on both macromolecule and ligand. The native ligand in the crystal structure was removed prior to docking. The search space was a 40×40×40 Å³ grid box covering the entire colchicine-binding site. The starting conformation of the ligand was randomly generated and the number of the random seeds was over 10 billion. A total of nine lowest-energy binding conformations were returned.

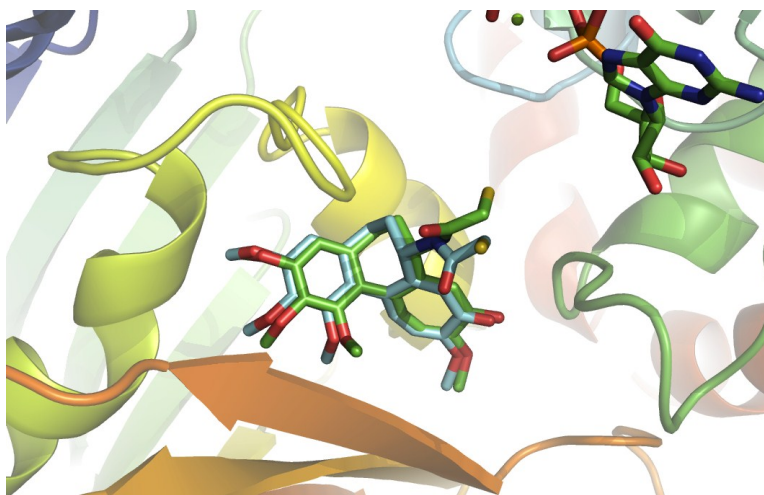


Figure 18 Superimposition of the docked conformation of 2-mercapto-colchicine (green) and the original crystal structure conformation (cyan); PDB: 1SA0; figure generated with Pymol 1.5.

A re-dock run was performed to validate of the program and the settings (**Figure 18**). Autodock Vina successfully reproduced the crystal structure conformation with RMSD less than 1 Å, which was lower than the general accepted cut-off limit of 2 Å.¹⁵¹

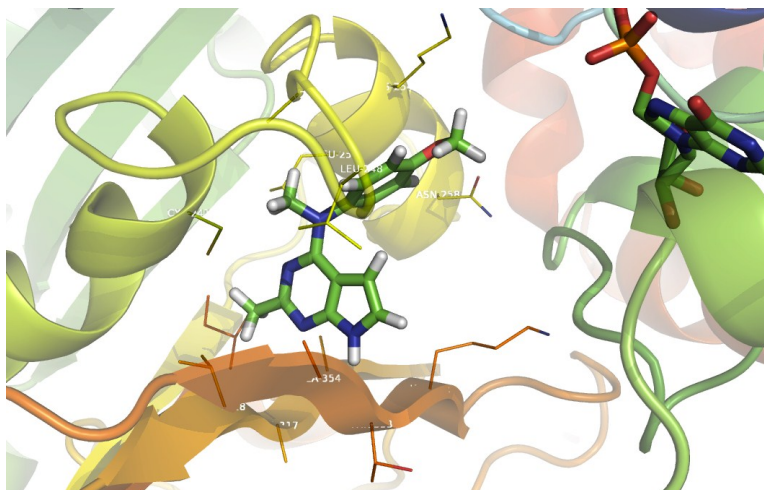


Figure 19 Lowest-energy conformation of **91** in the colchicine-binding site from the docked results; PDB: 1SA0; Autodock Vina; figure generated with Pymol 1.5.

The settings used in re-docking were repeated to dock **91** into the colchicine-binding site. The lowest-energy (-7.9 kcal/mol) conformation of **91** at colchicine-binding site was the same as the dominant conformation in solution (**Figure 19**). More importantly, all the nine top poses with binding energy in the range of -7.3 to -7.9 kcal/mol assumed highly similar conformations to the dominant one, though interactions with the binding site were different. These findings supported the hypothesis of the relationship between the conformation and activities.

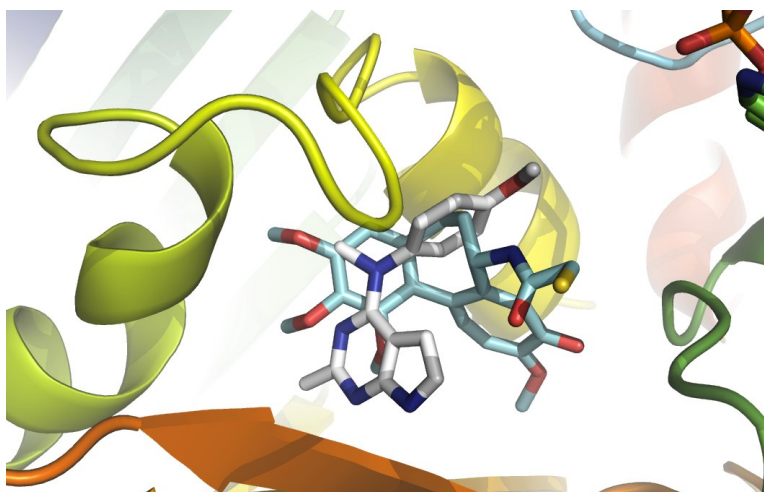
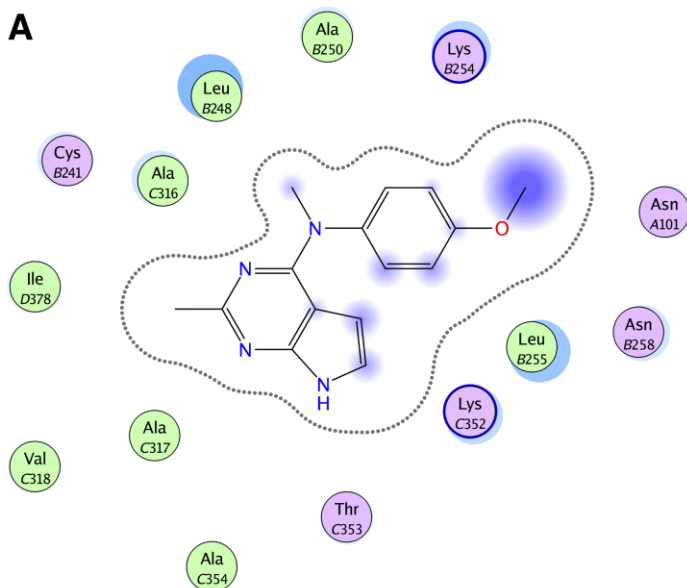


Figure 20 Overlap of **90** (white) and 2-mercapto-colchicine (**cyan**) at the colchicine-binding site

The colchicine site is able to hold structurally diverse compounds such as colchicine, combretastatin and 2-methoxyestradiol.^{1, 2} It is not surprising to see **90** would bind differently than colchicine at this relatively spacious site (**Figure 20**). From the docking result, **90** and colchicine were partly overlapped and some interactions with the binding pocket were shared.



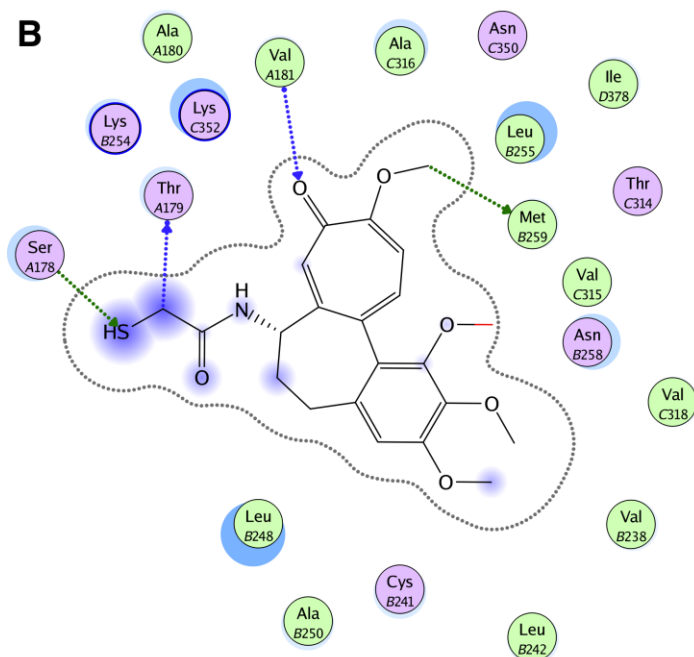


Figure 21 Interaction plots of A) 91 and B) 2-mercapto-colchicine at the colchicine-binding site generated by MOE 2011.10

The interactions of **91** (docked) and the binding pocket were mainly hydrophobic in nature (**Figure 21, A**). Notably, the *N*-methyl was enclosed in a “hydrophobic envelope” formed by Ala250, Leu248 and Ala316. The 2-methyl also pointed to the adjacent hydrophobic region surrounded by Ala316, Ile378, Val318 and Ala317. A potential hydrogen bond was formed between the N7-H and the backbone of Thr353. The 4-methoxy on phenyl was in the vicinity of Lys254, Asn101 and Asn258. However, no explicit hydrogen bond was identified.

Some of the hydrophobic bindings in **91** were also seen in colchicine, such as the interactions with Ala250, Leu248, Ala316, Ile378 and Val318 (**Figure 21, B**). In addition, colchicine formed four hydrogen bonds with the binding pocket (illustrated with arrows

in **Figure 21, B**). These hydrogen bonds might contribute to the higher potency of colchicine than **91**.

1.5) Analogs designed based on the hypothesis

Compounds of **Series I – VI** in the present work form parts of an extensive exploration of SAR of the pyrrolo[2,3-*d*]pyrimidines as colchicine-site binding agents.

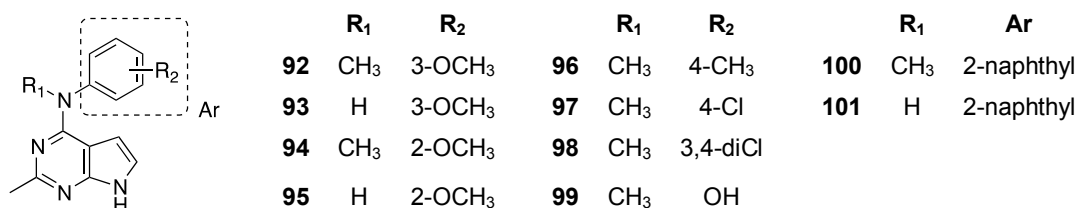


Figure 22 Series I

Compounds in **Series I (Figure 22)** serve two purposes. The first is to confirm the importance of *N*-methyl to the activities. This purpose is fulfilled by **92 – 95** and **100 – 101**. The second purpose is to observe the effect of different substitutions on the aniline to biological activity. A comparison between **91** and compounds in **Series I** would provide information on the preference of electron-donating or electron-withdrawing groups on the phenyl ring to biological activity. Since the 4-methoxy of **91** resided in a polar region of the colchicine-binding site in the docked pose, an analog with a hydrogen bond donor (**99**) is expected to be active if the docking prediction is accurate.

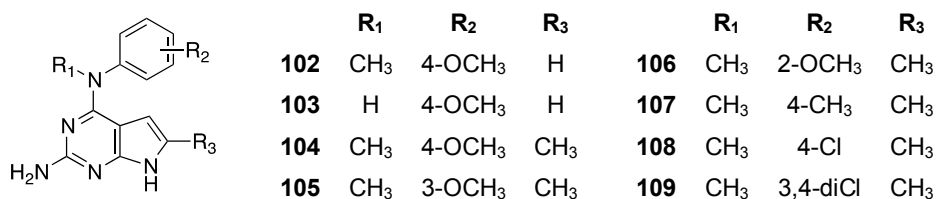


Figure 23 Series II

Series II also has two aims (**Figure 23**). The first is to observe the effect on biological activity when the 2-methyl is replaced with 2-amino (**102 – 103**). The second aim is to also check whether the involvement of a 6-methyl on the pyrrolo[2,3-*d*]pyrimidine scaffold (**104 – 109**) is conducive to activity. The 6-methyl was found to enhance the potency in structurally similar 4-*N*-methyl-aniline-substituted cyclopenta[*d*]pyrimidines.^{54, 61}

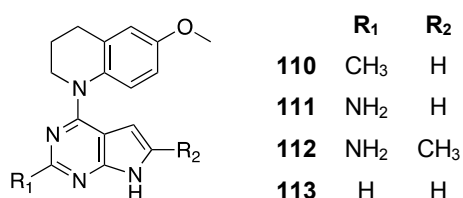


Figure 24 Series III

Series III takes a step beyond the anilines to incorporate the bicyclic 6-methoxy-tetrahydroquinoline onto the 4-position of the pyrrolo[2,3-*d*]pyrimidines with different 2- and 6-substitutions. This design focuses on the conformation of the phenyl ring. Compared to the *N*-methylaniline, the tetrahydroquinoline provides more restriction on the conformation of the phenyl ring, as the rotation around the N-phenyl bond is eliminated, thus affording a much more rigid structure than **91** but still maintaining the phenyl and alkyl substitutions on the *N4* as in **91**.

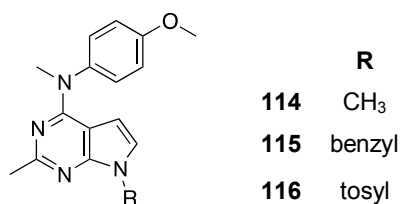


Figure 25 Series IV

Series IV aims at an exploration of substitutions at the N7 position (**Figure 25**). Three compounds including two non-polar groups (methyl and benzyl) and one polar group (tosyl) are included. This design is based on the docking of **91**, which suggests that the N7 substituent would extend into a region of the colchicine-binding site that consists of both non-polar residues (Ala317, Ala354) and a polar residue (Thr353).

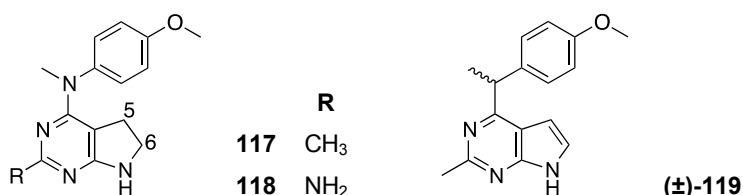


Figure 26 Series V

Series V contains two variations on the parent compound **91** (**Figure 26**). The first variation is the reduction of the 5,6-bond of **91**. Structurally, 5,6-dihydro-pyrrolo[2,3-*d*]pyrimidines **117** and **118** are akin to the cyclopenta[*d*]pyrimidine analogs, which are highly active colchicine-site binding agents.^{54, 61} Reduction of the 5,6-bond also allows less delocalization of the pyrrole N7-lone pair thus makes it somewhat more available for H-bonding acceptor and allows some flexibility in the 5,6-bond and 6,7-bond regions.

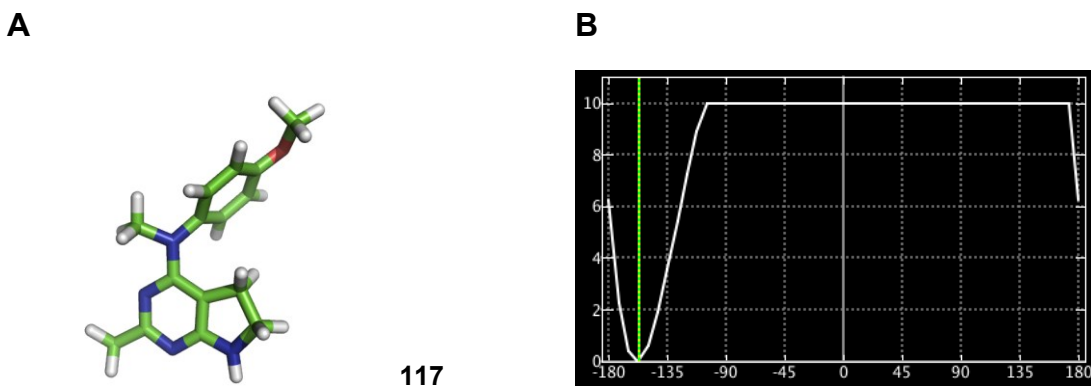


Figure 27 A) The lowest-energy conformation of **117**; B) plot of energy vs. dihedral angle between the pyrimidine and aniline in **117**. Energy in kcal/mol; green line in the plot indicates the current dihedral angle. Plot generated with MOE 2011.10; figure generated with Pymol 1.5.

In addition, the lowest-energy conformation is even more dominant in **117** compared with **91**, as no other competing energy minimum exists (**Figure 27**). An increase in the activity of **117** would support the modeling hypothesis that the lowest-energy conformation as in **91** is indeed the conformation at the colchicine-binding site.

The second variation in **Series V** is the isosteric replacement of the important *N4* with a carbon in **119** (**Figure 26**). If the H-bond acceptor attributes of the *N4* in **91** are critical to activity, **119** is expected to be inactive. In addition, the conformational energy profile of **119** (plot not shown) is similar to **90**, which is unable to maintain the productive binding conformation.

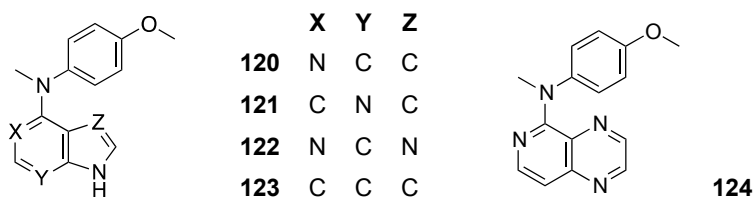


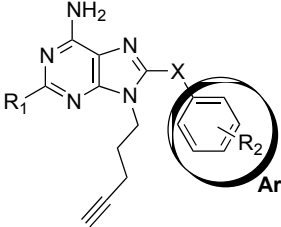
Figure 28 Series VI

Series VI aims to determine the contributions of the nitrogen atoms on the pyrimidine and pyrrole rings of **91** to biological activity (**Figure 28**). Five structurally related nitrogen-containing heterocyclic scaffolds are used to replace the pyrrolo[2,3-*d*]pyrimidine ring in **120 – 124**.

2) HSP90 inhibitors

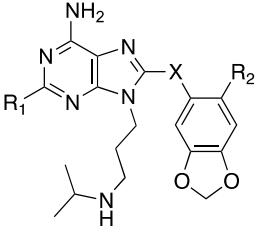
2.1) Reported HSP90 inhibitors based on 8-arylsulfanyl-adenine

Table 2 HSP90 inhibitors based on 8-arylsulfanyl-adenine with alkyne chain¹⁵²



	R ₁	X	Ar	EC ₅₀ Hsp90α (μM)	IC ₅₀ HER2 (μM)	IC ₅₀ SKBr3 (μM)
125	H	S	2-Br-4,5-(OCH ₂ O)-Ph	0.03 ± 0.005	0.3 ± 0.05	0.2 ± 0.01
126	H	S	2-Cl-3,4,5-(OCH ₃) ₃ -Ph	0.18 ± 0.05	9.1 ± 2.6	9.4 ± 0.9
127	F	S	2-Cl-3,4,5-(OCH ₃) ₃ -Ph	0.12 ± 0.03	1.3 ± 0.4	1.8 ± 0.2
PU24FCI	F	CH ₂	2-Cl-3,4,5-(OCH ₃) ₃ -Ph	0.17 ± 0.09	1.5 ± 0.5	1.8 ± 0.4

Table 3 HSP90 inhibitors based on 8-arylsulfanyl-adenine with amine chain¹⁵³



	R ₁	X	R ₂	EC ₅₀ Hsp90α (μM)	IC ₅₀ HER2 (μM)	IC ₅₀ SKBr3 (μM)
PU-H71	H	S	I	0.0161 ± 0.001	0.05 ± 0.006	0.05 ± 0.005
PU-H64	H	S	Br	0.0388 ± 0.003	0.205 ± 0.015	0.142 ± 0.022
128	F	CH ₂	I	0.0504 ± 0.004	0.08 ± 0.01	0.045 ± 0.006

Our initial interest in developing pyrrolo[2,3-*d*]pyrimidine-based HSP90 inhibitors was inspired in part by a series of 8-arylsulfanyl-adenine derivatives reported in 2005 (**Table 2**).¹⁵² These compounds showed moderate to good activities in both HSP90 inhibition assay and cell-based assay. Reports on a series of compounds with improved potency and water solubility followed shortly (**Table 3**).¹⁵³ Among them, **PU-H71** has progressed to Phase I clinical trial as an intravenous drug for both metastatic solid tumors and lymphoma (ClinicalTrials.gov Identifier: NCT01393509 and NCT01581541).

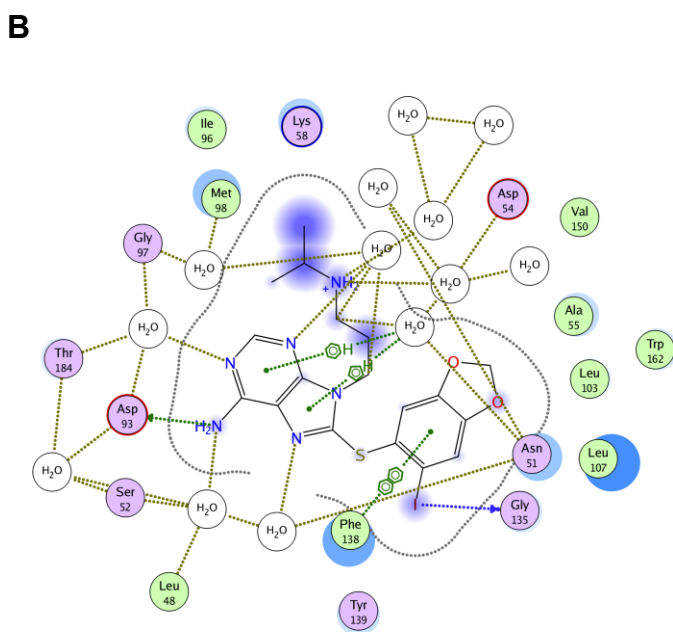
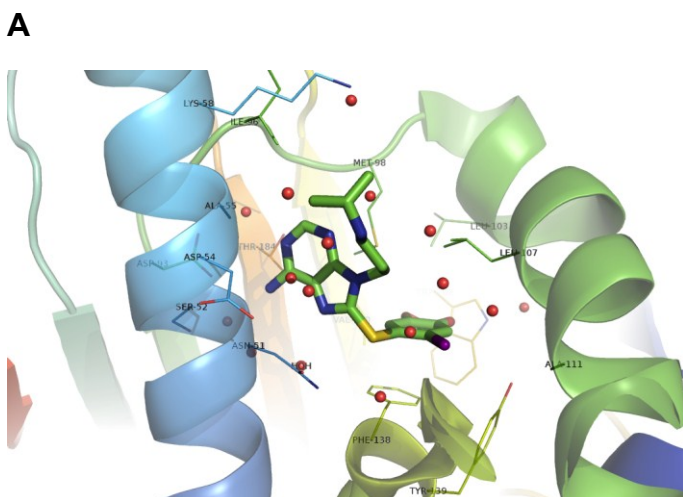


Figure 29 A) Crystal structure of PU-H71 (PDB: 2FWZ) at the ATP site of HSP90; B) Interaction plot of PU-H71 based on the crystal structure. Figure generated with Pymol 1.5; plot generated with MOE 2011.10.

The compounds in **Table 2** and **3** all bind to the ATP site on the N-domain of HSP90.^{152, 153} The ATP site is highly hydrated and the binding of **PU-H71** was facilitated by a complex network of water molecules (**Figure 29**). In addition to interactions present in ATP binding, **PU-H71** established additional bindings with the pocket through the benzodioxole ring. These added interactions have proved to be critical for the

activities.¹⁵²⁻¹⁵⁴ A comparison of the crystal structures of HSP90 with **PU24FC1** (PDB: 1UYF), **PU-H64** (PDB: 2FWY) and **PU-H71** (PDB: 2FWZ) indicated that these analogs shared a common binding mode.¹⁵⁴

Similar to purine in structure, pyrrolo[2,3-*d*]pyrimidines have been successfully designed by Gangjee et al.¹⁵⁵⁻¹⁶³ as receptor tyrosine kinase (RTK) inhibitors. It was reasoned that the pyrrolo[2,3-*d*]pyrimidine scaffolds could bind to the ATP-site in productive conformations and achieve certain degrees of selectivity with appropriate substitutions. For HSP90 inhibitors, the pyrrolo[2,3-*d*]pyrimidine scaffold provided functionalization opportunities at the 5-position, which was not possible with the aromatic N7 in 8-arylsulfanyl-adenine compounds.

2.2) Designed pyrrolo[2,3-*d*]pyrimidine analogs

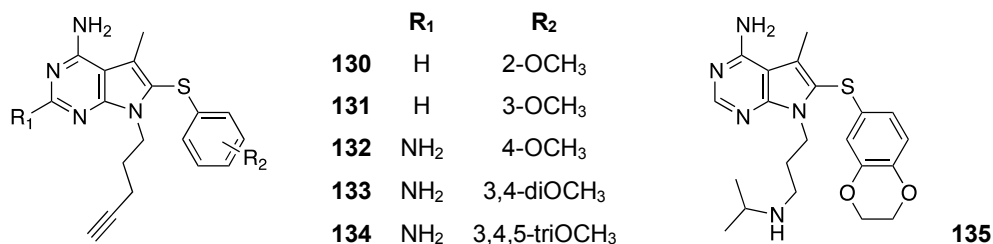
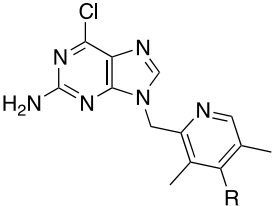


Figure 30 Series VII

Several pyrrolo[2,3-*d*]pyrimidine analogs based on the 8-arylsulfanyl-adenines were designed and synthesized in an effort to explore the SAR. Variations were attempted at the various positions of the pyrrolo[2,3-*d*]pyrimidine and the phenyl ring. Compounds included in the present work are listed in **Figure 30**. Among them, the 2-amino analogs were designed to establish additional hydrogen bonds with the help of a near-by water molecule present in the crystal structure and the 5-methyl was intended to displace the non-structural water molecule¹⁵⁴ for potential energy gains (**Figure 29**).

2.3) Reported HSP90 inhibitors based on 2-amino-6-halopurine

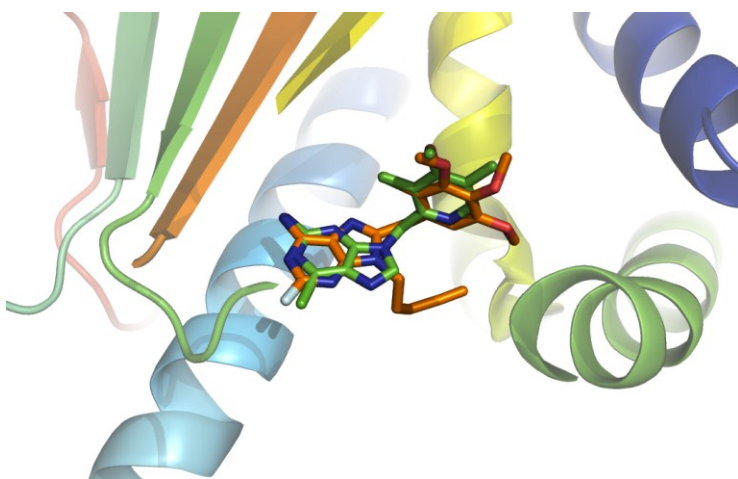
Table 4 BIIB021 and its activities (μM)

	R	IC ₅₀ HER2	IC ₅₀ rHSP90 binding	IC ₅₀ MCF7	Tumor growth inhibition
	17-AAG	*	0.007	0.7	0.01
PU24FCI	**	1.7	6.0	1.2	
129	H	0.02	0.9	0.5	83% @ 60 mg/kg
BIIB021	OCH ₃	0.03	0.9	0.15	87% @ 125 mg/kg

*structure in **Table 1, Part I**; ** structure in **Table 2**

The report of **PU-H71** and **PU24FCI** led an industrial group to the discovery of the 2-amino-6-halopurine-based HSP90 inhibitors (**Table 4**).¹⁰¹ This series has shown improved activities over the prior 8-arylsulfanyl-adenines. One of the most active compounds, **BIIB021**, has completed Phase II clinical trials as an orally active drug (ClinicalTrials.gov Identifier: NCT01004081 and NCT00618319).

A



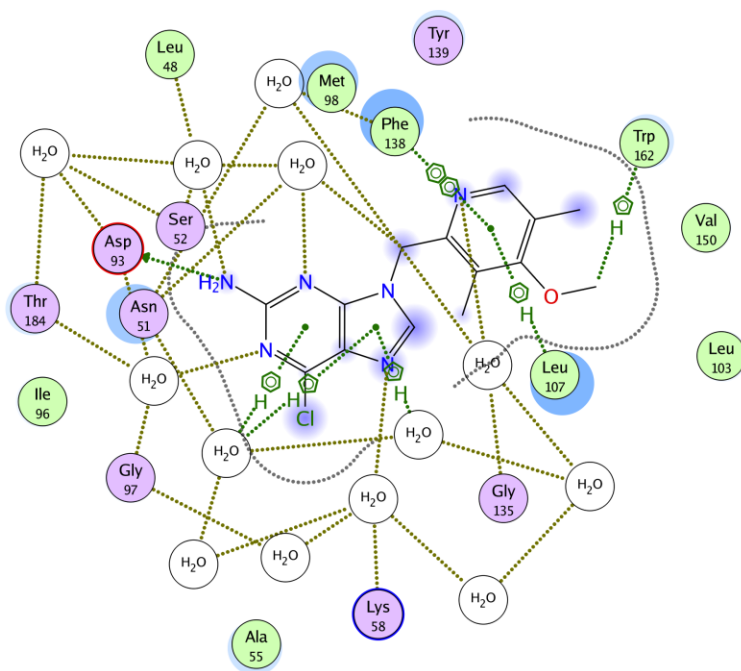
B

Figure 31 A) Superimposition view of BIIB021 (green) and PU24FCI (orange) in crystal structure; B) Interaction plot of BIIB021 based on the crystal structure (PDB: 3QDD). Figure generated with Pymol 1.5; plot generated with MOE 2011.10.

Despite different substitution patterns, the binding poses of BIIB021 (PDB: 3QDD⁹²) and PU24FCI (PDB: 1UYF¹⁶⁴) overlapped well when the two crystal structures were superimposed (Figure 31, A). Common interactions with the binding pocket were found in both inhibitors (Figure 31, B). Two hydrogen bonds were shared, including one between Asp93 and amino on both purines, four hydrogen bonds between the pocket and four nitrogen atoms of the purine mediated by structural water molecules. The π - π interactions between Phe138 and aromatic substitutions (phenyl in PU24FCI and pyridine in BIIB021) were also observed in both inhibitors.

2.4) Designed pyrrolo[2,3-*d*]pyrimidine analogs

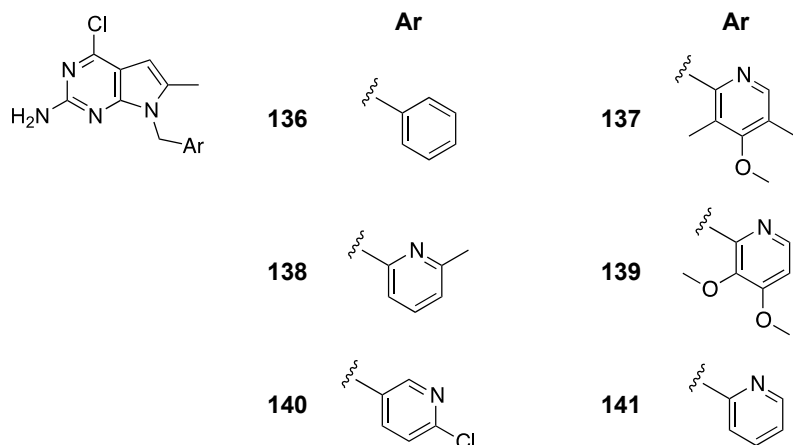


Figure 32 Series VIII

Similar to **Series VII**, **Series VIII** intends to explore the possibility of increasing the activities through the replacement of the purine scaffold with pyrrolo[2,3-*d*]pyrimidine (**Figure 32**). In addition to variations on the N7 substitution, the 6-methyl was designed for hydrophobic interaction with Leu107. In the crystal structure (PDB: 3QDD), a water molecule was found near-by (**Figure 31**). However, this water molecule was believed to be a non-structural water molecule, since it was not consistently seen in other crystal structures of HSP90.

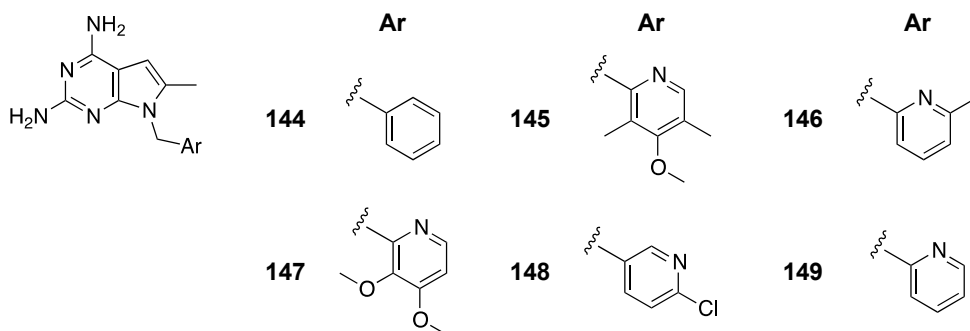


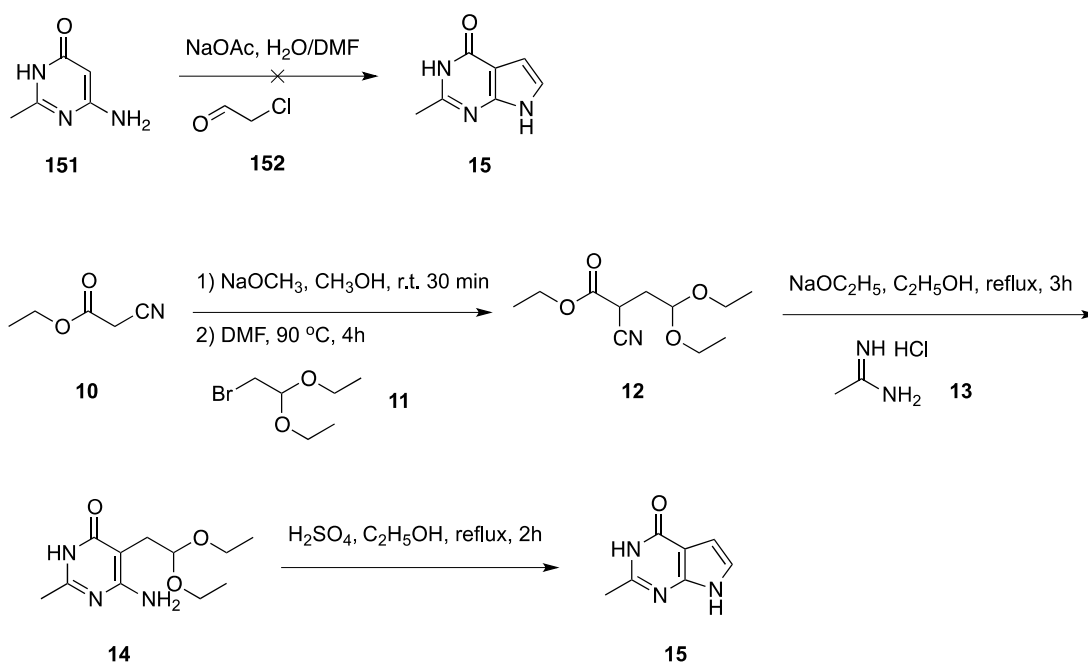
Figure 33 Series IX

The chlorine of **BIIB021** was surrounded by a group of water molecules in the crystal structure (**Figure 31, B**). It was reasoned that replacing this chlorine with an amino should be conducive to activity. **Series IX** serves this purpose by substituting the 4-chloro on the pyrrolo[2,3-*d*]pyrimidine in **Series VIII** with an amino moiety (**Figure 33**).

IV. CHEMICAL DISCUSSION

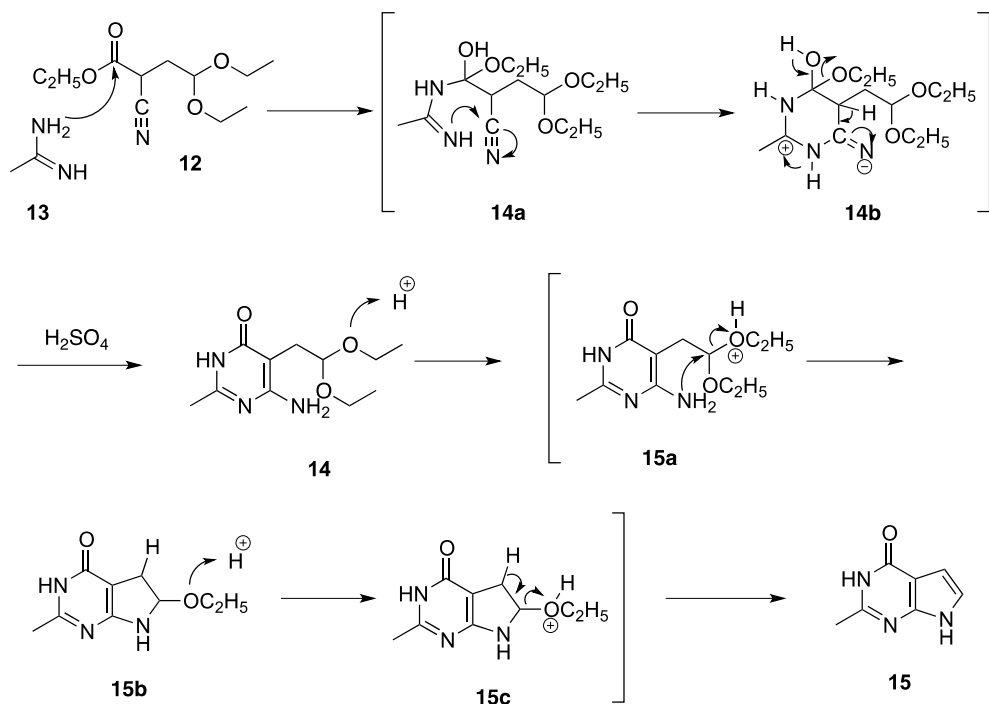
1) Synthesis of *N*-(4-methoxyphenyl)-2-dimethyl-7*H*-pyrrolo[2,3-*d*]pyrimidin-4-amines (90 – 98)

Scheme 17 Synthesis of the 2-methyl-3*H*-pyrrolo[2,3-*d*]pyrimidin-4(7*H*)-one (15)



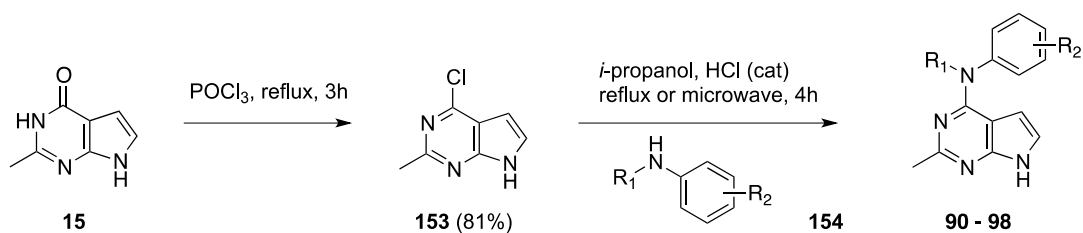
Direct cyclization to afford 2-methyl-pyrrolo[2,3-*d*]pyrimidine **15** (Scheme 17) by 6-amino-2-methylpyrimidin-4(3*H*)-one (**151**) and chloroacetaldehyde (**152**) was unsuccessful. A reported three-step process through the pyrimidine intermediate **14** afforded the desired scaffold **15**,¹²⁴ which was confirmed by ¹HNMR. The isolated yield over three steps was over 30%.

Scheme 18 Proposed mechanism for cyclization leading to 15



To help understand the two-step formation of the pyrrolo[2,3-*d*]pyrimidine **15** from **12** (Scheme 18), a stepwise mechanism is proposed.

Scheme 19 Synthesis of target compounds 90 – 98



	R ₁	R ₂		R ₁	R ₂
90	CH ₃	4-OCH ₃	95	H	2-OCH ₃
91	H	4-OCH ₃	96	CH ₃	4-CH ₃
92	CH ₃	3-OCH ₃	97	CH ₃	4-Cl
93	H	3-OCH ₃	98	CH ₃	3,4-diCl
94	CH ₃	2-OCH ₃			

The target compounds **90** – **98** were synthesized from the 2-methyl-pyrrolo[2,3-*d*]pyrimidine **15** in two steps (**Scheme 19**). Chlorination of **15** with phosphorus oxychloride gave the 4-chloro-pyrrolo[2,3-*d*]pyrimidine **153** in 81% yield. The following S_NAr displacements of 4-chloro with various anilines (**154**) afforded **90** – **98** (55 – 80% isolated). Catalytic amount of acid promoted the reaction. Anhydrous conditions were required to suppress hydrolysis of the 4-chloro in **153** to the 4-oxo **15**.

Both reflux in an oil bath and microwave irradiation (130 °C) were tried for the S_NAr displacement step. However, the outcomes of the reactions were close though the microwave reaction also requires a sealed vessel, which is advantageous in retaining the HCl gas. In terms of yield, the properties of the substrates had a greater impact, as *N*-methyl-anilines gave higher yields than anilines and anilines with electron-donating groups gave higher yields than those with electron-withdrawing groups. Complete disappearance of starting material was normally observed and the isolated yields ranged from 50% to 80%.

2) Synthesis of 4-(methyl(2-methyl-7*H*-pyrrolo[2,3-*d*]pyrimidin-4-yl)amino)phenol (**99**)

Scheme 20 Synthesis of target compound **99**

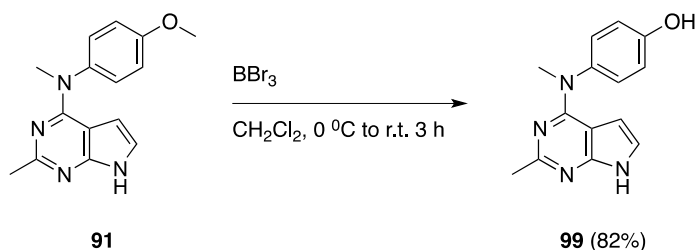


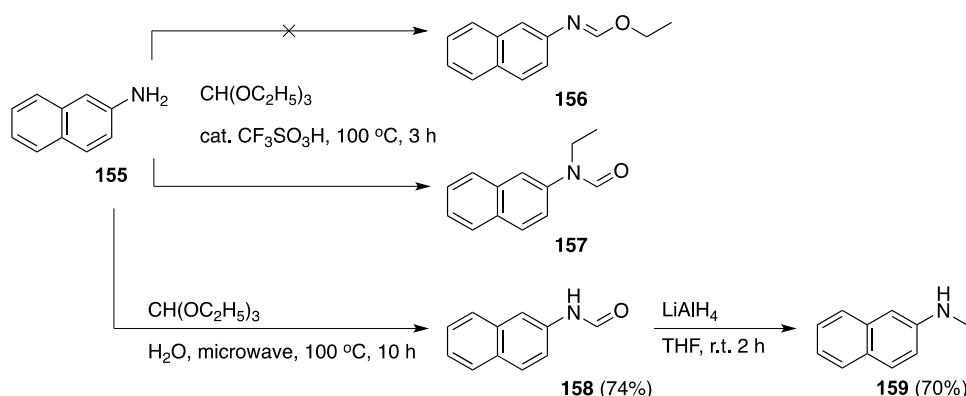
Table 5 Conditions attempted for de-methylation of the phenyl ether

Reagents	Conditions	Result
CF ₃ SO ₃ H	120 °C, 6 h	Sole product 99 formed, less than 50% isolated
(CH ₃) ₃ SiI, CHCl ₃	Microwave 120 °C, 6 h	Most of 90 recovered, minor new product identified
BBr ₃ , CH ₂ Cl ₂	0 °C to r.t. 4 h	Sole product 99 isolated

Instead of the same S_NAr displacement with the *O*-protected-*N*-methyl-aniline, a direct demethylation of **91** was carried out for the synthesis of **99** (Scheme 21). Three common reagents were tried (Table 5). Treatment with a strong Bronsted acid (CF₃SO₃H) generated the sole product **99**. However, the isolated yield was low, possibly due to the degradation under strong acidic condition. Milder conditions using iodotrimethylsilane did not effect any conversion up to 6 hours. Only the strong Lewis acid BBr₃ (3 eq.) was able to cleave the methylether on the electron-rich phenyl ring and gave the phenol (**99**) in satisfactory yield (82%).

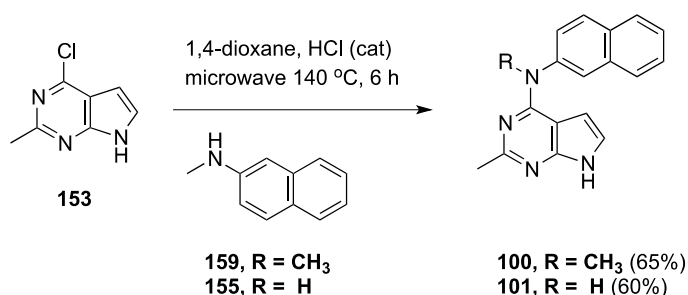
3) Synthesis of 2-methyl-*N*-(naphthalen-2-yl)-7*H*-pyrrolo[2,3-*d*]pyrimidin-4-amines (110 – 111)

Scheme 21 Synthesis of *N*-methylnaphthalen-2-amine (159)



Direct methylation of 2-amino-naphthalene **155** (Scheme 21) with iodomethane or dimethylsulfate, afforded mainly the N,N-dimethylated product. Reductive amination with formaldehyde was also expected to give the dimethylated amine. Using formic acid to generate the formamide with the amine under heating condition involves high hazardous risk. Using triethyl orthoformate as the surrogate of formaldehyde was supposed to produce the ethoxyimine **156**,¹⁶⁵ which could be reduced to monomethylated naphthalenamine **159**. However, treatment of the naphthalen-2-amine **155** with triethyl orthoformate and catalytic amount of strong acid afforded only the N-ethyl-formamide **157**, which was identified by ¹HNMR. Similar reaction was reported in literature,¹⁶⁶ while the mechanism was unclear. In the absence of acid, reaction between triethyl orthoformate and naphthalen-2-amine **155** in water under microwave irradiation¹⁶⁶ gave formamide **158** (74% isolated) as the sole product. Reduction of **158** by lithium aluminum hydride in short time afforded the monomethylated naphthalene-2-amine **159** (70%).

Scheme 22 Synthesis of target compounds 100 and 101

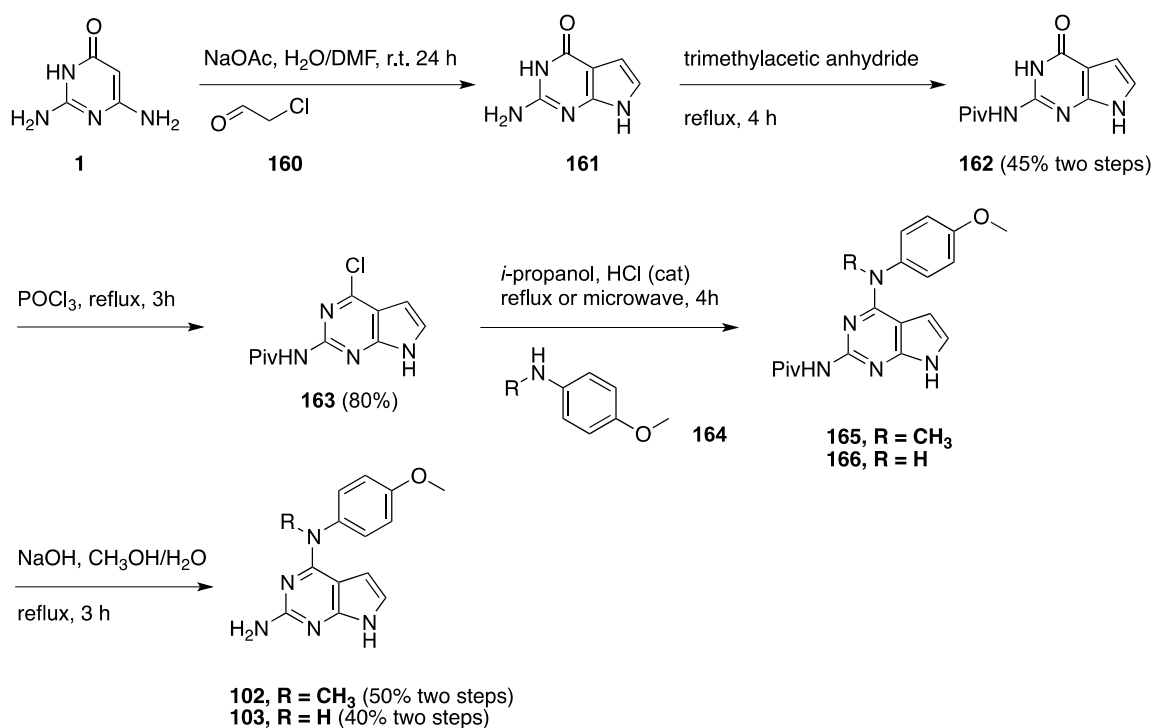


The S_NAr displacement of **153** with the naphthalen-2-amines **155** and **159** (Scheme 22) was performed in 1,4-dioxane at higher temperature in the microwave reactor (140 °C).

The yields were slightly lower than when carried out under reflux in isopropanol as for **90 – 98**.

4) Synthesis of *N*⁴-(4-methoxyphenyl)-7*H*-pyrrolo[2,3-*d*]pyrimidine-2,4-diamines (**102 – 103**)

Scheme 23 Synthesis of target compounds **102** and **103**

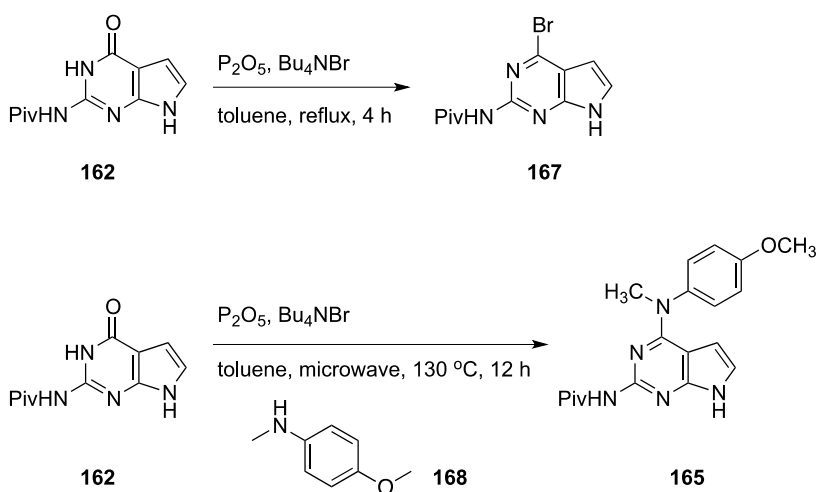


In contrast to 2-methyl-pyrrolo[2,3-*d*]pyrimidine **15**, the 2-amino-pyrrolo[2,3-*d*]pyrimidine **161** (Scheme 23) could be synthesized in a single step by cyclization of 2-amino-pyrimidine **1** with chloroacetaldehyde **161**. Variations of the reaction conditions were reported.¹¹³⁻¹¹⁵ The differences were mainly in temperature and solvents. Among the reactions attempted, the condition with DMF/H₂O 6:1 and room temperature 24 hours

gave the most reproducible result. The typical crude yield for **161** was about 70 to 80%. Other conditions included reflux in H₂O for five hours, under which the excess sodium acetate seemed to be detrimental to the yield.

A direct chlorination of **161** with phosphorus oxychloride was possible but suffered from low isolated yields (~30%). Further, the 2-amino-4-chloro-pyrrolo[2,3-*d*]pyrimidine formed was a poor reactant in the next S_NAr reaction with anilines. These problems were solved by adding the pivaloyl group to the 2-amino, which increased the solubility in organic solvents and decreased the electron density of the pyrimidine ring. The protected **162** was efficiently converted to the 4-bromo intermediate **163** and the following S_NAr reaction were performed under the same condition for 2-methyl-pyrrolo[2,3-*d*]pyrimidines. The removal of the pivaloyl group could be achieved in either basic (NaOH in methanol and water) or acidic (HCl in acetic acid) conditions.

Scheme 24 One-pot synthesis of **165** via 4-bromo-pyrrolo[2,3-*d*]pyrimidine



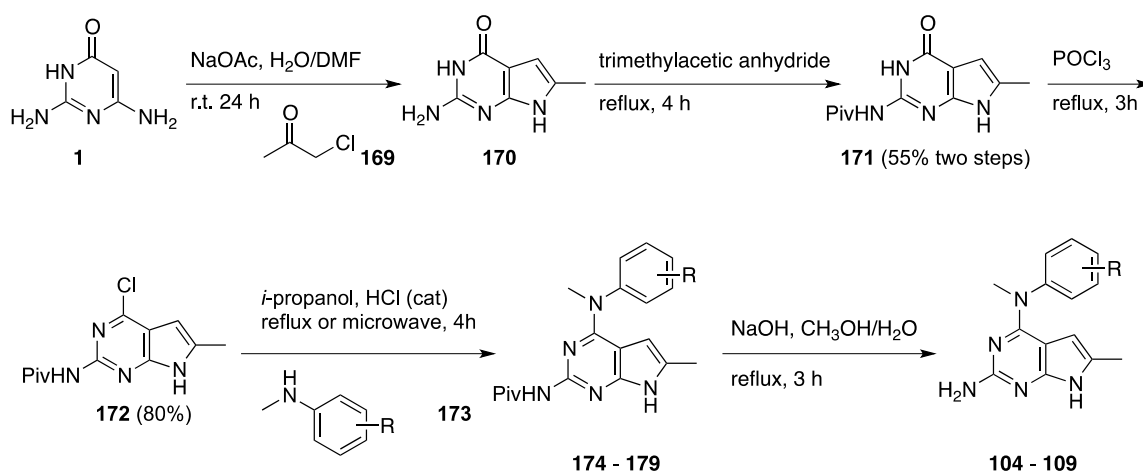
The synthesis of the more reactive 4-bromo-pyrrolo[2,3-*d*]pyrimidine **167** (Scheme 24) was also attempted. The obvious use of phosphorus oxybromide (POBr₃) was abandoned

due to the high chemical hazard involved. Alternatively, a combination of phosphorus pentoxide (dehydration reagent) and tetra-*n*-butylammonium bromide (anion source) in toluene at reflux was able to convert the 4-oxo-pyrrolo[2,3-*d*]pyrimidine **162** to the purported 4-bromo **167**. TLC monitoring indicated a roughly 60% yield in four hours. However, **167** was unstable and was completely hydrolyzed back to the starting **162** in the following aqueous workup.

To utilize the high reactivity of **167**, a one-pot procedure toward the 4-anilino-pyrrolo[2,3-*d*]pyrimidine **165** was next attempted (**Scheme 24**). In this case, a microwave reactor was used to ensure a strict anhydrous environment and high temperature. The target compound **165** was formed with an isolated yield around 40%.

5) Synthesis of *N*⁴,6-dimethyl-*N*⁴-phenyl-7*H*-pyrrolo[2,3-*d*]pyrimidine-2,4-diamines (104 – 109)

Scheme 25 Synthesis of target compounds 104 – 109

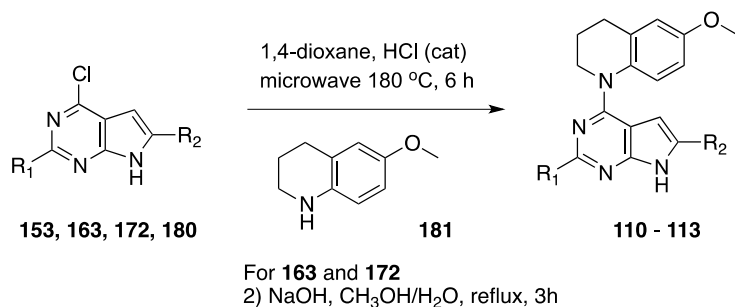


	R		R
174	4-OCH ₃	104	4-OCH ₃
175	3-OCH ₃	105	3-OCH ₃
176	2-OCH ₃	106	2-OCH ₃
177	4-CH ₃	107	4-CH ₃
178	4-Cl	108	4-Cl
179	3,4-diCl	109	3,4-diCl

The same sequence for the synthesis of **102** and **103** was applied to the 5-methyl analogs **104** – **109** without major modification (**Scheme 25**). The isolated yields of the last two steps (**172** to **104** – **109**) ranged from 40% to 65%.

6) Synthesis of 6-methoxy-1-(7H-pyrrolo[2,3-d]pyrimidin-4-yl)-1,2,3,4-tetrahydroquinolines (**110** – **113**)

Scheme 26 Synthesis of target compounds **110** – **113**



	R₁	R₂		R₁	R₂
153	CH ₃	H	110	CH ₃	H
163	PivNH	H	111	NH ₂	H
172	PivNH	CH ₃	112	NH ₂	CH ₃
180	H	H	113	H	H

Table 6 Experimented conditions for the reaction of **153** and **181**

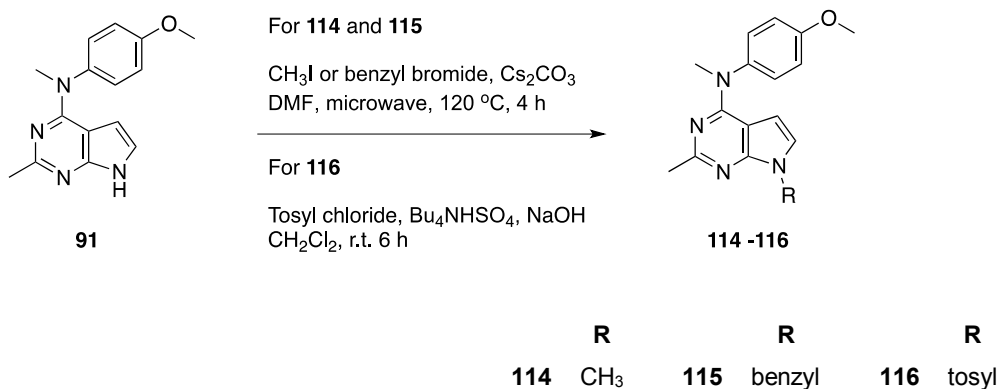
Solvent	Heat source	T °C	Acid	Result
isopropanol	oil bath	reflux	HCl (anhydrous)	Trace amount of product
isopropanol	Microwave	140 °C	HCl (anhydrous)	~ 20%
1,4-dioxane	Microwave	140 °C	HCl (anhydrous)	~ 20%
1,4-dioxane	Microwave	180 °C	HCl (anhydrous)	65% isolated
1,4-dioxane	Microwave	180 °C	CF ₃ COOH	~ 50%
1,4-dioxane	Microwave	180 °C	ZnCl ₂	~ 20%
DMF	Microwave	180 °C	HCl (anhydrous)	50% isolated

The S_NAr reactions of the 4-chloro-pyrrolo[2,3-*d*]pyrimidines were much more difficult and low-yielding when 6-methoxy-tetrahydroquinoline **181** (Scheme 26) was used as the nucleophile. A reproducible condition with isolated yield over 60% was established only after multiple trials. The factors including solvent, temperature and acid were investigated in the reaction of 2-methyl-4-chloro-pyrrolopyrimidine **153** and 6-methoxy-tetrahydroquinoline **181** (Table 6). Reaction times were fixed as six hours. The estimated yields were based on the observations of TLC.

Temperature was found to be the most important factor in this reaction (Table 6). The substitution of isopropanol with 1,4-dioxane was mainly for the control of the vapor pressure inside the microwave vial. DMF could achieve a similar yield (50% isolated), but 1,4-dioxane offered a more convenient workup. Interestingly, catalytic amounts of Lewis acid could also provide the same conversion, though the yield (~20%) with zinc chloride was low in this case. The methylphenyl ether remained intact in the presence of zinc chloride.

7) Synthesis of 7-substituted *N*-(4-methoxyphenyl)-*N*-methyl-7*H*-pyrrolo[2,3-*d*]pyrimidin-4-amines (114 – 116)

Scheme 27 Synthesis of target compounds 114 – 116



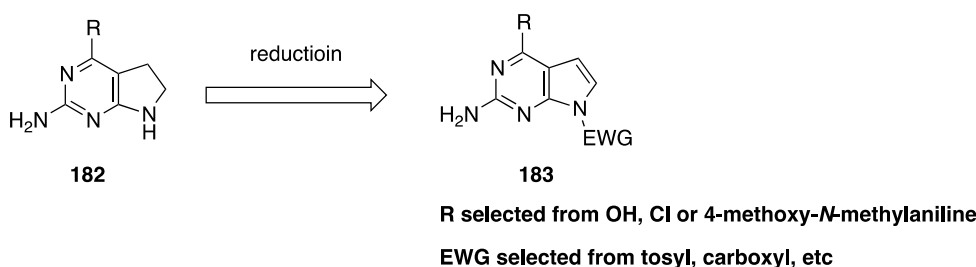
Sodium hydride is frequently used in electrophilic substitution at the N7 of the pyrrolo[2,3-*d*]pyrimidines. However, under such condition, excess quantities of highly toxic iodomethane were usually required for high yield. The polarity of the *N*-methyl analog **114** (Scheme 27) is close to its *N*-H precursor **91**, which makes the removal of the unreacted material very difficult. After multiple experiments, the combination of cesium carbonate and DMF in a sealed vial for four hours at 120 °C was found to be the optimal condition for both methylation and benzylation. It is noteworthy that the proper amount of DMF is critical for the outcome of the reaction. Excess solvent (over 10 times the weight of reactant) severely decreased the yield (lower than 20%) or gave no reaction at all.

The tosylation of N7 on the pyrrolo[2,3-*d*]pyrimidine was performed with sodium hydroxide as the base (Scheme 27). The room temperature reaction in methylene chloride

in the presence of the phase-transfer catalyst *n*-tetrabutylammonium hemisulfate afforded the N-tosyl analog **116** in better than 80% yield.

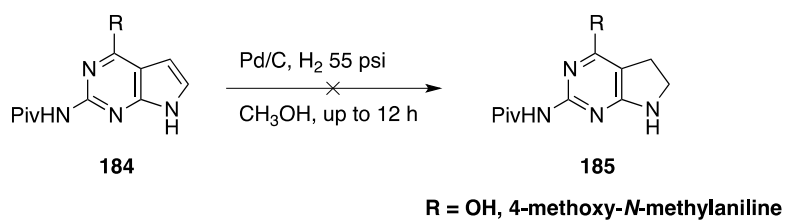
8) Synthesis of *N*⁴-(4-methoxyphenyl)-*N*⁴-methyl-6,7-dihydro-5*H*-pyrrolo[2,3-*d*]pyrimidine-2,4-diamine (**118**)

Scheme 28 The strategy toward the target compound **118**



The relatively quick access of the functionalized pyrrolo[2,3-*d*]pyrimidine **183** made direct reduction of the pyrrole ring a viable strategy for the synthesis of 5,6-dihydropyrrolo[2,3-*d*]pyrimidine **182** (Scheme 28). Successful application of this strategy has been reported for the synthesis of 6-substituted 5,6-dihydropyrrolo[2,3-*d*]pyrimidines.¹³³

Scheme 29 Hydrogenation without N-7 electron-withdrawing group



The direct palladium-catalyzed hydrogenation of the 5,6-bond on furo[2,3-*d*]pyrimidines was known (Gangjee et al. unpublished data). Although never reported, a direct hydrogenation of the pyrrolo[2,3-*d*]pyrimidines was attempted (**Scheme 29**). Both structures (R = OH or 4-methoxy-*N*-methylaniline) experimented remained intact after over night hydrogenation (55 psi) without any reduction.

Scheme 30 Hydrogenation in the presence of the 4-methoxy-*N*-methylaniline

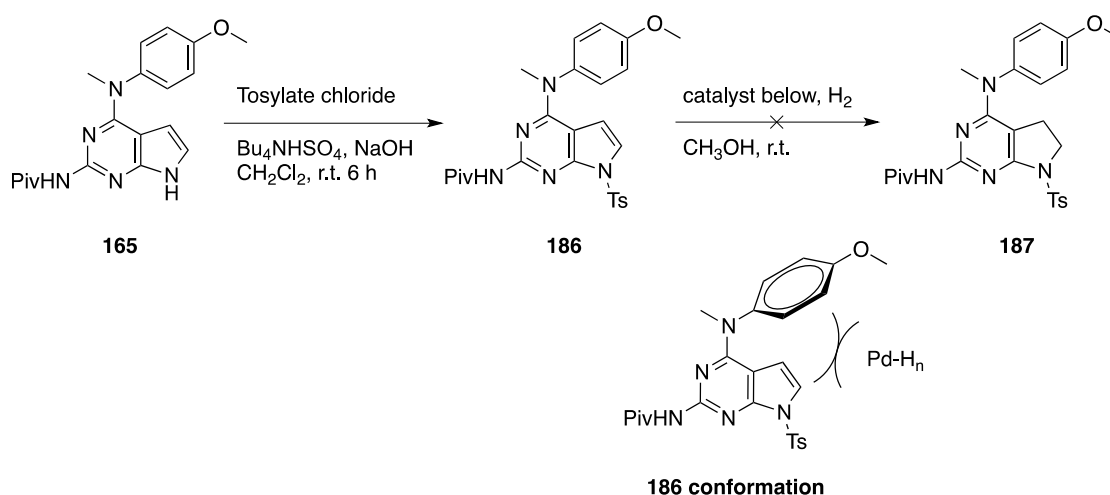


Table 7 Experimented hydrogenation conditions

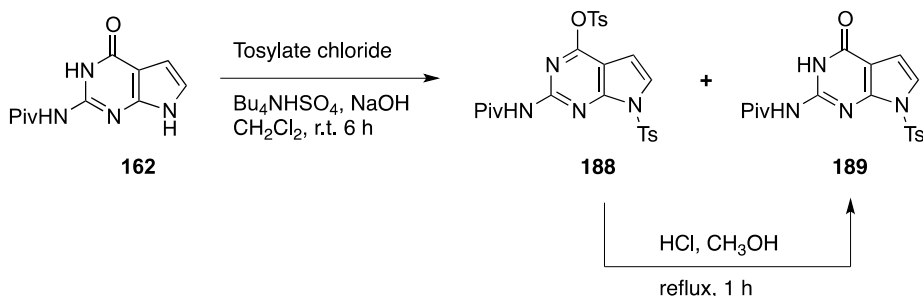
Catalyst	Conditions	Result
Pd(OH) ₂	15 – 55 psi, up to 12 h	No reaction
Pd/C	55 psi, up to 12 h	No reaction
PtO ₂	55 psi, up to 12 h	No reaction
Wilkinson's catalyst	15 – 55 psi, up to 12 h	No reaction

One of the shortest routes toward the target compound would be the hydrogenation on the N-tosyl analog of **165** (**Scheme 30**). The N-7 tosylation of pyrrolo[2,3-*d*]pyrimidines usually uses sodium hydride as the base.¹³³ However, in the conversion from **165** to **186**,

NaH/DMF combination did not afford a satisfactory yield (~50%). Instead, sodium hydroxide in tandem with a phase transfer catalyst (*n*-tetrabutylammonium hemisulfate) in dichloromethane gave a higher than 90% transformation and over 80% isolated yield.

The hydrogenation of N7 tosylated **186** was unsuccessful despite elevated hydrogen pressure or prolonged reaction time (**Table 7**). Switching the palladium catalyst to platinum was also in vain. The resistance to hydrogenation shown by **186** was likely due the dominance of its lowest-energy conformation in solution (“**186** conformation” in **Scheme 30**). A similar case was observed for **91** (discussed in **Part III**). In this conformation, the 4-methoxyphenyl effectively shielded the 5,6-double bond from the metal catalyst and rendered the reaction under room temperature impossible.

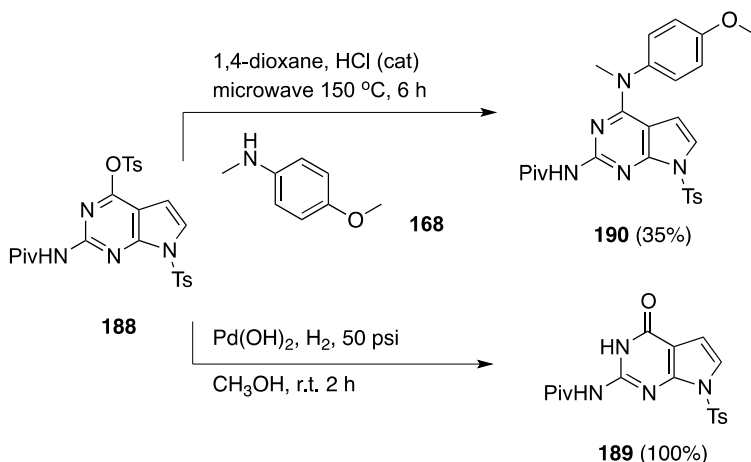
Scheme 31 Synthesis of N-7-tosylated pyrrolo[2,3-*d*]pyrimidines **189**



The tosylation of **162** took place at both the 4-oxo/hydroxyl and the N-7 position (**Scheme 31**). The formation of both products started almost simultaneously (observed on TLC), which made the adjustments on the reactant equivalent or addition sequence useless in controlling the reaction outcome. At the end of the reaction, **188** was the predominant product with the ratio of approximately 3:1 (**188:189**). Fortunately, it could be conveniently converted to the desired product **189** under acidic conditions. It was

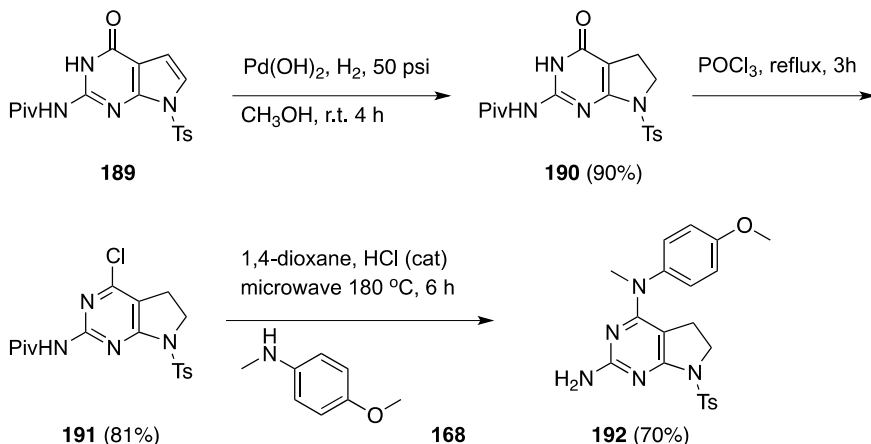
interesting to observe that the hydrolysis of O-tosyl proceeded more quickly in acidic conditions than in basic conditions (NaOH, CH₃OH, reflux).

Scheme 32 Reactions on *N,O*-distosyl-pyrrolo[2,3-*d*]pyrimidine **188**



The property of the O-tosyl as a leaving group prompted a S_NAr displacement with 4-methoxy-*N*-methylaniline **168** (Scheme 32). The reaction proceeded with relative low yield (~35%), comparing with higher than 70% isolated yield in reactions using the 4-chloro compounds. In addition, short duration (less than two hours) hydrogenation converted **188** to **189** quantitatively without 5,6-bond reduction.

Scheme 33 Synthesis of 5,6-dihydropyrrolo[2,3-*d*]pyrimidine **193**



The hydrogenation of **189** to **190** used a modified literature procedure (Scheme 33).¹³³ The increase of hydrogen pressure from 15 to 50 psi and four-hour duration resulted in an almost quantitative conversion. The chlorination of the reduced **190** by phosphorus oxychloride gave the same high yield as for other pyrrolopyrimidines. However, the S_NAr displacement of the reduced **191** was much more difficult than its aromatic counterpart. The harsher condition developed for the 6-methoxy-tetrahydroquinoline reactions were required to afford **192** in acceptable yield (60% isolated). Under this condition, the pivaloyl on the 2-amion was removed simultaneously. This observation highlights the influence of electron density on the reactivity of the aromatic rings in S_NAr reactions.

Scheme 34 Removal of the tosyl group from nitrogen

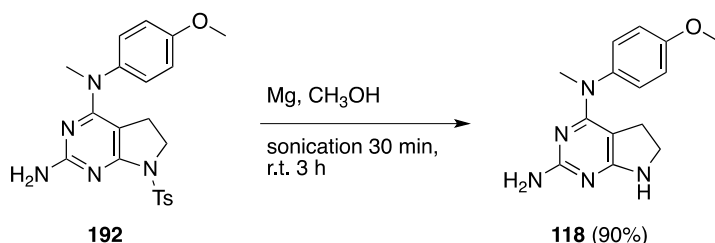


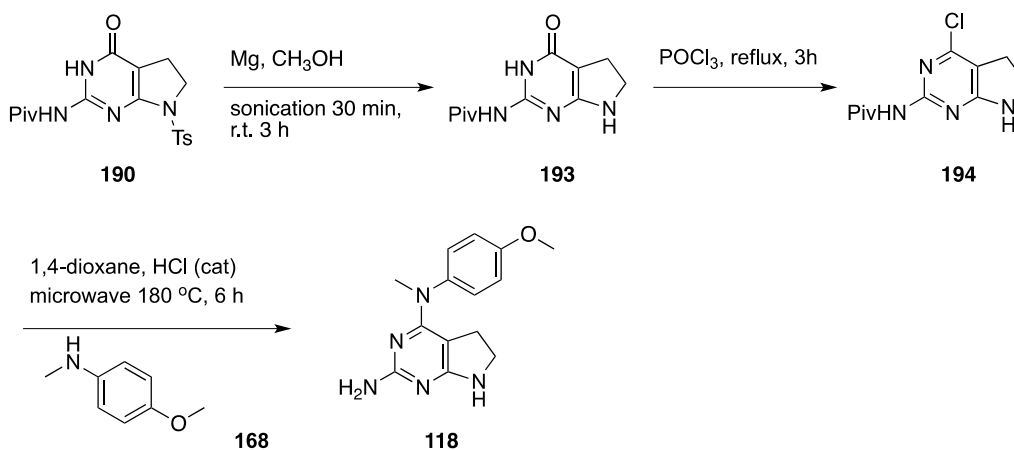
Table 8 Experimented conditions for the removal of N-tosyl

Reagent	Condition	Result
H ₂ SO ₄ (conc.)	90 °C, 1 h	Complete degradation of 193 , no product formed
H ₂ SO ₄ (70%)	90 °C, 4 h	No product formed
HBr / H ₂ O	Reflux, 2 h	Complete degradation of 193 , no product formed
HBr (30%) / AcOH	Reflux, 2 h	Complete degradation of 193 , no product formed
HBr (30%) / AcOH	r.t. 16 h	Multiple spots on TLC
HBr (30%) / AcOH, phenol	r.t. 16 h	No product formed
NaOH (3 N) / CH ₃ OH, H ₂ O	Reflux, 3 h	Removal of pivaloyl only
NaOC ₂ H ₅ / C ₂ H ₅ OH	Reflux, 3 h	Removal of pivaloyl only

Na/NH ₃ (liquid)	-78 to -30 °C, 3 h	Small quantities of 198 formed, most 193 recovered
Mg (turnings) / CH₃OH	Sonication 30 min, then r.t. 3 h	Complete reaction

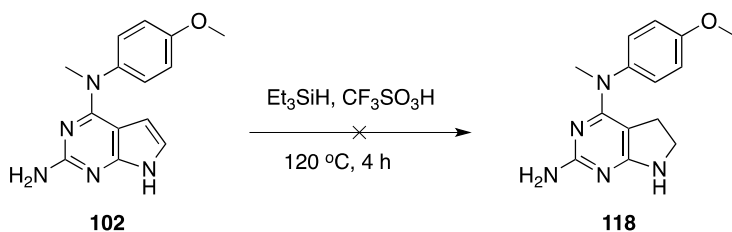
The most surprising moment during this project was when the removal of the tosyl group on the N-7 became a challenging task (**Scheme 34**). There is a report on removing the N-7 tosyl of the 4-oxo-5,6-dihydropyrrolo[2,3-*d*]pyrimidine **192**.¹³³ However, the two methods using concentrated sulfuric acid or sodium in liquid ammonia turned out to be ineffective in the reactions for **192** (**Table 8**). Harsh acidic conditions degraded the starting material into unidentifiable substances of black color. Basic conditions could only hydrolyze the pivaloyl group on the 2-amino within the given time. Reductive cleavage with sodium in liquid ammonia afforded small quantities of product. However, the complicated experiment setup made this method suboptimal in practice. Fortunately, the identification of magnesium turning in anhydrous methanol resulted in success (last entry in **Table 8**). The sonication as an activation mechanism for magnesium was necessary since the reaction rate under stirring was slow to the extent of being impractical. The isolated yield was over 90% with simple workup and purification procedures.

Scheme 35 Alternative synthetic sequence for the target compound **118**



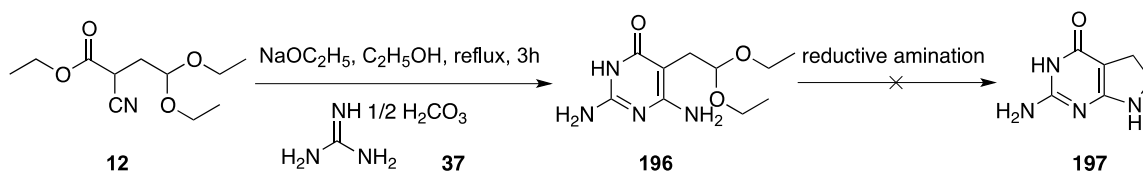
Alternatively, the removal of N7-tosyl could immediately follow the hydrogenation. This sequence was also attempted (**Scheme 35**). In sharp contrast with their N7-tosylated counterparts, both **194** and **195** displayed considerably lower reactivity under similar conditions. In the chlorination step, the reaction was not complete after three hours. In the subsequent S_NAr displacement with aniline **168**, the yield was lower than 30%. This provided another example of the close relationship between the electron density of the aromatic ring and its reactivity in S_NAr reactions.

Scheme 36 Attempted reduction of 102 by silane



The pyrrole ring of indoles was reported to undergo reduction by triethylsilane under strong acidic conditions. However, this method was not applicable to the pyrrolo[2,3-*d*]pyrimidines (**Scheme 36**). The sole product of this reaction was the de-methylated compound from the cleavage of the methoxy on phenyl.

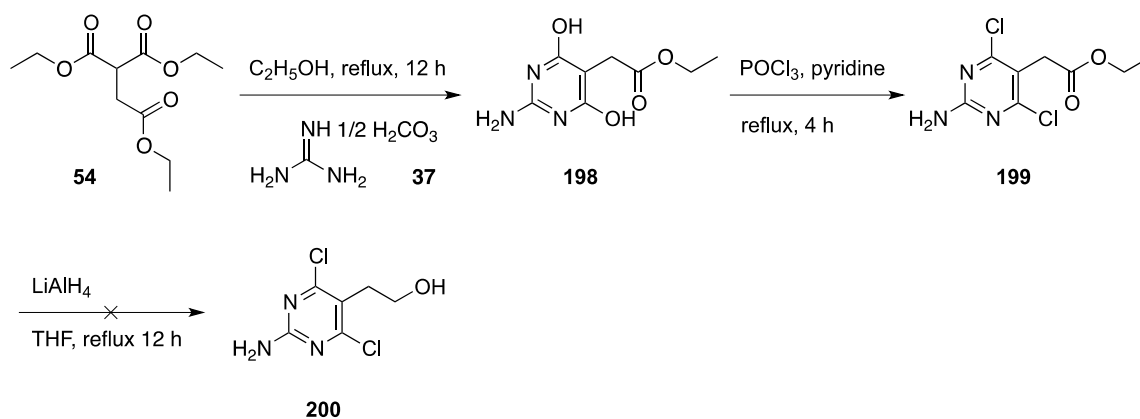
Scheme 37 Alternative strategy toward the 5,6-dihydropyrrolo[2,3-*d*]pyrimidine



Inspired by the synthesis of the 2-methyl-pyrrolo[2,3-*d*]pyrimidines, the 2-amino analog of the acetal intermediate **196** (**Scheme 37**) was synthesized with the intention of

a reductive amination to afford the 5,6-dihydropyrrolo[2,3-*d*]pyrimidine **197** in a single step. The explored reaction conditions included NaBH₄, NaBH(OAc)₃/AcOH, NaBH₄/AcOH (1:1). However, none of these experiments was successful. The main reason was attributed to the low nucleophilicity of the amino group on the pyrimidine. A combination of high temperature and strong electrophile is usually required to activate the amino group of this kind. In some experiments, it was suspected that the acetal was converted to aldehyde and reduced to alcohol. However, this observation was not confirmed since the products formed were not isolated.

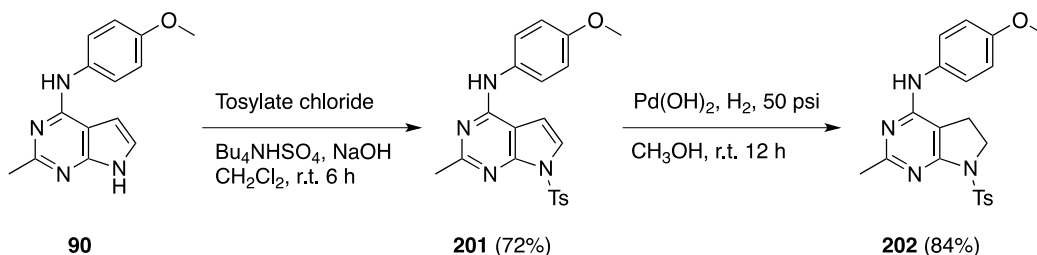
Scheme 38 Synthesis from functionalized pyrimidines



Intermediates like pyrimidinylethanol **200** (Scheme 38) could be a favorable precursor for the synthesis of 5,6-dihydropyrrolo[2,3-*d*]pyrimidines. Similar reactions are reported in the literature.^{132, 167} However, the practical value of this route was limited by the side reactions and low isolated yields. The reduction of the acetate **199** with LiAlH₄ generated highly polar compounds with unknown structures. Other reducing reagents were not experimented. The subsequent steps, including a Gabriel synthesis to convert the alcohol into an amine followed by an intramolecular S_NAr displacement, was not attempted.

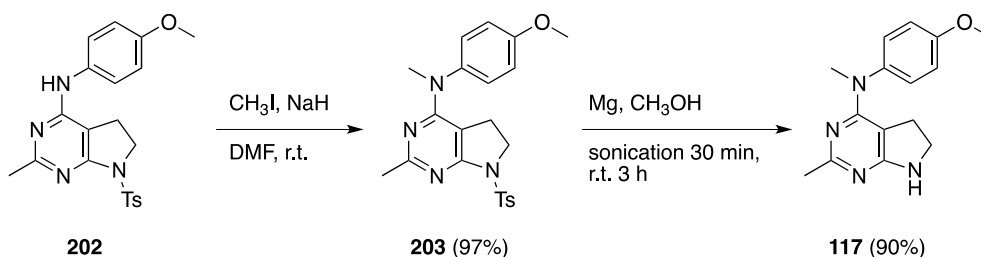
9) Synthesis of *N*-(4-methoxyphenyl)-*N*,2-dimethyl-6,7-dihydro-5*H*-pyrrolo[2,3-*d*]pyrimidin-4-amine (117)

Scheme 39 Direct hydrogenation with the 4-position substituted



On the basis on the observations during the synthesis of **118** (Scheme 39), the precursor toward the 2-methyl analog **117** was obtained in a much short sequence. This was made possible by the differences in the low-energy conformation between the *N*-methylaniline substituted **91** and aniline substituted **90**. This difference does not only influence the biological activity, but also has enormous impact on the reactivity. Since the access of the palladium catalyst to the 5,6-double bond of **90** was not hindered by the phenyl ring, a direct hydrogenation of the N7-tosylated derivative **201** becomes possible. The duration of the hydrogenation was much longer than the 4-oxo analogs under the same hydrogen pressure and catalyst conditions.

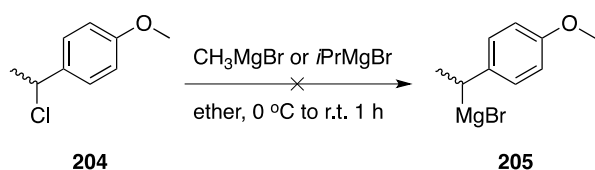
Scheme 40 Synthesis of the target compound 117



The methylation with iodomethane was carried out on the N7-tosylated **202** from the previous step (**Scheme 40**), followed by the removal of the tosyl group using the established procedure to afford the target compound **117**.

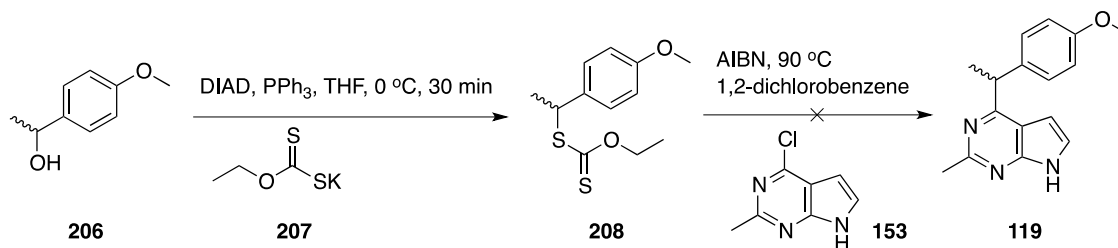
10) Synthesis of 4-(1-(4-methoxyphenyl)ethyl)-2-methyl-7H-pyrrolo[2,3-d]pyrimidine (**119**)

Scheme 41 Attempted synthesis of 1-(4-methoxyphenyl)ethyl Grignard reagent



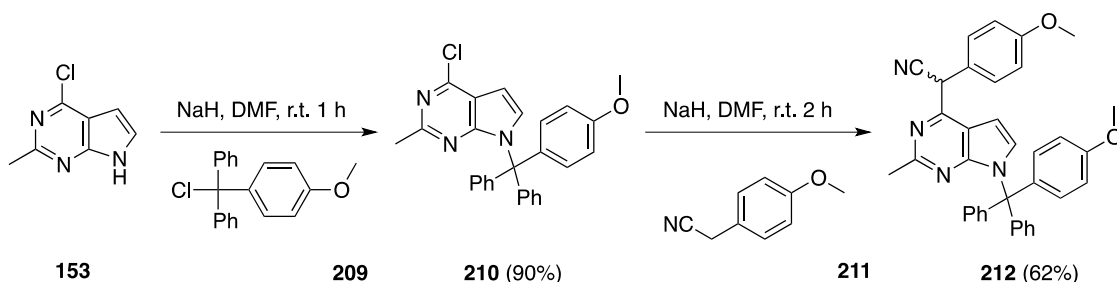
The initial plan for the synthesis of **119** was to utilize a ferric acetylacetonate [Fe(acac)₂] catalyzed coupling between the 4-chloropyrrolo[2,3-*d*]pyrimidine **153** and the Grignard reagent **205** (**Scheme 41**). There was no report or commercial source of **205**. This Grignard reagent is highly unstable and quickly rearranges into its 2-ethyl magnesium bromide analog. The attempt to generate **205** from **204** through the exchange reaction with another Grignard reagent was unsuccessful.

Scheme 42 Alkylation of the pyrrolopyrimidine through a free radical reaction



There are literature reports on the intramolecular displacement of halogen on the substituted pyrimidine through free radical reactions.^{168, 169} However, such intermolecular reactions through free radical mechanisms are not common in the literature. The precursor xanthate derivative **208** (Scheme 42) was synthesized from the alcohol **206** via a Mitsunobu reaction. The subsequent free radical reaction of **208** and 4-chloropyrrolo[2,3-*d*]pyrimidine **153** generated multiple products in similar quantities that were impractical to isolate and analyze individually.

Scheme 43 S_NAr displacement with a strong carbon nucleophile

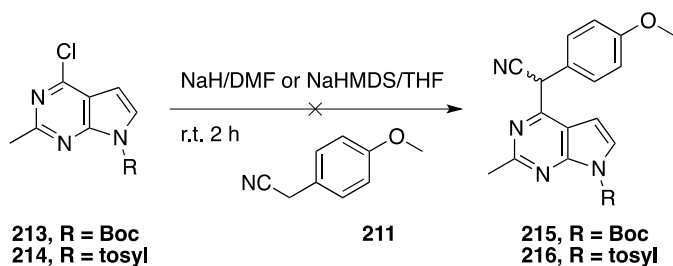


A direct S_NAr displacement of the 4-chloro of the pyrrolo[2,3-*d*]pyrimidine with a strong carbon nucleophile was contemplated and optimized (Scheme 43). The protection of the N7 of **153** was necessary, as no product was detected even under two equivalents of the base without the N7 protection. In the S_NAr reaction step (**210** to **212**), sodium hydride was found to give the best results (62% isolated). The main side product in this reaction was the carboxylic acid resulting from the hydrolysis of the nitrile. Using stronger bases like NaHMDS led to the formation of an unknown product.

Besides the acetonitrile **211**, methyl 2-(4-methoxyphenyl)acetate has also been attempted as the nucleophile in the S_NAr displacement. However, the outcome of the

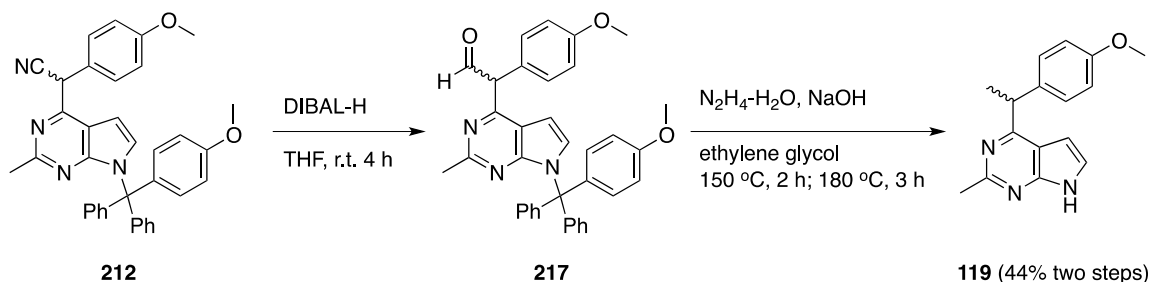
acetate reactions was less favorable as multiple products were formed. The side reactions were possibly due the hydrolysis of the acetate.

Scheme 44 Choice of protecting groups at the N7 position



Before the final selection of anisylidiphenylmethyl, the Boc and tosyl have been tried as the protecting group for the N-7 of pyrrolo[2,3-*d*]pyrimidine **153** (Scheme 44). Both of these protecting groups are stable under basic conditions for the protection of amines. However, instant cleavage of the Boc or tosyl from pyrrolo[2,3-*d*]pyrimidine was observed upon the exposure to NaH or NaHMDS. A change in the addition sequence of the reagents did not alter the outcome.

Scheme 45 Conversion of the nitrile to a methyl

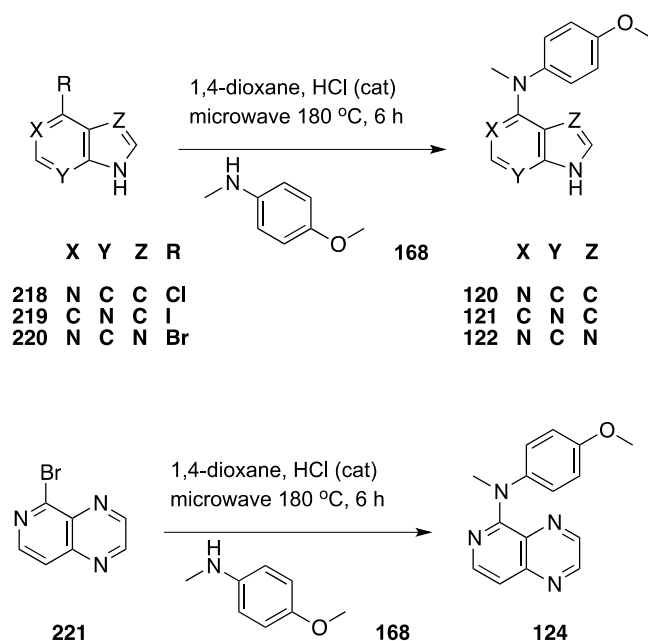


The reduction of nitriles to aldehydes was realized with diisobutylaluminum hydride (DIBAL-H) as expected (Scheme 45). The aldehyde **217** was unstable under room temperature and was immediately used for the next step. The following Wolff-Kishner-

Huang reaction accomplished both the reduction of aldehyde and the cleavage of anisyldiphenylmethyl in a single step. Trityl and anisyldiphenylmethyl are usually cleaved under strong acidic conditions. Hydrazine-promoted cleavage was uncommon and may be advantageous for acid-labile structures.

11) Synthesis of *N*-methyl-4-methoxyaniline-substituted bicyclic heterocycles (120 – 122 and 124)

Scheme 46 Synthesis of target compounds 120 – 122 and 124

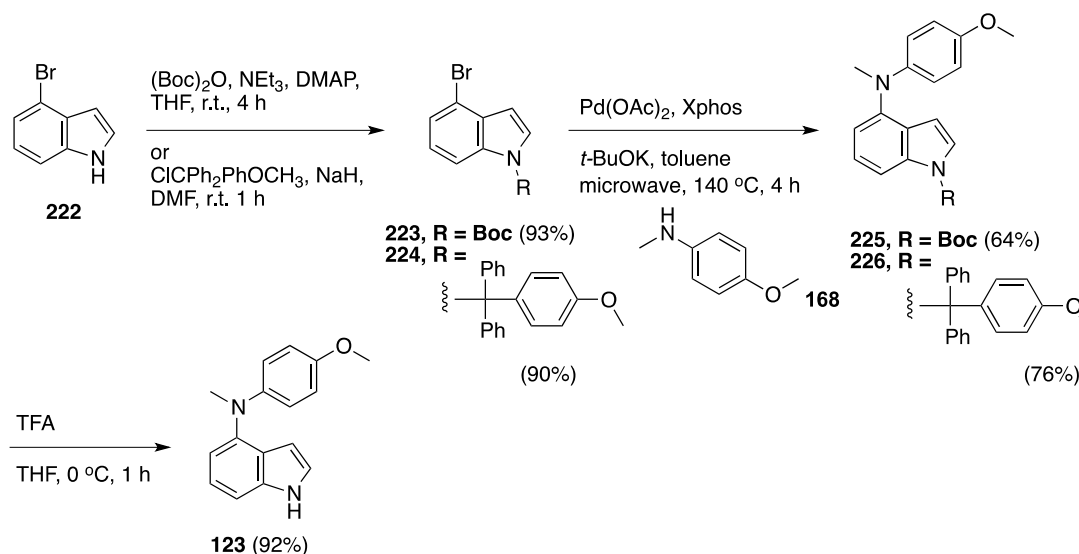


The synthesis of the target compounds 120 – 122 and 124 followed the same procedure established for the synthesis of tetrahydroquinoline-substituted analogs (Scheme 46). In general, to achieve reasonable yields on these reactions elevated temperature and strictly anhydrous condition are required. Even if these requirements were satisfied, complete conversion within the attempted time was rare. The isolated

yield in these reaction ranged from 40% to 63%. The physical states of the products were different. For example, **122** and **124** remained semi-solid despite multiple rounds of recrystallization. Formation of the hydrochloride salts did not promote the formation of a solid.

12) Synthesis of *N*-(4-methoxyphenyl)-*N*-methyl-1*H*-indol-4-amine (**123**)

Scheme 47 Synthesis of the target compound **123** via Buchwald-Hartwig reaction



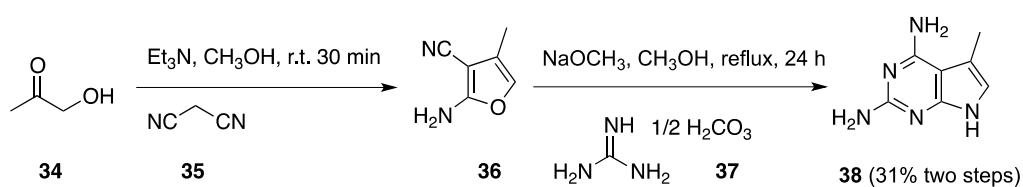
A Buchwald-Hartwig amination was the obvious choice for the synthesis of indole-based **123** (Scheme 47). The removal of the NH hydrogen on the 4-bromo-indole **222** was necessary as shown by experiment. Boc group was selected in this structure for its expedient formation and removal. Anticipating the strong basic condition of the coupling reaction, the more base-resistant anisylidiphenylmethyl was also employed. Another benefit of anisylidiphenylmethyl is the solid form of its protected product **224** while the

Boc-protected **223** was a oil-like liquid. Both formation and removal of these two protecting group proceeded with high yields (> 90%).

Palladium acetate and Xphos, a typical catalyst-ligand pair for Buchwald-Hartwig coupling, turned out to be the most efficient combination for the synthesis of **225** and **226** after a short screening. Other attempted combinations included Pd₃(dba)₂/tBu-Dave-phos, Pd(OAc)₂/tBu-Dave-phos, Pd(OAc)₂/BINAP. The Pd₃(dba)₂/tBu-Dave-phos pair gave very low yield (~10%) in this case, while the other two did not afford the product under the same condition.

13) Synthesis of 5-methyl-7-(pent-4-yn-1-yl)-6-(phenylthio)-7H-pyrrolo[2,3-*d*]pyrimidin-4-amines (130 – 134) and 6-(benzo[*d*][1,3]dioxol-5-ylthio)-7-(3-(isopropylamino)propyl)-5-methyl-7H-pyrrolo[2,3-*d*]pyrimidin-4-amine (135)

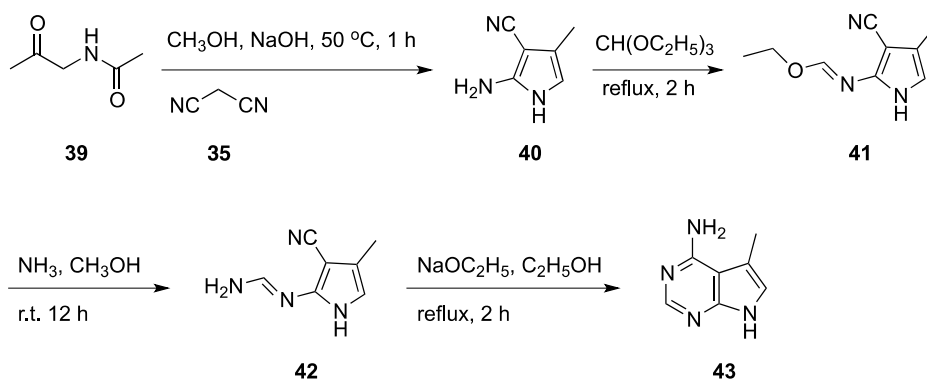
Scheme 48 Synthesis of 5-methyl-7H-pyrrolo[2,3-*d*]pyrimidine-2,4-diamine (38)



The synthesis of the 2-amino-5-methyl-pyrrolo[2,3-*d*]pyrimidine **38** (Scheme 48) followed a literature reported method.¹²⁹ The 2-amino-3-cyano-furan **36** was unstable and was used immediately without isolation. Under basic conditions, the furan ring of **35** opened and rearranged into the product **38** upon the attack of guanidine. The reaction was

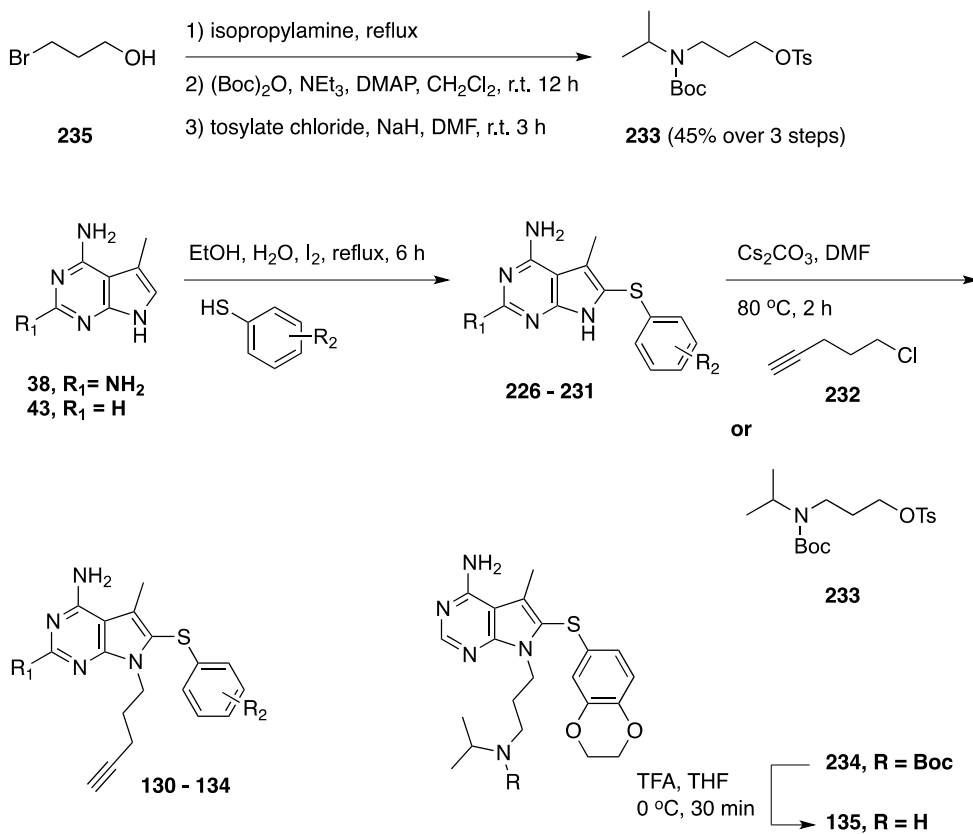
slow and strict anhydrous condition was required to attain a reasonable isolated yield (31% over two steps).

Scheme 49 Synthesis of 5-methyl-7H-pyrrolo[2,3-*d*]pyrimidin-4-amine (43)



The synthesis of 4-amino-5-methyl-pyrrolo[2,3-*d*]pyrimidine **43** (Scheme 49) also followed a literature reported method.¹³⁰ A modified Knorr pyrrole synthesis afforded the 2-amino-3-cyano-4-methyl-pyrrole **40** in a crude yield around 60%. Reflux of **40** in triethyl orthoformate gave the ethoxyimine **41** followed by amination with the commercially available 7N ammonia in methanol in a sealed vial under room temperature for 12 hours to afford **42** (crude yield ~30% over two steps). The redundant sequence was deemed necessary when a direct cyclization between **40** and formimidamide failed to produce **43**. Finally, the intramolecular cyclization of **42** under basic conditions afforded the pyrrolo[2,3-*d*]pyrimidine **43** in 70% yield.

Scheme 50 Synthesis of target compounds 130 – 135



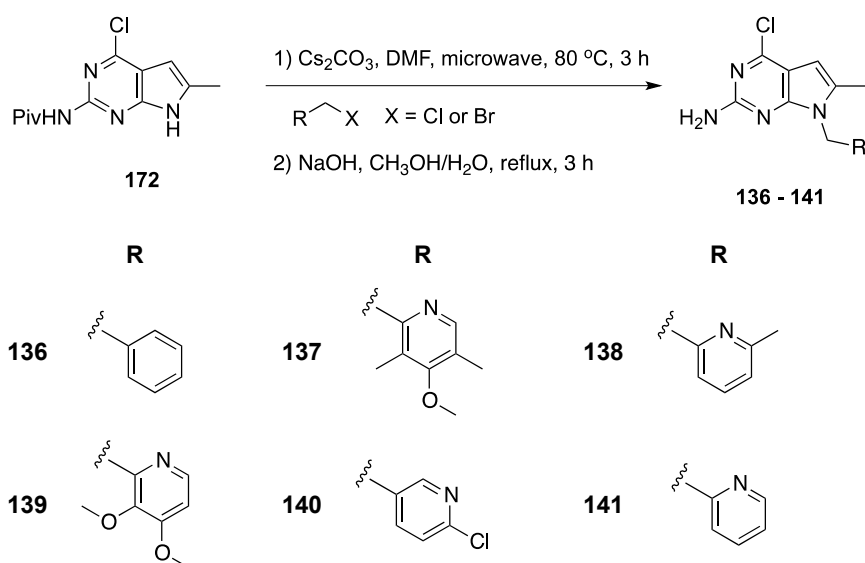
	R ₁	R ₂
130	H	2-OCH ₃
131	H	3-OCH ₃
132	NH ₂	4-OCH ₃
133	NH ₂	3,4-diOCH ₃
134	NH ₂	3,4,5-triOCH ₃

The substitutions of selected thiophenols to the 6-position of pyrrolo[2,3-*d*]pyrimidines **226 – 231** followed a reported procedure (Scheme 50).¹⁷⁰ The iodine in these reactions was added in portions to ensure the maximal catalytic performance. The yields for the substitution reaction ranged from 30% to 45%. The secondary amine **233** was converted from bromopropanol **235** in three steps. In the N7 alkylation step, higher concentrations of reactants were found to be critical to achieve the high yields (~ 90%). Excess solvent,

for example over ten times the weight of **226 – 231**, severely decreased the yield (~ 20%) or resulted in no product at all.

14) Synthesis of 7-substituted-4-chloro-6-methyl-7*H*-pyrrolo[2,3-*d*]pyrimidin-2-amine (**136 – 143**)

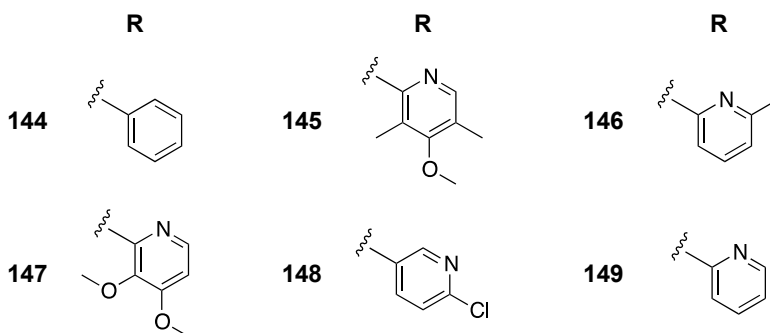
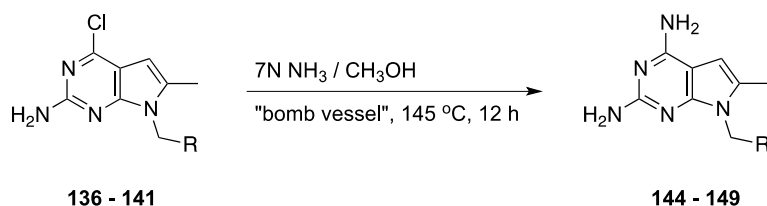
Scheme 51 Synthesis of target compounds **136 – 141**



The synthesis of target compounds **136 – 141** (Scheme 51) followed the same procedure for the synthesis of N7-benzyl analogs **115**. Similar yields (71% to 85%) were also obtained for this series of compounds.

16) Synthesis of 7-substituted-4-amino-6-methyl-7*H*-pyrrolo[2,3-*d*]pyrimidin-2-amine (149 – 154)

Scheme 52 Synthesis of target compounds 144 – 149



The target compounds 144 – 149 (Scheme 52) were synthesized from their corresponding 4-chloro analogs in a single amination step using the commercially available 7N ammonia in methanol. The yields of this amination step ranged from 54% to 89%.

V. EXPERIMENTAL

Microwave reactions were performed on the Biotage® Initiator EXP US microwave reactor. A model ROBOT EIGHT 355380 30522-17A robot was used in combination. Analytical samples were dried *in vacuo* in a CHEM-DRY drying apparatus over P₂O₅ at 50 °C. Melting points were determined on either on a MEL-TEMP II melting point apparatus with FLUKE 51 K/J electronic thermometer or a MPA100 OptiMelt Automated Melting Point System. Nuclear magnetic resonance spectra for proton (¹H NMR) were recorded on the Bruker WH-300 (300 MHz), Bruker Avance II 400 (400 MHz) or Bruker Avance II 500 (500 MHz) NMR systems with TopSpin processing software. The chemical shift values are expressed in ppm (parts per million) relative to the tetramethylsilane as an internal standard: s, singlet; d, doublet; dd, doublet of doublet; t, triplet; q, quartet; m, multiplet; br, broad singlet. Thin-layer chromatography (TLC) was performed on Whatman® PE SIL G/UV254 flexible silica gel plates with fluorescent indicator. The spots were visualized under 254 and 365 nm illumination. Proportions of solvents used for TLC are by volume. Column chromatography was performed on the silica gel (70 to 230 meshes, Fisher Scientific) column. Flash chromatography was carried out on the CombiFlash® Rf systems, model COMBIFLASH RF. Pre-packed RediSep® Rf normal-phase flash columns (230 to 400 meshes) of various sizes were used. Elemental analyses were performed by Atlantic Microlab, Inc., Norcross, GA. Element compositions are within ±0.4% of the calculated values. Fractional moles of water or organic solvents frequently found in some analytical samples could not be prevented despite 24 to 48 hours of drying *in vacuo* and were confirmed where possible by their presence in the ¹H NMR spectra. Mass spectrum data was acquired on the

Agilent G6220AA TOF LC/MS system using the nano ESI (Agilent chip tube system with infusion chip). Solvents and chemicals were purchased from Sigma-Aldrich Co. or Thermo Fisher Scientific Inc. and were used as received.

2-Methyl-3*H*-pyrrolo[2,3-*d*]pyrimidin-4(7*H*)-one (15)

To solution of ethyl-2-cyanoacetate **10** (1.13 g, 10 mmol) in anhydrous DMF (20 mL) was added the sodium methoxide (0.54 g, 10 mmol). After stirring for 30 min, the precipitated salt was filtered off and to the clear solution 2-bromo-1,1-diethoxyethane **11** (1.97 g, 10 mmol) was added. The reaction was heated at 90 °C for 4 hours. After cooled to room temperature, the reaction solution was extracted with diethyl ether (2 × 20 mL). The ether layer was collected, dried over sodium sulfate and evaporated to give a pale yellow liquid. The liquid was then added to a solution of acetamidine hydrochloride **13** (0.94 g, 10 mmol) and sodium ethoxide (0.68 g, 10 mmol) in ethanol (20 mL), followed by reflux for 3 hours. By the end of the reflux, the reaction solution was evaporated to dryness, extracted by ethyl acetate and water. The organic layer was collected and evaporated to afford a solid. Then the solid was added concentrated sulfuric acid (2 mL) in ethanol (10 mL) and reflux for 2 hours. Water (10 mL) was added at the end of the reaction followed by ammonia hydroxide to adjust the pH to 8. The precipitate formed was collected and dried to give **15** as an off-white powder (850 mg) and used without further purification. An analytical sample was purified and analyzed by ¹HNMR (500 MHz, DMSO-*d*6): δ 2.30 (s, 3 H, 2-CH₃), 6.37 (d, 1 H, 5-H, *J* = 1.15), 6.94 (d, 1 H, 6-H, *J* = 0.6), 11.61 – 11.67 (d, 1 H, N7-H, *J* = 26.35, D₂O exchanged).

4-Chloro-2-methyl-7H-pyrrolo[2,3-*d*]pyrimidine (153)

To the POCl₃ (10 mL) in a round-bottom flask was added **15** (745 mg, 5 mmol) and the mixture was refluxed for 3 hours. After the removal of remaining POCl₃ under vacuum, saturated solution of sodium bicarbonate (10 mL) was carefully added. The mixture was extraction with ethyl acetate (2 × 20 mL). After evaporation, **153** was obtained as a pale yellow powder (668 mg, 81%) and used without further purification. R_f 0.45 (CH₃OH/CHCl₃, 1:10). An analytical sample was purified and analyzed by ¹HNMR (DMSO-*d*₆): δ 2.28 (s, 3 H, 2-CH₃), 6.35 (d, 1 H, 5-H, *J* = 3.28), 6.93 (d, 1 H, 6-H, *J* = 3.28), 11.67 (s, 1 H, N7-H, D₂O exchanged).

General procedures for the synthesis of 90 – 98

To the solution of compound **153** (334 mg, 2 mmol) in isopropanol (5 mL) was added the corresponding aniline **154** (2.2 mmol). Anhydrous HCl gas was bubbled through the mixture under stirring until the solution became clear. The solution was then either refluxed in oil bath or heated in microwave reactor (130 °C) for 4 hours. At the end of the reaction, the reaction mixture was evaporated to dryness, added saturated sodium bicarbonate (10 mL) and extracted with ethyl acetate (2 × 20 mL). Silica gel was added to the organic layer followed by column chromatography or flash chromatography.

***N*-(4-methoxyphenyl)-2-methyl-7H-pyrrolo[2,3-*d*]pyrimidin-4-amine (90)**

After column chromatography (1 – 3% methanol in chloroform), **90** was obtained as white solid (305 mg, 60%). ¹H NMR (400 MHz, DMSO-d₆): δ 2.42 (s, 3 H, 2-CH₃), 3.73 (s, 3 H, OCH₃), 6.55 (d, 1 H, 5-H, *J* = 3.24), 6.91 (d, 2 H, phenyl, *J* = 8.96), 7.05 (d, 1 H, 6-H, *J* = 3.44), 7.74 (d, 2 H, phenyl, *J* = 8.92), 9.02 (s, 1H, *N*-H), 11.41 (s, 1 H, N7-H, D₂O exchanged). R_f 0.42 (CH₃OH/CHCl₃, 1:5); m.p. 258.7 – 259.9 °C. HRMS *m/z* calculated for C₁₄H₁₅N₄O [M+H]⁺, 255.1240; found, 255.1234. Elemental analysis calculated for C₁₄H₁₄N₄O: C, 66.13; H, 5.55; N, 22.03. Found: C, 66.09; H, 5.68; N, 21.86.

***N*-(4-methoxyphenyl)-*N*,2-dimethyl-7H-pyrrolo[2,3-*d*]pyrimidin-4-amine (91)**

After column chromatography (1 – 2% methanol in chloroform), **91** was obtained as a white solid (425 mg, 80%). R_f 0.65 (CH₃OH/CHCl₃, 1:5); m.p. 229.3 – 229.5 °C. ¹H NMR (400 MHz, DMSO-*d*₆): δ 2.45 (s, 3 H, 2-CH₃), 3.45 (s, 3 H, *N*CH₃), 3.82 (s, 3 H, OCH₃), 4.52 – 4.53 (d, 1 H, 5-H, *J* = 3.50), 6.73 – 6.74 (d, 1 H, 6-H, *J* = 3.35), 7.03 – 7.04 (d, 2 H, phenyl, *J* = 8.85), 7.26 – 7.28 (d, 2 H, phenyl, *J* = 6.7), 11.27 (s, 1 H, N7-H, D₂O exchanged). HRMS *m/z* calculated for C₁₅H₁₇N₄O [M+H]⁺, 269.1397; found, 269.1385. Elemental analysis calculated for C₁₅H₁₆N₄O·0.3045CHCl₃: C, 60.33; H, 5.39; N, 18.39. Found: C, 60.20; H, 5.74; N, 18.66.

***N*-(4-methoxyphenyl)-*N*,2-dimethyl-7*H*-pyrrolo[2,3-*d*]pyrimidin-4-amine hydrochloride (91·HCl)**

To the solution of **91** (1 mmol, 268 mg) in diethyl ether in the ice bath was bubbled anhydrous HCl gas for 5 min. The salt precipitated from the solution and was collected to give a white solid after drying (180 mg, 60%); m.p. 247.5 – 249.7 °C. ¹H NMR (500 MHz, DMSO-*d*₆): δ 2.70 (s, 3 H, 2-CH₃), 3.66 (s, 3 H, NCH₃), 3.85 (s, 3 H, OCH₃), 4.59 (s, 1 H, 5-H), 7.00 (s, 1 H, 6-H), 7.12 – 7.14 (d, 2 H, phenyl, *J* = 8.45), 7.42 – 7.43 (d, 2 H, phenyl, *J* = 8.30), 11.59 (s, 1 H, N7-H, D₂O exchanged). Elemental analysis calculated for C₁₅H₁₇ClN₄O·0.5256H₂O: C, 57.33; H, 5.79; N, 17.83; Cl, 11.28. Found: C, 57.33; H, 5.68; N, 17.77; Cl, 11.33.

***N*-(3-methoxyphenyl)-*N*,2-dimethyl-7*H*-pyrrolo[2,3-*d*]pyrimidin-4-amine (92)**

After column chromatography (1 – 2% methanol in chloroform), **92** was obtained as white solid (370 mg, 70%). R_f 0.60 (CH₃OH/CHCl₃, 1:10); m.p. 174.8 – 176.3 °C. ¹H NMR (DMSO-*d*₆): δ 2.47 (s, 3 H, 2-CH₃), 3.50 (s, 3 H, NCH₃), 3.75 (s, 3 H, OCH₃), 4.63 – 4.64 (d, 1 H, 5-H, *J* = 3.48 Hz), 6.77 – 6.78 (d, 1 H, 6-H, *J* = 3.52 Hz), 6.91 (m, 1 H, phenyl), 6.92 (s, 1 H, phenyl), 6.97 – 6.99 (m, 1 H, phenyl), 7.37 – 7.41 (t, 1 H, phenyl), 11.53 (s, 1 H, N7-H, D₂O exchanged). HRMS *m/z* calculated for C₁₅H₁₆N₄O [M+H]⁺, 269.1397; found, 269.1392. Elemental analysis calculated for C₁₅H₁₆N₄O: C, 67.15; H, 6.01; N, 20.88. Found: C, 67.23; H, 6.15; N, 20.80.

***N*-(3-methoxyphenyl)-2-methyl-7*H*-pyrrolo[2,3-*d*]pyrimidin-4-amine (93)**

After column chromatography (1 – 3% methanol in chloroform), **93** was obtained as white solid (278 mg, 55%). R_f 0.50 (CH₃OH/CHCl₃, 1:10); m.p. 180.3 – 182.1 °C. ¹H NMR (DMSO-*d*₆): δ 2.38 (s, 3 H, 2-CH₃), 3.83 (s, 3 H, OCH₃), 6.70 – 6.71 (d, 1 H, 5-H, J = 3.64 Hz), 6.90 – 6.91 (d, 1 H, 6-H, J = 3.48 Hz), 7.04 (s, 1 H NH, D₂O exchanged), 7.41 – 7.50 (m, 4 H, phenyl), 11.41 (s, 1 H, 7-H, D₂O exchanged). HRMS m/z calculated for C₁₄H₁₄N₄O [M+H]⁺, 255.1240; found, 255.1250. Elemental analysis calculated for C₁₄H₁₄N₄O·0.0623 CHCl₃: C, 64.53; H, 5.42; N, 21.41. Found: C, 64.63; H, 5.70; N, 21.09.

***N*-(2-methoxyphenyl)-*N*,2-dimethyl-7*H*-pyrrolo[2,3-*d*]pyrimidin-4-amine (94)**

After column chromatography (1 – 2% methanol in chloroform), **94** was obtained as white solid (340 mg, 65%). R_f 0.55 (CH₃OH/CHCl₃, 1:10); m.p. 234.0 – 236.9 °C. ¹H NMR (DMSO-*d*₆): δ 2.45 (s, 3 H, 2-CH₃), 3.39 (s, 3 H, NCH₃), 3.68 (s, 3 H, OCH₃), 4.44 (s, 1 H, 5-H), 6.68 – 6.70 (d, 1 H, 6-H, J = 3.56 Hz), 7.04 – 7.07 (m, 1 H, phenyl), 7.18 – 7.20 (m, 1 H, phenyl), 7.29 – 7.31 (m, 1 H, phenyl), 7.43 – 7.47 (m, 1 H, phenyl), 11.25 (s, 1 H, N7-H, D₂O exchanged). HRMS m/z calculated for C₁₅H₁₆N₄O [M+H]⁺, 269.1397; found, 269.1383. Elemental analysis calculated for C₁₅H₁₆N₄O·0.0899 CH₃CO₂C₂H₅: C, 66.78; H, 6.10; N, 20.28. Found: C, 67.07; H, 6.28; N, 20.13.

***N*-(2-methoxyphenyl)-2-methyl-7*H*-pyrrolo[2,3-*d*]pyrimidin-4-amine (95)**

After column chromatography (1 – 3% methanol in chloroform), **95** was obtained as white solid (255 mg, 50%). R_f 0.40 (CH₃OH/CHCl₃, 1:10); m.p. 207.7 – 209.6 °C. ¹H NMR (DMSO-*d*₆): δ 2.28 (s, 3 H, 2-CH₃), 3.73 (s, 3 H, OCH₃), 6.62 – 6.63 (d, 1 H, 5-H, J = 3.52 Hz), 6.93 (s, 1 H, NH, D₂O exchanged), 7.08 (d, 1 H, 6-H, J = 3.40 Hz), 7.09 (m, 1 H, phenyl), 7.22 – 7.24 (m, 1 H, phenyl), 7.35 – 7.37 (m, 1 H, phenyl), 7.41 – 7.43 (m, 1 H, phenyl), 11.36 (s, 1 H, 7-H, D₂O exchanged). HRMS m/z calculated for C₁₄H₁₄N₄O [M+H]⁺, 255.1240; found, 255.1227. Elemental analysis calculated for C₁₄H₁₄N₄O: C, 66.13; H, 5.55; N, 22.03. Found: C, 66.16; H, 5.67; N, 21.70.

***N*,2-dimethyl-*N*-(*p*-tolyl)-7*H*-pyrrolo[2,3-*d*]pyrimidin-4-amine (96)**

After column chromatography (1 – 2% methanol in chloroform), **96** was obtained as white solid (397 mg, 75%). R_f 0.48 (CH₃OH/CHCl₃, 1:10); m.p. 265.8 – 268.7 °C. ¹H NMR (400 MHz, DMSO-*d*₆): δ 2.38 (s, 3 H, phenyl-CH₃), 2.46 (s, 3 H, 2-CH₃), 3.47 (s, 3 H, NCH₃), 4.53 – 4.54 (d, 1 H, 5-H, J = 3.48), 6.73 – 6.74 (d, 1 H, 6-H, J = 3.48), 7.21 – 7.23 (d, 2 H, phenyl, J = 8.28), 7.28 – 7.30 (d, 2 H, phenyl, J = 8.12), 11.30 (s, 1 H, N7-H, D₂O exchanged). HRMS m/z calculated for C₁₅H₁₆N₄ [M+H]⁺, 253.1448; found, 253.1435. Elemental analysis calculated for C₁₅H₁₆N₄·0.0625CHCl₃: C, 69.64; H, 6.23; N, 21.57. Found: C, 69.68; H, 6.30; N, 21.44.

***N*-(4-chlorophenyl)-*N*,2-dimethyl-7*H*-pyrrolo[2,3-*d*]pyrimidin-4-amine (97)**

After column chromatography (1 – 2% methanol in chloroform), **97** was obtained as white solid (322 mg, 60%). R_f 0.50 (CH₃OH/CHCl₃, 1:10); m.p. 219.6 – 221.8 °C. ¹H NMR (400 MHz, DMSO-*d*6): δ 2.47 (s, 3 H, 2-CH₃), 3.50 (s, 3 H, NCH₃), 4.68 – 4.69 (d, 1 H, 5-H, $J = 3.52$), 6.83 – 6.84 (d, 1 H, 6-H, $J = 3.52$), 7.37 – 7.39 (d, 2 H, phenyl, $J = 8.64$), 7.52 – 7.55 (d, 2 H, phenyl, $J = 8.64$), 11.41 (s, 1 H, N7-H, D₂O exchanged). HRMS m/z calculated for C₁₄H₁₃N₄Cl [M+H]⁺, 273.0902; found, 273.0889. Elemental analysis calculated for C₁₄H₁₃N₄Cl: C, 61.65; H, 4.80; N, 20.54; Cl, 13.00. Found: C, 61.79; H, 4.82; N, 20.46; Cl, 12.77.

***N*-(3,4-dichlorophenyl)-*N*,2-dimethyl-7*H*-pyrrolo[2,3-*d*]pyrimidin-4-amine (98)**

After column chromatography (1 – 2% methanol in chloroform), **97** was obtained as white solid (364 mg, 60%). R_f 0.55 (CH₃OH/CHCl₃, 1:10); m.p. 250.3 – 252.2 °C. ¹H NMR (400 MHz, DMSO-*d*6): δ 2.48 (s, 3 H, 2-CH₃), 3.52 (s, 3 H, NCH₃), 4.87 – 4.88 (d, 1 H, 5-H, $J = 3.56$), 6.92 – 6.93 (d, 1 H, 6-H, $J = 3.60$), 7.36 – 7.38 (m, 1 H, phenyl), 7.70 – 7.73 (m, 2 H, phenyl), 11.50 (s, 1 H, N7-H, D₂O exchanged). HRMS m/z calculated for C₁₄H₁₂N₄Cl₂ [M+H]⁺, 307.0512; found, 307.0504. Elemental analysis calculated for C₁₄H₁₂N₄Cl₂·0.0316CHCl₃: C, 54.20; H, 3.90; N, 18.02; Cl, 23.88. Found: C, 54.03; H, 3.85; N, 17.84; Cl, 23.72.

4-(methyl(2-methyl-7H-pyrrolo[2,3-d]pyrimidin-4-yl)amino)phenol (99)

To the solution of **91** (134 mg, 0.5 mmol) in CH₂Cl₂ (5 mL) under ice bath (0 °C) was slowly added BBr₃ (0.142 mL, 376 mg, 1.5 mmol). The reaction mixture was stirred under 0 °C for 30 min before brought to room temperature. After three hours, saturated sodium bicarbonate (5 mL) was carefully added. Extraction with CH₂Cl₂ (2 × 10 mL) was followed by column chromatography (1 – 3% methanol in chloroform) before **99** was obtained as a yellow solid (104 mg, 82%). R_f 0.60 (CH₃OH/CHCl₃, 1:5); m.p. 225.7 – 229.2 °C. ¹HNMR (400 MHz, DMSO-*d*₆): δ 2.48 (s, 3 H, 2-CH₃), 3.46 (s, 3 H, *N*-CH₃), 4.54 – 4.55 (d, 1 H, 5-H, *J* = 2.72), 6.77 (d, 1 H, 6-H, *J* = 2.68), 9.74 (s, 1 H, OH), 11.45 (s, 1 H, N7-H). Elemental analysis calculated for C₁₄H₁₄N₄O·0.2287CHCl₃: C, 60.69; H, 5.09; N, 19.90. Found: C, 60.75; H, 5.36; N, 19.68.

N-(naphthalen-2-yl)formamide (158)

To the suspension of naphthalen-2-amine **155** (218 mg, 1.5 mmol) in water (3 mL) was added triethyl orthoformate (1 mL, 6 mmol). The reaction mixture was sealed in a microwave vial and irradiated in the microwave reactor at 100 °C for 10 hours. At the end of the reaction, the mixture was extracted with ethyl acetate (2 × 10 mL) and the organic layer was evaporated and subjected to flash chromatography (gradient from 0 to 20% ethyl acetate in hexane, 18 mL/min). The product **158** was obtained in a yellow powder (190 mg, 74%). R_f 0.30 (hexane/ethyl acetate, 2:1); ¹HNMR (400 MHz, DMSO-*d*₆): δ 7.40 – 7.68 (m, 3 H, naphthyl), 7.79 – 7.91 (m, 2 H, naphthyl), 8.30 (s, 1 H,

naphthyl), 8.37 (d, 1 H, naphthyl, $J = 2$), 8.94 – 8.97 (d, 1 H, CHO, $J = 10.92$), 10.42 (s, 1 H, NH, D₂O exchanged).

***N*-methylnaphthalen-2-amine (159)**

To the solution of **158** (102 mg, 0.6 mmol) in anhydrous THF (2 mL) at room temperature was slowly added LiAlH₄ (1 mL, 1M solution) in THF under a stream of nitrogen. The resulted solution was stirred under room temperature for two hours, during which the reaction progress was monitored by TLC. At the end of the reaction, methanol (5 mL) was slowly poured into the solution and the solution was evaporated to dryness. The mixture was then suspended in saturated ammonium chloride in water (5 mL) and extracted with ethyl acetate (2 × 10 mL). The organic layer was evaporated and purified through flash chromatography (gradient from 0 to 10% ethyl acetate in hexane, 18 mL/min). The product **158** was obtained as dark red oil (65 mg, 70%). R_f 0.65 (hexane/ethyl acetate, 2:1); ¹HNMR (400 MHz, DMSO-*d*₆): δ 2.76 – 2.78 (d, 3 H, CH₃, $J = 5.04$), 5.96 – 5.97 (d, 1 H, NH, D₂O exchanged, $J = 4.88$), 6.65 (d, 1 H, naphthyl, $J = 1.96$), 6.93 – 6.96 (dd, 1 H, naphthyl), 7.08 – 7.12 (t, 1 H, naphthyl), 7.27 – 7.30 (t, 1 H, naphthyl), 7.32 – 7.64 (m, 4 H, naphthyl), 10.42 (s, 1 H, NH).

General procedure for the synthesis of *N*,2-dimethyl-*N*-(naphthalen-2-yl)-7*H*-pyrrolo[2,3-*d*]pyrimidin-4-amine (100) and 2-methyl-*N*-(naphthalen-2-yl)-7*H*-pyrrolo[2,3-*d*]pyrimidin-4-amine (101)

To **153** (167 mg, 1 mmol) and **159** or **155** (1.2 mmol) in a microwave vial was added anhydrous 1,4-dioxane (1 mL). HCl gas was bubbled through the vial before it was sealed and placed in the microwave reactor. The reaction condition was set for 140 °C and six hours. At the end of the reaction, the mixture was evaporated to dryness and suspended in brine (5 mL). After extraction with ethyl acetate (2 × 10 mL), the organic layer was evaporated to dryness and purified by flash chromatography (gradient from 0% to 3% methanol in chloroform).

***N*,2-dimethyl-*N*-(naphthalen-2-yl)-7*H*-pyrrolo[2,3-*d*]pyrimidin-4-amine (100)**

After flash chromatography, the target compound **100** was obtained as an off-white powder (193 mg, 65%). R_f 0.50 (CH₃OH/CHCl₃, 1:10); m.p. 213.0 – 215.2 °C. ¹HNMR (400 MHz, DMSO-*d*₆): δ 2.50 (s, 3 H, 2-CH₃), 2.70 (s, 3 H, *N*-CH₃), 4.7 (d, 1 H, 5-H, *J* = 1.36), 6.69 – 6.70 (t, 1 H, 6-H), 7.48 – 7.51 (dd, 1 H, naphthyl), 7.55 – 7.57 (m, 1 H, naphthyl), 7.91 (m, 1 H, naphthyl), 7.90 – 8.04 (m, 4 H, naphthyl), 11.34 (s, 1 H, N7-H, D₂O exchanged). Elemental analysis calculated for C₁₈H₁₆N₄·0.1756 CH₃CO₂C₂H₅: C, 73.94; H, 5.77; N, 18.44. Found: C, 73.83; H, 5.77; N, 18.55.

2-methyl-*N*-(naphthalen-2-yl)-7*H*-pyrrolo[2,3-*d*]pyrimidin-4-amine (101)

After flash chromatography, the target compound **101** was obtained as a pale yellow powder (173 mg, 60%). R_f 0.40 (CH₃OH/CHCl₃, 1:10); m.p. 272.8 – 275.3 °C. ¹HNMR (400 MHz, DMSO-*d*₆): δ 2.55 (s, 3 H, 2-CH₃), 6.75 – 6.76 (d, 1 H, 5-H, *J* = 3.2), 7.16 –

7.17 (d, 1 H, 6-H, $J = 3.2$), 7.35 – 7.39 (m, 2 H, naphthyl), 7.45 – 7.47 (m, 2 H, naphthyl), 7.81 – 7.88 (m, 1 H, naphthyl), 7.97 – 8.00 (m, 1 H, naphthyl), 8.61 (s, 1 H, naphthyl), 9.43 (s, 1 H, NH), 11.56 (d, 1 H, N7-H, D₂O exchanged, $J = 0.4$). Elemental analysis calculated for C₁₇H₁₄N₄·0.0618CHCl₃: C, 72.75; H, 5.03; N, 19.89. Found: C, 72.83; H, 5.10; N, 19.61.

***N*-(4-oxo-4,7-dihydro-3*H*-pyrrolo[2,3-*d*]pyrimidin-2-yl)pivalamide (162)**

To the mixture of DMF (120 mL) and water (20 mL) at room temperature was added 2,4-diamino-6-hydroxypyrimidine **1** (6.3 g, 50 mmol) and NaOAc (4.1 g, 50 mmol). After the solution turned clear, chloroacetaldehyde **160** (7.2 mL 50% aqueous solution, 7.9 g, 50 mmol) was added. The reaction mixture was stirred for 24 hours. Then the solvent was removed under vacuum and water (5 mL) was added. The suspension was ice cooled and filtered. The solid containing 2-amino-3*H*-pyrrolo[2,3-*d*]pyrimidin-4(7*H*)-one **161** was thoroughly dried under vacuum. To the dried solid was added trimethylacetic anhydride (20 mL) and refluxed for four hours. The remaining trimethylacetic anhydride was removed under vacuum at the end of the reaction. The remaining solid was added saturated sodium bicarbonate solution (20 mL) and extracted with ethyl acetate (2 × 40 mL). The organic layer was evaporated and purified through column chromatography (1 – 3% methanol in chloroform) to afford **162** in the form of white solid (5.3 g, 45% over two steps). R_f 0.30 (CH₃OH:CHCl₃, 1/10). ¹HNMR (400 MHz, DMSO-*d*₆): δ 1.24 (s, 9 H, Piv), 6.41 (d, 1 H, 5-H, $J = 1.24$), 6.96 (t, 1 H, 6-H), 10.81 (s, 1 H, N7-H, D₂O

exchanged), 11.59 (s, 1 H, NHPiv, D₂O exchanged), 11.85 (s, 1 H, 3-NH, D₂O exchanged).

***N*-(4-chloro-7*H*-pyrrolo[2,3-*d*]pyrimidin-2-yl)pivalamide (163)**

To the POCl₃ (10 mL) in a round-bottom flask was added **162** (1.17 g, 5 mmol) and the mixture was refluxed for 3 hours. After the removal of remaining POCl₃ under vacuum, saturated solution of sodium bicarbonate (10 mL) was carefully added. The mixture was extraction with ethyl acetate (2 × 20 mL). After evaporation, **163** was obtained as a pale yellow powder (1 g, 80%) and used without further purification. R_f 0.45 (CH₃OH/CHCl₃, 1:10). An analytical sample was purified and analyzed by ¹HNMR (400 MHz, DMSO-*d*₆): δ 1.23 (s, 9 H, Piv), 6.53 – 6.54 (d, 1 H, 5-H, *J* = 3.56 Hz), 7.55 – 7.56 (d, 1 H, 6-H, *J* = 3.56 Hz), 10.05 (s, 1 H, N7-H, D₂O exchanged), 12.32 (s, 1 H, NHPiv, D₂O exchanged).

General procedure for the synthesis of *N*⁴-(4-methoxyphenyl)-*N*⁴-methyl-7*H*-pyrrolo[2,3-*d*]pyrimidine-2,4-diamine (102) and *N*⁴-(4-methoxyphenyl)-7*H*-pyrrolo[2,3-*d*]pyrimidine-2,4-diamine (103)

To the solution of **163** (504 mg, 2 mmol) in isopropanol (5 mL) was added the corresponding aniline **164** (2.2 mmol). Anhydrous HCl gas was bubbled through the mixture under stirring until the solution became clear. The solution was refluxed for 4 hours. At the end of the reaction, the reaction mixture was evaporated to dryness, added

saturated sodium bicarbonate (10 mL) and extracted with ethyl acetate (2 × 20 mL). The organic layer containing the pivaloyl-protected **165** or **166** was evaporated and dissolved in methanol (5 mL). Sodium hydroxide solution (2 N, 5 mL) was added and the solution was refluxed for three hours. The reaction mixture was evaporated to dryness at the end of the reaction and suspended in water (10 mL). After extraction with ethyl acetate (2 × 20 mL), silica gel was added to the organic layer followed by flash chromatography (2 – 4% methanol in chloroform).

***N*-(4-((4-methoxyphenyl)(methyl)amino)-7*H*-pyrrolo[2,3-*d*]pyrimidin-2-yl)pivalamide (165)**

A sample of **165** was analyzed with ¹HNMR (500 MHz, DMSO-*d*6): δ 1.24 (s, 9 H, Piv), 3.47 (s, 3 H, *N*CH₃), 3.83 (s, 3 H, OCH₃), 4.52 (d, 1 H, 5-H, *J* = 1.45), 6.73 – 6.74 (d, 1 H, 6-H, *J* = 1.00), 7.04 – 7.06 (d, 2 H, phenyl, *J* = 8.8), 7.27 – 7.28 (d, 2 H, phenyl, *J* = 8.75), 9.20 (s, 1 H, N7-H, D₂O exchanged), 11.32 (s, 1 H, NHPiv, D₂O exchanged).

***N*⁴-(4-methoxyphenyl)-*N*⁴-methyl-7*H*-pyrrolo[2,3-*d*]pyrimidine-2,4-diamine (102)**

After flash chromatography, **102** was obtained as a white solid (270 mg, 50% over two steps). *R*_f 0.40 (CH₃OH/CHCl₃, 1:10); m.p. 202.8 – 205.7 °C. ¹HNMR (400 MHz, DMSO-*d*6): δ 3.39 (s, 3 H, *N*CH₃), 3.81 (s, 3 H, OCH₃), 4.39 – 4.40 (d, 1 H, 5-H, *J* = 2.04), 5.59 (s, 2 H, NH₂, D₂O exchanged), 6.39 (d, 1 H, 6-H, *J* = 2.16), 7.00 – 7.03 (d, 2 H, phenyl, *J* = 8.76), 7.22 – 7.25 (d, 2 H, phenyl, *J* = 8.76), 10.64 (s, 1 H, N7-H, D₂O

exchanged). Elemental analysis calculated for $C_{14}H_{15}N_5O \cdot 0.0492CH_3(CH_2)_4CH_3$: C, 62.77; H, 5.78; N, 25.60. Found: C, 62.38; H, 5.79; N, 25.28.

***N*⁴-(4-methoxyphenyl)-7*H*-pyrrolo[2,3-*d*]pyrimidine-2,4-diamine (103)**

After flash chromatography, **103** was obtained as a white solid (205 mg, 40% over two steps). R_f 0.45 ($CH_3OH/CHCl_3$, 1:5); m.p. 189.5 – 192.9 °C. ¹HNMR (400 MHz, DMSO-*d*6): ¹HNMR (400 MHz, DMSO-*d*6): δ 3.74 (s, 3 H, OCH₃), 5.63 (s, 2 H, NH₂, D₂O exchanged), 6.46 (s, 1 H, 5-H), 6.62 (s, 1 H, 6-H), 6.72 (s, 2 H, phenyl), 7.78 (s, 2 H, phenyl), 8.76 (s, 1 H, NH, D₂O exchanged) 10.64 (s, 1 H, N7-H, D₂O exchanged). Elemental analysis calculated for $C_{13}H_{13}N_5O \cdot 0.1759CH_3CO_2C_2H_5$: C, 60.79; H, 5.36; N, 25.86; O, 6.27. Found: C, 61.08; H, 5.51; N, 25.81.

***N*-(6-methyl-4-oxo-4,7-dihydro-3*H*-pyrrolo[2,3-*d*]pyrimidin-2-yl)pivalamide (171)**

To the mixture of DMF (120 mL) and water (20 mL) at room temperature was added 2,4-diamino-6-hydroxypyrimidine **1** (6.3 g, 50 mmol) and NaOAc (4.1 g, 50 mmol). After the solution turned clear, chloroacetone **169** (4.6 g, 50 mmol) was added. The reaction mixture was stirred for 24 hours. Then the solvent was removed under vacuum and water (5 mL) was added. The suspension was ice cooled and filtered. The solid containing 2-amino-6-methyl-3*H*-pyrrolo[2,3-*d*]pyrimidin-4(7*H*)-one **170** was thoroughly dried under vacuum. To the dried solid was added trimethylacetic anhydride (20 mL) and refluxed for four hours. The remaining trimethylacetic anhydride was removed under

vacuum at the end of the reaction. The remaining solid was added saturated sodium bicarbonate solution (20 mL) and extracted with ethyl acetate (2 × 40 mL). The organic layer was evaporated and purified through column chromatography (1 – 3% methanol in chloroform) to afford **171** in the form of white solid (6.82 g, 55% over two steps). R_f 0.35 (CH₃OH:CHCl₃, 1/10). ¹HNMR (500 MHz, DMSO-*d*₆): δ 1.24 (s, 9 H, Piv), 1.76 (s, 3 H, 6-CH₃), 2.26 (s, 3 H, 2-CH₃), 6.08 (s, 1 H, 5-H), 10.75 (s, 1 H, N7-H, D₂O exchanged), 11.35 (s, 1 H, NHPiv, D₂O exchanged), 11.79 (s, 1 H, 3-NH, D₂O exchanged).

General procedure for the synthesis of 104 - 109

To the solution of **172** (266 mg, 1 mmol) in isopropanol (5 mL) was added the corresponding *N*-methyl-aniline **173** (1.1 mmol). Anhydrous HCl gas was bubbled through the mixture under stirring until the solution became clear. The solution was refluxed or microwave-irradiated (140 °C) for 4 hours. At the end of the reaction, the reaction mixture was evaporated to dryness, added saturated sodium bicarbonate (10 mL) and extracted with ethyl acetate (2 × 20 mL). The organic layer containing the pivaloyl-protected intermediate (**174** – **179**) was evaporated and dissolved in methanol (5 mL). Sodium hydroxide solution (2 N, 5 mL) was added and the solution was refluxed for three hours. The reaction mixture was evaporated to dryness at the end of the reaction and suspended in water (10 mL). After extraction with ethyl acetate (2 × 20 mL), silica gel was added to the organic layer followed by flash chromatography (2 – 4% methanol in chloroform).

***N*⁴-(4-methoxyphenyl)-*N*⁴,6-dimethyl-7*H*-pyrrolo[2,3-*d*]pyrimidine-2,4-diamine (104)**

After flash chromatography, **104** was obtained as a pale yellow solid (170 mg, 60% over two steps). *R*_f 0.45 (CH₃OH/CHCl₃, 1:10); m.p. 194.3 – 198.2 °C. ¹HNMR (500 MHz, DMSO-*d*₆): δ 2.01 (s, 1 H, 6-CH₃), 3.50 (s, 3 H, *N*CH₃), 3.84 (s, 3 H, OCH₃), 4.19 (s, 1 H, 5-H), 6.35 (s, 2 H, NH₂, D₂O exchanged), 7.08 – 7.09 (d, 2 H, phenyl, *J* = 8.90), 7.32 (d, 2 H, phenyl, *J* = 8.76), 11.61 (s, 1 H, N7-H, D₂O exchanged). HRMS *m/z* calculated for C₁₅H₁₇N₅O [M+H]⁺, 284.1506; found, 284.1502. Elemental analysis calculated for C₁₅H₁₇N₅O·0.9321CH₃CN·0.1155CHCl₃: C, 60.81; H, 5.98; N, 24.77. Found: C, 60.81; H, 5.89; N, 24.79.

***N*⁴-(3-methoxyphenyl)-*N*⁴,6-dimethyl-7*H*-pyrrolo[2,3-*d*]pyrimidine-2,4-diamine (105)**

After flash chromatography, **105** was obtained as an off-white solid (127 mg, 45% over two steps). *R*_f 0.45 (CH₃OH/CHCl₃, 1:10); m.p. 178.5 – 181.4 °C. ¹HNMR (400 MHz, DMSO-*d*₆): δ 1.98 (s, 1 H, 6-CH₃), 3.41 (s, 3 H, *N*CH₃), 3.75 (s, 3 H, OCH₃), 4.29 (s, 1 H, 5-H), 5.55 (s, 2 H, NH₂, D₂O exchanged), 6.82 – 6.84 (m, 1 H, phenyl), 6.90 – 6.92 (m, 1 H, phenyl), 7.31 – 7.33 (m, 1 H, phenyl), 10.55 (s, 1 H, N7-H, D₂O exchanged). HRMS *m/z* calculated for C₁₅H₁₇N₅O [M+H]⁺, 284.1506; found, 284.1497. Elemental analysis calculated for C₁₅H₁₇N₅O·0.0321CH₃(CH₂)₄CH₃: C, 63.78; H, 6.15; N, 24.48. Found: C, 64.00; H, 6.14; N, 24.65.

***N*⁴-(2-methoxyphenyl)-*N*⁴,6-dimethyl-7*H*-pyrrolo[2,3-*d*]pyrimidine-2,4-diamine (106)**

After flash chromatography, **106** was obtained as an off-white solid (127 mg, 45% over two steps). *R*_f 0.40 (CH₃OH/CHCl₃, 1:10); m.p. 148.4 – 151.3 °C. ¹HNMR (400 MHz, DMSO-*d*₆): δ 1.93 (s, 1 H, 6-CH₃), 3.34 (s, 3 H, *N*CH₃), 3.70 (s, 3 H, OCH₃), 4.04 (s, 1 H, 5-H), 5.45 (s, 2 H, NH₂, D₂O exchanged), 7.02 (t, 1 H, phenyl), 7.15 – 7.18 (t, 1 H, phenyl), 7.21 – 7.23 (t, 1 H, phenyl), 7.41 (t, 1 H, phenyl), 10.46 (s, 1 H, N7-H, D₂O exchanged). HRMS *m/z* calculated for C₁₅H₁₇N₅O [M+H]⁺, 284.1506; found, 284.1500. Elemental analysis calculated for C₁₅H₁₇N₅O·0.5297CH₃OH: C, 62.11; H, 6.42; N, 23.32. Found: C, 62.09; H, 6.08; N, 23.25.

***N*⁴,6-dimethyl-*N*⁴-(*p*-tolyl)-7*H*-pyrrolo[2,3-*d*]pyrimidine-2,4-diamine (107)**

After flash chromatography, **107** was obtained as a white solid (147 mg, 55% over two steps). *R*_f 0.40 (CH₃OH/CHCl₃, 1:10); m.p. 230.4 – 233.3 °C. ¹HNMR (400 MHz, DMSO-*d*₆): δ 1.96 (s, 1 H, 6-CH₃), 2.09 (s, 3 H, phenyl-CH₃), 3.40 (s, 3 H, *N*CH₃), 4.19 (s, 1 H, 5-H), 5.76 (s, 2 H, NH₂, D₂O exchanged), 7.16 – 7.18 (d, 2 H, phenyl, *J* = 8.2), 7.25 – 7.27 (d, 1 H, phenyl, *J* = 8.12), 10.69 (s, 1 H, N7-H, D₂O exchanged). HRMS *m/z* calculated for C₁₅H₁₇N₅ [M+H]⁺, 268.1557; found, 268.1573. Elemental analysis calculated for C₁₅H₁₇N₅: C, 67.39; H, 6.41; N, 26.20. Found: C, 67.11; H, 6.30; N, 25.82.

***N*⁴-(4-chlorophenyl)-*N*⁴,6-dimethyl-7*H*-pyrrolo[2,3-*d*]pyrimidine-2,4-diamine (108)**

After flash chromatography, **108** was obtained as a pale yellow solid (115 mg, 40% over two steps). *R*_f 0.45 (CH₃OH/CHCl₃, 1:10); m.p. 223.7 – 226.4 °C. ¹HNMR (400 MHz, DMSO-*d*₆): δ 2.01 (s, 1 H, 6-CH₃), 3.41 (s, 3 H, NCH₃), 4.36 (s, 1 H, 5-H), 5.59 (s, 2 H, NH₂, D₂O exchanged), 7.28 – 7.30 (d, 2 H, phenyl, *J* = 8.68), 7.47 – 7.49 (d, 2 H, phenyl, *J* = 8.6), 10.63 (s, 1 H, N7-H, D₂O exchanged). HRMS *m/z* calculated for C₁₅H₁₇ClN₅ [M+H]⁺, 288.1010; found, 288.1036. Elemental analysis calculated for C₁₄H₁₄ClN₅·0.0711H₂O·0.0262CHCl₃: C, 57.66; H, 4.89; N, 23.97, Cl, 13.09. Found: C, 57.81; H, 4.88; N, 23.62; Cl, 13.07.

***N*⁴-(3,4-dichlorophenyl)-*N*⁴,6-dimethyl-7*H*-pyrrolo[2,3-*d*]pyrimidine-2,4-diamine (109)**

After flash chromatography, **109** was obtained as a pale yellow solid (128 mg, 40% over two steps). *R*_f 0.42 (CH₃OH/CHCl₃, 1:10); m.p. 239.2 – 243.9 °C. ¹HNMR (400 MHz, DMSO-*d*₆): δ 2.05 (s, 1 H, 6-CH₃), 3.44 (s, 3 H, NCH₃), 4.58 (s, 1 H, 5-H), 5.69 (s, 2 H, NH₂, D₂O exchanged), 7.24 – 7.27 (m, 1 H, phenyl), 7.57 – 7.65 (m, 2 H, phenyl), 10.74 (s, 1 H, N7-H, D₂O exchanged). HRMS *m/z* calculated for C₁₄H₁₃Cl₂N₅ [M+H]⁺, 322.0621; found, 322.0632. Elemental analysis calculated for C₁₄H₁₃N₅Cl₂·1.1117CH₃CN·0.2422CHCl₃: C, 49.85; H, 4.21; N, 21.58, Cl, 24.36. Found: C, 49.80; H, 4.27; N, 21.49; Cl, 24.31.

6-methoxy-1-(2-methyl-7*H*-pyrrolo[2,3-*d*]pyrimidin-4-yl)-1,2,3,4-tetrahydroquinoline (110)

To the solution of 6-methoxy-1,2,3,4-tetrahydroquinoline **181** (180 mg, 1.1 mmol) in 1,4-dioxane was added 2-methyl-4-chloro-pyrrolopyrimidine **153** (167 mg, 1 mmol). Dry HCl gas was bubbled through before the solution was sealed in a microwave vial. The vial was placed in a microwave reactor and irradiated at 180 °C for six hours. At the end of the reaction, the reaction mixture was evaporated to dryness and suspended in saturated sodium bicarbonate solution (5 mL). The suspension was extracted with ethyl acetate (2 × 20 mL). The organic layer was evaporated and purified through flash chromatography (1 – 2% methanol in chloroform) before **110** was obtained as a white powder (190 mg, 65%). R_f 0.41 (CH₃OH/CHCl₃, 1:10); m.p. 176.1 – 177.5 °C. ¹HNMR (500 MHz, DMSO-*d*₆): δ 1.92 (q, 2 H, CH₂), 2.47 (s, 3 H, 2-CH₃), 2.72 (t, 2 H, CH₂), 3.76 (s, 3 H, OCH₃), 3.99 (t, 2 H, NCH₂), 5.42 – 5.43 (d, 1 H, 5-H, $J = 3.45$), 6.70 – 6.71 (d, 1 H, phenyl, $J = 8.75$), 6.82 – 6.83 (d, 1 H, 6-H, $J = 2.85$), 6.95 – 6.96 (d, 1 H, phenyl, $J = 5.8$), 7.58 (s, 1 H, phenyl), 11.45 (s, 1 H, N7-H, D₂O exchanged). HRMS m/z calculated for C₁₇H₁₈N₄O [M+H]⁺, 295.1553; found, 295.1540. Elemental analysis calculated for C₁₇H₁₈N₄O: C, 69.37; H, 6.16; N, 19.13. Found: C, 69.00; H 6.21; N, 19.13.

4-(6-methoxy-3,4-dihydroquinolin-1(2*H*)-yl)-7*H*-pyrrolo[2,3-*d*]pyrimidin-2-amine (111)

To the solution of 6-methoxy-1,2,3,4-tetrahydroquinoline **181** (180 mg, 1.1 mmol) in 1,4-dioxane was added the pivaloyl protected 2-amino-4-chloro-pyrrolopyrimidine **163**

(252 mg, 1 mmol). Dry HCl gas was bubbled through before the solution was sealed in a microwave vial. The vial was placed in a microwave reactor and irradiated at 180 °C for six hours. At the end of the reaction, the reaction mixture was evaporated to dryness and suspended in saturated sodium bicarbonate solution (5 mL). The suspension was extracted with ethyl acetate (2 × 20 mL). The organic layer was evaporated and dissolved in methanol (5 mL). Sodium hydroxide solution (2 N, 5 mL) was added and the solution was refluxed for three hours. The reaction mixture was evaporated to dryness at the end of the reaction and suspended in water (10 mL). After extraction with ethyl acetate (2 × 20 mL), silica gel was added to the organic layer followed by flash chromatography (1 – 2% methanol in chloroform). The target compound **111** was obtained as a white powder (135 mg, 45% over two steps). R_f 0.27 (CH₃OH/CHCl₃, 1:10); m.p. 192.5 – 195.0 °C. ¹HNMR (500 MHz, DMSO-*d*₆): δ 1.86 – 1.88 (q, 2 H, CH₂), 2.47 (s, 3 H, 2-CH₃), 2.72 (t, 2 H, CH₂), 3.75 (s, 3 H, OCH₃), 3.91 (t, 2 H, NCH₂), 5.27 – 5.28 (d, 1 H, 5-H, $J = 3.6$), 5.64 (s, 2 H, 2-NH₂, D₂O exchanged), 6.60 (d, 1 H, phenyl, $J = 3.55$), 6.68 – 6.69 (d, 1 H, 6-H, $J = 2.9$), 6.70 – 6.71 (d, 1 H, phenyl, $J = 3$), 7.00 – 7.02 (d, 1 H, phenyl, $J = 8.8$), 10.79 (s, 1 H, N7-H, D₂O exchanged). HRMS m/z calculated for C₁₆H₁₇N₅O [M+H]⁺, 296.1506; found, 296.1525. Elemental analysis calculated for C₁₆H₁₇N₅O·0.0451CHCl₃: C, 64.08; H, 5.71; N, 23.29. Found: C, 64.22; H 5.96; N, 22.91.

4-(6-methoxy-3,4-dihydroquinolin-1(2H)-yl)-6-methyl-7H-pyrrolo[2,3-d]pyrimidin-2-amine (112)

To the solution of 6-methoxy-1,2,3,4-tetrahydroquinoline **181** (180 mg, 1.1 mmol) in 1,4-dioxane was added the pivaloyl protected 2-amino-4-chloro-6-methyl-pyrrolopyrimidine **172** (266 mg, 1 mmol). Dry HCl gas was bubbled through before the solution was sealed in a microwave vial. The vial was placed in a microwave reactor and irradiated at 180 °C for six hours. At the end of the reaction, the reaction mixture was evaporated to dryness and suspended in saturated sodium bicarbonate solution (5 mL). The suspension was extracted with ethyl acetate (2 × 20 mL). The organic layer was evaporated and dissolved in methanol (5 mL). Sodium hydroxide solution (2 N, 5 mL) was added and the solution was refluxed for three hours. The reaction mixture was evaporated to dryness at the end of the reaction and suspended in water (10 mL). After extraction with ethyl acetate (2 × 20 mL), silica gel was added to the organic layer followed by flash chromatography (1 – 2% methanol in chloroform). The target compound **112** was obtained as a white powder (154 mg, 50% over two steps). R_f 0.30 (CH₃OH/CHCl₃, 1:10); m.p. 191.6 – 194.2 °C ¹HNMR (500 MHz, DMSO-*d*₆): δ 1.88 (q, 2 H, CH₂), 2.09 (s, 3 H, 6-CH₃), 2.66 (s, 3 H, 2-CH₃), 2.72 (t, 2 H, CH₂), 3.76 (s, 3 H, OCH₃), 3.90 (t, 2 H, NCH₂), 5.03 (s, 1 H, 5-H), 6.35 (s, 2 H, 2-NH₂, D₂O exchanged), 6.70 – 6.72 (d, 1 H, phenyl, $J = 5.9$), 6.80 (d, 1 H, phenyl, $J = 2.75$), 7.00 – 7.02 (d, 1 H, phenyl, $J = 8.8$), 8.33 (s, 1 H, phenyl), 10.91 (s, 1 H, N7-H). HRMS m/z calculated for C₁₇H₁₉N₅O [M+H]⁺, 310.1662; found, 310.1649. Elemental analysis calculated for C₁₇H₁₉N₅O·0.5288H₂O: C, 64.03; H, 6.34; N, 21.96. Found: C, 64.00; H 6.19; N, 22.01.

6-methoxy-1-(7*H*-pyrrolo[2,3-*d*]pyrimidin-4-yl)-1,2,3,4-tetrahydroquinoline (113)

To the solution of 6-methoxy-1,2,3,4-tetrahydroquinoline **181** (180 mg, 1.1 mmol) in 1,4-dioxane was added 4-chloro-pyrrolopyrimidine **180** (153 mg, 1 mmol). Dry HCl gas was bubbled through before the solution was sealed in a microwave vial. The vial was placed in a microwave reactor and irradiated at 180 °C for six hours. At the end of the reaction, the reaction mixture was evaporated to dryness and suspended in saturated sodium bicarbonate solution (5 mL). The suspension was extracted with ethyl acetate (2 × 20 mL). The organic layer was evaporated and purified through flash chromatography (2 – 4% methanol in chloroform) before **113** was obtained as a white powder (210 mg, 75%). R_f 0.50 (CH₃OH/CHCl₃, 1:10); m.p. 173.8 – 175.1 °C ¹H NMR (500 MHz, DMSO-*d*₆): δ 1.90 – 1.93 (q, 2 H, CH₂), 2.72 – 2.75 (t, 2 H, CH₂), 3.77 (s, 3 H, OCH₃), 3.98 – 4.01 (t, 2 H, NCH₂), 5.52 – 5.53 (d, 1 H, 5-H, $J = 1.8$), 6.72 – 6.73 (d, 1 H, phenyl, $J = 5.85$), 6.84 (d, 1 H, 6-H, $J = 2.9$), 7.05 – 7.06 (d, 1 H, phenyl, $J = 8.8$), 8.30 (s, 1 H, phenyl), 11.69 (s, 1 H, N7-H). HRMS m/z calculated for C₁₆H₁₆N₄O [M+H]⁺, 281.1397; found, 281.1424. Elemental analysis calculated for C₁₆H₁₆N₄O: C, 68.38; H, 6.02; N, 19.73. Found: C, 68.38; H 6.02; N, 19.73.

***N*-(4-methoxyphenyl)-*N*,2,7-trimethyl-7*H*-pyrrolo[2,3-*d*]pyrimidin-4-amine (114)**

To **91** (134 mg, 0.5 mmol) in a microwave vial was added anhydrous cesium carbonate (195 mg, 0.6 mmol), anhydrous DMF (1 mL) and iodomethane (0.037 mL, 85 mg, 0.6 mmol). The vial was quickly sealed and reaction mixture was irradiated by microwave under 120 °C for four hours. At the end of the reaction, DMF was evaporated

under vacuum and the dried mixture was suspended in water (5 mL). The suspension was extracted with ethyl acetate (2 × 20 mL). The organic layer was evaporated and purified through flash chromatography (2 – 4% methanol in chloroform) before **114** was obtained as a yellow powder (120 mg, 85%). R_f 0.60 (CH₃OH/CHCl₃, 1:10); m.p. deg. 190 °C. ¹H NMR (400 MHz, DMSO-*d*₆): δ 2.49 (s, 3 H, 2-CH₃), 3.46 (s, 3 H, NCH₃), 3.82 (s, 3 H, OCH₃), 4.52 – 4.53 (d, 1 H, 5-H, $J = 3.2$), 6.78 – 6.79 (d, 1 H, 6-H, $J = 3.6$), 7.03 – 7.05 (d, 2 H, phenyl, $J = 9.2$), 7.25 – 7.28 (d, 2 H, phenyl, $J = 9.2$). Elemental analysis calculated for C₁₆H₁₈N₄O: C, 68.06; H, 6.43; N, 19.84. Found: C, 68.06; H, 6.48; N, 19.75.

***N*-(4-methoxyphenyl)-*N*,2,7-trimethyl-7*H*-pyrrolo[2,3-*d*]pyrimidin-4-amine hydrochloride salt (114·HCl)**

To the solution of **114** (85 mg, 0.3 mmol,) in diethyl ether in the ice bath was bubbled anhydrous HCl gas for 5 min. The salt precipitated from the solution and was collected to give a white solid after drying (68 mg, 70%). Elemental analysis calculated for C₁₆H₁₈N₄O·HCl: C, 60.28; H, 6.01; N, 17.57, Cl, 11.12. Found: C, 59.91; H, 6.04; N, 17.47; Cl, 11.19.

**7-benzyl-N-(4-methoxyphenyl)-N,2-dimethyl-7H-pyrrolo[2,3-d]pyrimidin-4-amine
(115)**

To **91** (134 mg, 0.5 mmol) in a microwave vial was added anhydrous cesium carbonate (195 mg, 0.6 mmol), anhydrous DMF (1 mL) and benzyl bromide (0.072 mL, 103 mg, 0.6 mmol). The vial was quickly sealed and reaction mixture was irradiated by microwave under 120 °C for four hours. At the end of the reaction, DMF was evaporated under vacuum and the dried mixture was suspended in water (5 mL). The suspension was extracted with ethyl acetate (2 × 20 mL). The organic layer was evaporated and purified through flash chromatography (0 – 15% ethyl acetate in hexane) before **115** was obtained as a yellow oil. Recrystallization from acetone/hexane provided **115** as a yellow powder (302 mg, 85%). R_f 0.75 (ethyl acetate/hexane, 1:1); m.p. 102.1 – 103.4 °C. ^1H NMR (400 MHz, DMSO-*d*6): δ 2.48 (s, 3 H, 2-CH₃), 3.47 (s, 3 H, NCH₃), 3.82 (s, 3 H, OCH₃), 4.56 – 4.57 (d, 1 H, 5-H, J = 3.52), 5.27 (s, 1 H, 6-H), 6.86 – 6.87 (d, 1 H, benzyl, J = 3.48), 7.03 – 7.05 (d, 2 H, phenyl, J = 8.84), 7.11 – 7.13 (d, 2 H, phenyl, J = 7.48), 7.23 – 7.30 (m, 4 H, benzyl). Elemental analysis calculated for C₂₂H₂₂N₄O: C, 73.72; H, 6.19; N, 15.63. Found: C, 73.39; H, 6.27; N, 15.58.

**N-(4-methoxyphenyl)-N,2-dimethyl-7-tosyl-7H-pyrrolo[2,3-d]pyrimidin-4-amine
(116)**

To the stirred solution of **91** (134 mg, 0.5 mmol) in dichloromethane (5 mL) was added sodium hydroxide (80 mg, 2 mmol) and tetrabutylammonium hydrogensulfate (33.9 mg, 0.1 mmol). After the solution turned clear, tosyl chloride (190 mg, 1 mmol)

was added and the reaction mixture was stirred at room temperature for six hours. At the end of the reaction, the organic layer was collected and washed with water (2 × 5 mL). The solvent was evaporated under vacuum and the mixture was purified through flash chromatography (0 – 20% ethyl acetate in hexane) before **116** was obtained as a white powder (310 mg, 75%). R_f 0.65 (ethyl acetate/hexane, 1:1); m.p. 195.7 – 197.1 °C. $^1\text{H NMR}$ (500 MHz, DMSO-*d*6): δ 2.36 (s, 3 H, tosyl-CH₃), 2.42 (s, 3 H, tosyl-CH₃), 2.49 (s, 3 H, 2-CH₃), 3.46 (s, 3 H, NCH₃), 3.86 (s, 3 H, OCH₃), 4.65 – 4.66 (d, 1 H, 5-H, $J = 4.05$), 7.05 – 7.06 (d, 2 H, phenyl, $J = 8.8$), 7.27 – 7.28 (d, 2 H, phenyl, $J = 8.8$), 7.42 – 7.43 (d, 2 H, tosyl, $J = 8.1$), 7.95 – 7.97 (d, 2 H, tosyl, $J = 8.35$). HRMS m/z calculated for C₂₂H₂₂N₄O₃S [M+H]⁺, 423.1485; found, 423.1499. Elemental analysis calculated for C₂₂H₂₂N₄O₃S·0.1944CH₃CO₂C₂H₅: C, 62.23; H, 5.40; N, 12.74; S, 7.29. Found: C, 62.10; H 5.41; N, 12.72; S, 7.47.

2-pivalamido-7-tosyl-7H-pyrrolo[2,3-d]pyrimidin-4-yl 4-methylbenzenesulfonate (188)

To the stirred solution of **162** (234 mg, 1 mmol) in dichloromethane (10 mL) was added sodium hydroxide (160 mg, 4 mmol) and tetrabutylammonium hydrogensulfate (68 mg, 0.2 mmol). After the solution turned clear, tosyl chloride (475 mg, 2.5 mmol) was added and the reaction mixture was stirred at room temperature for six hours. At the end of the reaction, the organic layer was collected and washed with water (2 × 10 mL). Small quantity of mono-tosylated product **189** was also present in the organic layer. The solvent was evaporated under vacuum and the mixture was used for next step without

further purification. R_f 0.60 (ethyl acetate/hexane, 1:1). A sample of **188** was purified through flash chromatography (0 – 20% ethyl acetate in hexane) and analyzed by ^1H NMR (400 MHz, DMSO- d_6): δ 1.31 (s, 9 H, Piv), 2.36 (s, 3 H, tosyl- CH_3), 2.42 (s, 3 H, tosyl- CH_3), 6.58 – 6.59 (d, 1 H, 5-H, $J = 4.04$), 7.41 – 7.43 (d, 2 H, tosyl, $J = 8$), 7.45 – 7.47 (d, 2 H, tosyl, $J = 8.16$), 7.79 – 7.80 (d, 1 H, 6-H, $J = 4.08$), 8.08 – 8.10 (d, 2 H, tosyl, $J = 8.4$), 8.31 – 8.33 (d, 2 H, tosyl, $J = 8.44$), 10.15 (s, 1 H, NHPiv, D_2O exchanged).

***N*-(4-oxo-7-tosyl-4,7-dihydro-3*H*-pyrrolo[2,3-*d*]pyrimidin-2-yl)pivalamide (189)**

The mixture containing **188** from the previous step was dissolved in methanol (10 mL). To the solution was added concentrated HCl (1 mL) followed by reflux for one hour. The solvent was then removed under vacuum. The resulted mixture was suspended in saturated sodium bicarbonate solution (10 mL) and extracted with ethyl acetate (2×10 mL). The organic layer was evaporated and purified through flash chromatography (0 – 30% ethyl acetate in hexane) before **189** was obtained as a white solid (290 mg, 75% over two steps). R_f 0.45 (ethyl acetate/hexane, 1:1). ^1H NMR (400 MHz, DMSO- d_6): δ 1.30 (s, 9 H, Piv), 2.39 (s, 3 H, tosyl- CH_3), 6.65 – 6.66 (d, 1 H, 5-H, $J = 3.04$), 7.39 – 7.40 (d, 1 H, 6-H, $J = 3$), 7.44 – 7.45 (d, 2 H, tosyl, $J = 6.62$), 8.18 – 8.19 (d, 2 H, tosyl, $J = 6.52$), 10.15 (s, 1 H, NHPiv, D_2O exchanged), 12.20 (s, 1 H, 3-NH, D_2O exchanged).

***N*-(4-oxo-7-tosyl-4,5,6,7-tetrahydro-3*H*-pyrrolo[2,3-*d*]pyrimidin-2-yl)pivalamide**

(190)

To the solution of **189** (194 mg, 0.5 mmol) in methanol (10 mL) was added palladium hydroxide (45%) on carbon (150 mg). The resulted suspension was hydrogenated (50 psi) in a Parr apparatus under room temperature for four hours. At the end of the reaction, the suspension was filtered through a layer of celite and washed with methanol (40 mL). The filtrate was evaporated to afford **190** (175 mg, 90%) in pure form. R_f 0.43 (ethyl acetate/hexane, 1:1). $^1\text{H NMR}$ (400 MHz, DMSO-*d*₆): δ 1.28 (s, 9 H, Piv), 2.38 (s, 3 H, tosyl-CH₃), 2.64 – 2.68 (t, 2 H, 5-H), 3.88 – 3.92 (t, 2 H, 6-H), 7.37 – 7.39 (d, 2 H, tosyl, $J = 8.04$), 8.03 – 8.05 (d, 2 H, tosyl, $J = 8.08$), 10.97 (s, 1 H, NHPiv, D₂O exchanged), 11.95 (s, 1 H, 3-NH, D₂O exchanged).

***N*-(4-chloro-7-tosyl-6,7-dihydro-5*H*-pyrrolo[2,3-*d*]pyrimidin-2-yl)pivalamide (191)**

To the POCl₃ (5 mL) in a round-bottom flask was added **190** (170 mg, 0.5 mmol) and the mixture was refluxed for 3 hours. After the removal of remaining POCl₃ under vacuum, saturated solution of saturated sodium bicarbonate (10 mL) was carefully added. The mixture was extracted with ethyl acetate (2 × 20 mL). After evaporation, **191** was obtained as a white solid (155 mg, 80%) and used without further purification. R_f 0.60 (ethyl acetate/hexane, 1:1). An analytical sample was purified and analyzed by $^1\text{H NMR}$ (400 MHz, DMSO-*d*₆): δ 1.26 (s, 9 H, Piv), 2.37 (s, 3 H, tosyl-CH₃), 2.99 – 3.03 (t, 2 H, 5-H), 4.06 – 4.09 (t, 2 H, 6-H), 7.36 – 7.38 (d, 2 H, tosyl, $J = 8.08$), 8.21 – 8.23 (d, 2 H, tosyl, $J = 8.04$), 10.16 (s, 1 H, NHPiv, D₂O exchanged).

***N*⁴-(4-methoxyphenyl)-*N*⁴-methyl-7-tosyl-6,7-dihydro-5*H*-pyrrolo[2,3-*d*]pyrimidine-2,4-diamine (192)**

To **191** (122 mg, 0.3 mmol) in a microwave vial was added 4-methoxy-*N*-methylaniline **168** (69 mg, 0.5 mmol) and 1,4-dioxane (3 mL). Anhydrous hydrochloride gas was bubbled through the solution before the vial was sealed. The reaction mixture was then irradiated under microwave at 180 °C for six hours. At end of the reaction, the solvent was removed under vacuum and saturated sodium bicarbonate solution (10 mL) was added to suspend the mixture. After extraction with ethyl acetate (2 × 20 mL), the organic layer was evaporated and purified through flash chromatography (0 – 30% ethyl acetate in hexane) before **192** was obtained as a pale yellow solid (90 mg, 70%). *R*_f 0.52 (ethyl acetate/hexane, 1:1); m.p. 163.9 – 166.4 °C. ¹HNMR (400 MHz, DMSO-*d*₆): δ 2.38 (s, 3 H, tosyl-CH₃), 1.73 (t, 2 H, 5-H), 3.23 (s, 1 H, NCH₃), 3.51 (t, 2 H, 6-H), 3.75 (s, 1 H, OCH₃), 6.20 (s, 2 H, 2-NH₂, D₂O exchanged), 6.90 – 6.93 (d, 2 H, phenyl, *J* = 8.84), 7.10 – 7.13 (d, 2 H, phenyl, *J* = 8.8), 7.34 – 7.36 (d, 2 H, tosyl, *J* = 8.24), 7.91 – 7.93 (d, 2 H, tosyl, *J* = 8.28).

***N*⁴-(4-methoxyphenyl)-*N*⁴-methyl-6,7-dihydro-5*H*-pyrrolo[2,3-*d*]pyrimidine-2,4-diamine (118)**

To the solution of **192** (85 mg, 0.2 mmol) in anhydrous methanol (10 mL) was added magnesium turnings (100 mg). The resulted suspension was sonicated by an ultrasound sonicator for 30 minutes and stirred under room temperature for additional three hours, during which the change of magnesium turnings into cloudy precipitate was observed. At

the end of reaction, the precipitate was filtered through celite and washed with methanol (30 mL). The filtrate was evaporated to afford **118** (77 mg, 90%) in pure form. R_f 0.40 (CH₃OH/CHCl₃, 1:5); m.p. 150.7 – 153.4 °C. ¹HNMR (400 MHz, DMSO-*d*₆): δ 1.79 – 1.83 (t, 2 H, 5-H), 3.05 – 3.09 (t, 2 H, 6-H), 3.26 (s, 1 H, NCH₃), 3.51 (t, 2 H, 6-H), 3.76 (s, 1 H, OCH₃), 5.58 (s, 1 H, N7-H, D₂O exchanged), 6.01 (s, 2 H, 2-NH₂, D₂O exchanged), 6.91 – 6.93 (d, 2 H, phenyl, $J = 8.88$), 7.10 – 7.12 (d, 2 H, phenyl, $J = 8.84$). Elemental analysis calculated for C₁₄H₁₇N₅O·0.1284CH₃CO₂C₂H₅: C, 61.98; H, 6.32; N, 25.81. Found: C, 61.83; H, 6.39; N, 24.73.

***N*-(4-methoxyphenyl)-2-methyl-7-tosyl-7*H*-pyrrolo[2,3-*d*]pyrimidin-4-amine (201)**

To the solution of **90** (127 mg, 0.5 mmol) in dichloromethane (5 mL) was added sodium hydroxide (160 mg, 4 mmol) and tetrabutylammonium hydrogensulfate (68 mg, 0.2 mmol). After the solution turned clear, tosyl chloride (285 mg, 1.5 mmol) was added and the reaction mixture was stirred at room temperature for six hours. At the end of the reaction, the organic layer was collected and washed with water (2 × 5 mL) before the solvent was evaporated under vacuum. The dried mixture was purified through flash chromatography (0 – 20% ethyl acetate in hexane) to afford **201** as a white solid (146 mg, 72%). R_f 0.32 (ethyl acetate/hexane, 1:2); m.p. 215.5 – 218.1 °C. ¹HNMR (400 MHz, DMSO-*d*₆): δ 2.37 (s, 3 H, tosyl-CH₃), 2.46 (s, 3 H, 2-CH₃), 3.75 (s, 3 H, OCH₃), 6.85 (s, 1 H, 5-H), 6.92 – 6.94 (d, 2 H, tosyl, $J = 9.04$), 7.44 – 7.46 (d, 2 H, phenyl, $J = 8.4$), 7.53 – 7.54 (d, 1 H, 6-H, $J = 3.92$), 7.61 – 7.63 (d, 2 H, phenyl, $J = 8.76$), 8.00 – 8.02 (d, 2 H, tosyl, $J = 8.4$), 9.41 (s, 1 H, NH, D₂O exchanged).

***N*-(4-methoxyphenyl)-2-methyl-7-tosyl-6,7-dihydro-5*H*-pyrrolo[2,3-*d*]pyrimidin-4-amine (202)**

To the solution of **201** (122 mg, 0.3 mmol) in methanol (10 mL) was added palladium hydroxide (45%) on carbon (150 mg). The resulted suspension was hydrogenated (50 psi) in a Parr apparatus under room temperature for four hours. At the end of the reaction, the suspension was filtered through a layer of celite and washed with methanol (40 mL). The filtrate was evaporated to afford **202** (104 mg, 84%) in pure form. R_f 0.30 (ethyl acetate/hexane, 1:2). $^1\text{H NMR}$ (400 MHz, DMSO-*d*₆): δ 2.33 (s, 3 H, 2-CH₃), 2.37 (s, 3 H, tosyl-CH₃), 2.78 – 2.81 (t, 2 H, 5-H), 3.72 (s, 3 H, OCH₃), 3.92 – 3.96 (t, 2 H, 6-H), 6.85 – 6.88 (d, 2 H, phenyl, $J = 9$), 7.39 – 7.41 (d, 2 H, tosyl, $J = 6.2$), 7.45 – 7.47 (d, 2 H, phenyl, $J = 8.92$), 7.89 – 7.91 (d, 2 H, tosyl, $J = 8.16$), 8.61 (s, 1 H, NH, D₂O exchanged).

***N*-(4-methoxyphenyl)-*N*,2-dimethyl-7-tosyl-6,7-dihydro-5*H*-pyrrolo[2,3-*d*]pyrimidin-4-amine (203)**

To the solution of **202** (100 mg, 0.24 mmol) in anhydrous DMF (1 mL) was added sodium hydride (12 mg, 0.5 mmol) and iodomethane (0.019 mL, 43 mg, 0.3 mmol). The resulted suspension was stirred under room for 30 min. Then the DMF was removed under vacuum and the reaction mixture was suspended in water (5 mL). Extraction with ethyl acetate (2 × 10 mL) and evaporation of the organic layer afford **203** in pure form (98 mg, 97%). R_f 0.60 (ethyl acetate/hexane, 1:2). $^1\text{H NMR}$ (400 MHz, CDCl₃): δ 1.85 – 1.89 (t, 2 H, 5-H), 2.36 (s, 3 H, 2-CH₃), 2.40 (s, 3 H, tosyl-CH₃), 3.39 (s, 3 H, NCH₃), 3.65 (t, 2 H, 6-H), 3.72 (s, 3 H, OCH₃), 6.86 – 6.88 (d, 2 H, phenyl, $J = 8.84$), 7.17 – 7.19

(d, 2 H, phenyl, $J = 10.56$), 7.25 – 7.29 (d, 2 H, tosyl, $J = 7.2$), 7.98 – 8.00 (d, 2 H, tosyl, $J = 8.28$).

***N*-(4-methoxyphenyl)-*N*,2-dimethyl-6,7-dihydro-5*H*-pyrrolo[2,3-*d*]pyrimidin-4-amine (117)**

To the solution of **203** (90 mg, 0.21 mmol) in anhydrous methanol (10 mL) was added magnesium turnings (100 mg). The resulted suspension was sonicated by an ultrasound sonicator for 30 minutes and stirred under room temperature for additional three hours, during which the change of magnesium turnings into cloudy precipitate was observed. At the end of reaction, the precipitate was filtered through celite and washed with methanol (30 mL). The filtrate was evaporated to afford **117** (52 mg, 90%) in pure form. R_f 0.40 (CH₃OH/CHCl₃, 1:10); m.p. 179.4 – 181.4°C ¹HNMR (400 MHz, DMSO-*d*₆): δ 1.85 – 1.89 (t, 2 H, 5-H), 2.23 (s, 3 H, 2-CH₃), 3.10 – 3.15 (t, 2 H, 6-H), 3.30 (s, 1 H, NCH₃), 3.76 (s, 1 H, OCH₃), 6.30 (s, 1 H, N7-H, D₂O exchanged), 6.92 – 6.94 (d, 2 H, phenyl, $J = 8.24$), 7.13 – 7.15 (d, 2 H, phenyl, $J = 8.2$). Elemental analysis calculated for C₁₅H₁₈N₄O·0.2758CH₃CO₂C₂H₅: C, 65.65; H, 6.91; N, 19.02;. Found: C, 65.41; H, 6.83; N, 19.14.

4-chloro-7-((4-methoxyphenyl)diphenylmethyl)-2-methyl-7H-pyrrolo[2,3-*d*]pyrimidine (210)

To the solution of **153** (160 mg, 1 mmol) and (chloro(4-methoxyphenyl)methylene)dibenzene (339 mg, 1.1 mmol) in anhydrous DMF (1 mL) was added sodium hydride (27 mg, 1.1 mmol). The resulted suspension was stirred under room temperature for 1 hour. Then water (5 mL) was added to the reaction mixture and extracted with *tert*-butyl methyl ether (2 × 10 mL). The organic layer was dried over sodium sulfate and evaporated to afford **210** in a yellow solid (364 mg, 83%). R_f 0.65 (ethyl acetate/hexane, 1:2). $^1\text{H-NMR}$ (400 MHz, DMSO): δ 2.23 (s, 3 H, 2-CH₃), 3.74 (s, 3 H, OCH₃), 6.63 – 6.64 (d, 1 H, 5-H, $J = 3.84$), 6.89 – 6.91 (d, 2 H, phenyl, $J = 8.96$), 7.03 – 7.05 (d, 2 H, phenyl, $J = 8.92$), 7.10 – 7.12 (d, 1 H, 6-H, $J = 6.96$), 7.28 – 7.33 (m, 10 H, benzene).

(±)-2-(4-methoxyphenyl)-2-(7-((4-methoxyphenyl)diphenylmethyl)-2-methyl-7H-pyrrolo[2,3-*d*]pyrimidin-4-yl)acetonitrile (±-212)

To the solution of **210** (351 mg, 0.8 mmol) and 2-(4-methoxyphenyl)acetonitrile (0.136 mL, 1 mmol) in anhydrous DMF (1 mL) was added sodium hydride (24 mg, 1 mmol). The resulted suspension was stirred under room temperature for two hours. Then water (5 mL) was added to the reaction mixture and extracted with *tert*-butyl methyl ether (2 × 10 mL). The organic layer was evaporated and purified through flash chromatography to afford (±)-**212** (272 mg, 62%) in a yellow solid. R_f 0.45 (ethyl acetate/hexane, 1:2); $^1\text{H-NMR}$ (400 MHz, CDCl₃): δ 2.38 (s, 3 H, 2-CH₃), 3.81 (s, 6 H, OCH₃), 5.40 (s, 1 H, CH), 6.43 – 6.44 (d, 1 H, 5-H, $J = 3.8$), 6.78 – 6.79 (d, 2 H, phenyl,

$J = 8.92$), 6.90 – 6.93 (d, 2 H, phenyl, $J = 11.8$), 7.07 (d, 1 H, 6-H, $J = 2.04$), 7.08 – 7.26 (m, 10 H, benzene).

(±)-4-(1-(4-methoxyphenyl)ethyl)-2-methyl-7H-pyrrolo[2,3-*d*]pyrimidine (119)

To the solution of **212** (220 mg, 0.4 mmol) in anhydrous THF (1 mL) was added diisobutylaluminium hydride (0.5 mL, 1 M). The solution was stirred under room temperature for four hours. The formation of aldehyde **217** was detected on TLC and ^1H NMR. Then methanol (5 mL) was added to quench the unreacted DIBAL-H and the solution was evaporated to dryness. Water (5 mL) was added to the mixture followed by extraction with *tert*-butyl methyl ether (2×10 mL). The organic layer was evaporated and to the mixture containing the aldehyde **217** was added potassium hydroxide (100 mg), water (1 mL), ethylene glycol (5 mL) and hydrazine hydrate (1 mL). The resulting reaction mixture was heated at 150 °C for two hours with reflux condenser. Then the reaction temperature was elevated to 180 °C and the condenser was replaced with a Dean-Stark apparatus to collect the evaporated water and hydrazine. The temperature was maintained at 180 °C for three hours before cooled to room temperature. Water (5 mL) was added to the reaction mixture and extracted with ethyl acetate (2×10 mL). The organic layer was evaporated and purified through flash chromatography (2 – 4% methanol in chloroform) before **119** was obtained as a white powder. R_f 0.40 (CH₃OH/CHCl₃, 1:10); m.p. 167.8 – 171.6 °C. ^1H NMR (400 MHz, CDCl₃): δ 1.27 (s, 3 H, CH-CH₃), 2.13 (s, 3 H, 2-CH₃), 3.84 (s, 3 H, OCH₃), 4.23 – 4.25 (q, 1 H, CH), 6.75 (d,

1 H, 5-H, $J = 2.28$), 7.05 – 7.09 (d, 2 H, phenyl, $J = 13$), 7.61 – 7.63 (d, 2 H, phenyl, $J = 8.68$), 8.14 (s, 1 H, 6-H), 9.08 (s, 1 H, N7-H, D₂O exchanged).

General procedure for the synthesis of 120 – 122, 124

To the solution of 4-methoxy-*N*-methylaniline **168** (151 mg, 1.1 mmol) in 1,4-dioxane (2 mL) was added the corresponding halo-substituted bicyclic heterocycles (1 mmol of **218**, **219**, **220** or **221**). Dry HCl gas was bubbled through before the solution was sealed in a microwave vial. The vial was placed in a microwave reactor and irradiated at 180 °C for six hours. At the end of the reaction, the reaction mixture was evaporated to dryness and suspended in saturated sodium bicarbonate solution (5 mL). The suspension was extracted with ethyl acetate (2 × 20 mL) and purified by flash chromatography.

N-(4-methoxyphenyl)-*N*-methyl-1*H*-pyrrolo[3,2-*c*]pyridin-4-amine (**120**)

After flash chromatography (0 – 1% methanol in chloroform), **120** was obtained as an off-white solid (172 mg, 68%). R_f 0.20 (CH₃OH/CHCl₃, 1:10); m.p. 192.9 – 195.8 °C. ¹HNMR (400 MHz, DMSO-*d*₆): δ 3.40 (s, 3 H, *N*CH₃), 3.79 (2s, 3 H, OCH₃), 4.88 (s, 1 H, 3-H), 6.79 – 6.80 (d, 2 H, phenyl, $J = 5.8$), 6.90 – 6.91 (d, 1 H, 2-H, $J = 2.12$), 6.95 – 6.97 (d, 2 H, phenyl, $J = 6.96$), 7.14 – 7.16 (d, 1 H, 7-H, $J = 8.72$), 7.76 – 7.77 (d, 1 H, 6-H, $J = 5.76$), 11.16 (s, 1 H, N1-H, D₂O exchanged). Elemental analysis calculated for C₁₅H₁₅N₃O·0.2284H₂O: C, 69.99; H, 6.05; N, 16.32. Found: C, 70.03; H, 5.89; N, 16.09.

***N*-(4-methoxyphenyl)-*N*-methyl-1*H*-pyrrolo[2,3-*b*]pyridin-4-amine (121)**

After flash chromatography (0 – 1% methanol in chloroform), **121** was obtained as a white solid (106 mg, 42%). R_f 0.48 (CH₃OH/CHCl₃, 1:5); m.p. 179.7 – 182.2 °C. ¹HNMR (400 MHz, DMSO-*d*₆): δ 3.33 (s, 3 H, NCH₃), 3.79 (s, 3 H, OCH₃), 5.01 (s, 1 H, 3-H), 6.38 – 6.40 (d, 2 H, phenyl, $J = 5.52$), 6.91 (d, 1 H, 2-H, $J = 2.12$), 6.96 – 6.98 (d, 2 H, phenyl, $J = 7.52$), 7.15 – 7.17 (t, 1 H, 5-H), 7.94 – 7.95 (t, 1 H, 6-H), 11.20 (s, 1 H, N1-H, D₂O exchanged). Elemental analysis calculated for C₁₅H₁₅N₃O·0.1169 CH₃CO₂C₂H₅: C, 70.48; H, 6.09; N, 15.94. Found: C, 70.66; H, 6.18; N, 15.77.

***N*-(4-methoxyphenyl)-*N*-methyl-1*H*-imidazo[4,5-*c*]pyridin-4-amine (122)**

After flash chromatography (0 – 1% methanol in chloroform), **122** was obtained as a brown oil-like liquid (157 mg, 62%). R_f 0.55 (CH₃OH/CHCl₃, 1:5). ¹HNMR (400 MHz, DMSO-*d*₆): δ 3.63 (s, 3 H, NCH₃), 3.75 (s, 3 H, OCH₃), 6.85 – 6.88 (d, 2 H, phenyl, $J = 8.84$), 6.93 – 6.94 (d, 1 H, 7-H, $J = 5.56$), 7.08 – 7.10 (d, 2 H, phenyl, $J = 8.88$), 7.78 – 7.80 (d, 1 H, 6-H, $J = 5.56$), 7.98 (s, 1 H, 2-H), 12.53 (s, 1 H, N1-H, D₂O exchanged).

***N*-(4-methoxyphenyl)-*N*-methylpyrido[3,4-*b*]pyrazin-5-amine (124)**

After flash chromatography (0 – 1% methanol in chloroform), **124** was obtained as a dark oil-like liquid (138 mg, 52%). R_f 0.40 (CH₃OH/CHCl₃, 1:5). ¹HNMR (400 MHz, DMSO-*d*₆): δ 3.52 (s, 3 H, NCH₃), 3.73 (s, 3 H, OCH₃), 6.82 – 6.85 (d, 2 H, phenyl, $J =$

8.84), 7.01 – 7.03 (d, 2 H, phenyl, $J = 8.88$), 7.31 – 7.32 (d, 1 H, 8-H, $J = 5.76$), 8.34 – 8.35 (d, 1 H, 7-H, $J = 5.76$), 8.49 (d, 1 H, 3-H, $J = 1.72$), 8.86 (d, 1 H, 2-H, $J = 1.72$).

***tert*-Butyl 4-bromo-1*H*-indole-1-carboxylate (223)**

To the solution of 4-bromoindole **222** (196 mg, 1 mmol) in anhydrous THF (5 mL) was added triethylamine (0.139 mL, 1 mmol), 4-dimethylaminopyridine (20 mg) and di-*tert*-butyl dicarbonate (240 mg, 1.1 mmol). The reaction mixture was stirred under room temperature for four hours. At the end of reaction, methanol (5 mL) was added to the solution to quench the unreacted Boc anhydride. The reaction mixture was then evaporated to dryness and suspended in water (10 mL). After extraction with *tert*-butyl methyl ether (2 × 20 mL), the organic layer was dried and evaporated to give **233** as a colorless liquid (275 mg, 93%). R_f 0.80 (ethyl acetate/hexane, 1:2). $^1\text{H NMR}$ (400 MHz, DMSO- d_6): δ 1.64 (s, 9 H, Boc-CH₃), 6.67 – 6.68 (d, 1 H, 3-H, $J = 3.72$), 7.26 – 7.31 (t, 1 H, 6-H), 7.48 – 7.49 (d, 1 H, 6-H, $J = 7.72$), 7.80 – 7.81 (d, 1 H, 2-H, $J = 3.76$), 8.08 – 8.10 (d, 1 H, 5-H, $J = 8.32$).

4-Bromo-1-((4-methoxyphenyl)diphenylmethyl)-1*H*-indole (224)

To the solution of 4-bromoindole **222** (196 mg, 1 mmol) and (chloro(4-methoxyphenyl)methylene) dibenzene (339 mg, 1.1 mmol) in anhydrous DMF (1 mL) was added sodium hydride (27 mg, 1.1 mmol). The resulted suspension was stirred under room temperature for 1 hour. Then water (5 mL) was added to the reaction mixture and

extracted with *tert*-butyl methyl ether (2 × 10 mL). The organic layer was dried over sodium sulfate and evaporated to afford **224** in a white solid (421 mg, 90%). R_f 0.70 (ethyl acetate/hexane, 1:2). ¹HNMR (400 MHz, DMSO): δ 3.74 (s, 3 H, OCH₃), 6.40 – 6.42 (d, 1 H, 3-H, *J* = 6.84), 6.49 – 6.50 (d, 2 H, phenyl, *J* = 3.96), 6.70 – 6.73 (t, 1 H, 6-H), 6.92 – 7.11 (m, 15 H, aromatic H).

***tert*-butyl 4-((4-methoxyphenyl)(methyl)amino)-1*H*-indole-1-carboxylate (225)**

Into a microwave vial was added the Boc-protected **223** (236 mg, 0.8 mmol), 4-methoxy-*N*-methylaniline **168** (137 mg, 1 mmol), palladium acetate (11.2 mg, 5 mol%), Xphos (47.6 mg, 10 mol%), potassium *tert*-butoxide (112 mg, 1 mmol). The vial was sealed, connected to vacuum to remove the oxygen and back-filled with nitrogen. After three rounds of vacuum-fill cycle, toluene (3 mL) was injected through the polymer septum. The vial was then placed in a microwave reactor and irradiated at 140 °C for four hours. At the end of the reaction, ethyl acetate (10 mL) was added to the vial and the mixture was filtered. The filtrate was evaporated to dryness and purified through flash chromatography (0 – 10% ethyl acetate in hexane) before **225** was afforded as a white solid (180 mg, 64%). R_f 0.55 (ethyl acetate/hexane, 1:2). ¹HNMR (400 MHz, DMSO-*d*₆): δ 1.61 (s, 9 H, Boc-CH₃), 3.28 (s, 3 H, NCH₃), 3.70 (s, 3 H, OCH₃), 5.86 – 5.87 (d, 1 H, 3-H, *J* = 3.80), 6.83 (s, 1h, 5-H), 6.91 – 6.93 (d, 2 H, phenyl, *J* = 7.76), 7.26 – 7.31 (t, 1 H, 6-H), 7.43 – 7.44 (d, 1 H, 2-H, *J* = 3.8), 7.74 – 7.77 (d, 2 H, phenyl, *J* = 8.28), 8.32 (s, 1 H, 7-H).

***N*-(4-methoxyphenyl)-1-((4-methoxyphenyl)diphenylmethyl)-*N*-methyl-1*H*-indol-4-amine (226)**

Into a microwave vial was added the N1-protected **224** (374 mg, 0.8 mmol), 4-methoxy-*N*-methylaniline **168** (137 mg, 1 mmol), palladium acetate (11.2 mg, 5 mol%), Xphos (47.6 mg, 10 mol%), potassium *tert*-butoxide (112 mg, 1 mmol). The vial was sealed, connected to vacuum to remove the oxygen and back-filled with nitrogen. After three rounds of vacuum-fill cycle, toluene (3 mL) was injected through the polymer septum. The vial was then placed in a microwave reactor and irradiated at 140 °C for four hours. At the end of the reaction, ethyl acetate (10 mL) was added to the vial and the mixture was filtered. The filtrate was evaporated to dryness and purified through flash chromatography (0 – 10% ethyl acetate in hexane) before **226** was afforded as a pale yellow solid (318 mg, 76%). R_f 0.60 (ethyl acetate/hexane, 1:2). $^1\text{H NMR}$ (400 MHz, CDCl_3): δ 3.40 (s, 3 H, NCH_3), 3.80 (s, 3 H, OCH_3), 3.82 (s, 3 H, OCH_3), 5.93 – 5.94 (d, 1 H, 3-H, $J = 3.36$), 6.26 – 6.28 (d, 2 H, phenyl, $J = 8.16$), 6.71 – 7.19 (m, 20 H, aromatic H).

***N*-(4-methoxyphenyl)-*N*-methyl-1*H*-indol-4-amine (123)**

To the solution of **225** or **226** (0.5 mmol) in THF (2 mL) under 0 °C was added trifluoroacetic acid (0.5 mL). The reaction mixture was continued to stirred under 0 °C for one hour before evaporated to dryness. Saturated sodium bicarbonate solution (5 mL) was added to the mixture. After extraction with *tert*-butyl methyl ether (2 × 20 mL), the organic layer was evaporated and purified through flash chromatography (0 – 10% ethyl

acetate in hexane) before **123** was obtained as an oil-like liquid (115 mg, 92%). R_f 0.52 (CH₃OH/CHCl₃, 1:10). ¹HNMR (400 MHz, DMSO-*d*₆): δ 3.28 (s, 3 H, NCH₃), 3.69 (s, 3 H, OCH₃), 5.71 – 5.72 (d, 1 H, 3-H, $J = 3.76$), 6.67 – 6.68 (d, 2 H, phenyl, $J = 7.28$), 6.79 – 7.11 (m, 5 H, aromatic H), 8.33 (s, 1 H, 7-H), 11.03 (s, 1 H, N1-H, D₂O exchanged).

5-methyl-7H-pyrrolo[2,3-*d*]pyrimidine-2,4-diamine (38)

To the solution of hydroxyacetone (6.85 mL, 7.4 g, 0.1 mol) and triethylamine (14 mL) in methanol (70 mL) was slowly added malononitrile (6.30 mL, 6.61 g, 0.1 mol). The resulted dark red solution was stirred under room temperature for 30 min. After evaporating the solvent and dried under vacuum, the residue containing the furan **36** was dissolved in anhydrous methanol (120 mL). To the resulted solution was added guanidine carbonate (5.4 g, 0.6 mol) and sodium methoxide (3.24 g, 0.6 mol) and reflux for 24 hours. Then the solvent was evaporated and the residue was purified with column chromatography (2 – 5% methanol in chloroform) to afford **38** as a yellow solid (5.05 g, 31% over two steps). R_f 0.35 (CH₃OH/CHCl₃, 1:5). ¹HNMR (300 MHz, DMSO-*d*₆): δ 2.23 (s, 3 H, 5-CH₃), 5.65 (s, 2 H, 4-NH₂, D₂O exchanged), 6.24 (s, 2 H, 2-NH₂, D₂O exchanged), 6.48 (s, 1 H, 6-H), 10.32 (s, 1 H, N7-H, D₂O exchanged).

5-methyl-7H-pyrrolo[2,3-*d*]pyrimidin-4-amine (43)

To the solution of acetamide **39** (2.30 g, 20 mmol) and malononitrile (1.32 g, 20 mmol) in methanol (10 mL) was slowly added sodium hydroxide (2 N solution in water) until

pH 12. The reaction mixture was stirred under 50 °C for one hour. Then hydrochloric acid (1 N) was added to adjust the pH to 7. After the evaporation of methanol, the remaining mixture was extracted with ethyl acetate (2 × 20 mL). The organic layer containing the pyrrole **40** was dried with sodium sulfate before evaporated to dryness. Then the residue was added triethyl orthoformate (5 mL) and refluxed for two hours. At the end of the reaction, the remaining triethyl orthoformate was removed under vacuum and the residue containing the ethoxyimine **41** was dissolved in 7 N solution of ammonia in methanol (15 mL) at 0 °C. The solution was then sealed in a microwave vessel and stirred under room temperature for 12 hours. After removing the methanol under vacuum, the residue containing **42** was dissolved in anhydrous ethanol (10 mL) and added sodium methoxide (1.08 g, 20 mmol). The resulted mixture was reflux for two hours before evaporated to dryness and purified through column chromatography (2 – 5% methanol in chloroform) to afford **43** as a yellow solid (355 mg, 12% over four steps). R_f 0.50 (CH₃OH/CHCl₃, 1:5). ¹HNMR (300 MHz, DMSO-*d*₆): δ 2.33 (s, 3 H, 6-CH₃), 6.40 (s, 2 H, 4-NH₂, D₂O exchanged), 6.80 (s, 1 H, 6-H), 7.95 (s, 1 H, 2-H), 11.12 (s, 1 H, N7-H, D₂O exchanged).

General procedure for the synthesis of target compounds 130 – 135

To the solution of pyrrolo[2,3-*d*]pyrimidine **38** or **43** (1 mmol) and the thiophenol (2 mmol) in ethanol (10 mL) under reflux was added iodine (254 mg, 2 mmol) in several portions. The reflux continued for six hours before cooled to room temperature and added 1 N sodium thiosulfate solution in water (10 mL). After the evaporation of ethanol, the

remaining water layer was extracted with ethyl acetate (2×20 mL). The organic layer was then evaporated to dryness and purified through column chromatography. The purified intermediate **226 – 231** was dissolved in anhydrous DMF (1 mL). To the solution was added cesium carbonate (326 mg, 1 mmol) and 5-chloropent-1-yne **232** (0.11 mL, 103 mg, 1 mmol). The reaction mixture was sealed in a microwave vial and irradiated in a microwave reactor at 80 °C for two hours. At the end of the reaction, the solvent was removed under vacuum and the residues were suspended in water (5 mL). The suspension was extracted by ethyl acetate (2×15 mL) before the organic layer was evaporated and purified through column chromatography.

6-((2-methoxyphenyl)thio)-5-methyl-7-(pent-4-yn-1-yl)-7H-pyrrolo[2,3-d]pyrimidin-4-amine (130)

After column chromatography (0 – 1% methanol in chloroform), **130** was afforded as a yellow solid (92 mg, 25% over two steps). R_f 0.40 (CH₃OH/CHCl₃, 1:10); m.p. 116.9 – 119.2 °C. ¹HNMR (400 MHz, DMSO-*d*₆): δ 1.69 – 1.73 (t, 2 H, CH₂), 2.07 – 2.11 (m, 2 H, CH₂), 2.47 (s, 3 H, 5-CH₃), 2.76 (s, 1 H, CH), 3.69 (s, 3 H, OCH₃), 4.14 (t, 2 H, CH₂), 6.50 – 6.52 (d, 1 H, phenyl, $J = 7.8$), 6.55 – 6.56 (m, 1 H, phenyl), 6.75 – 6.77 (d, 1 H, phenyl, $J = 8.08$), 6.88 (s, 2 H, 4-NH₂, D₂O exchanged), 7.19 – 7.23 (t, 1 H, phenyl), 8.10 (s, 1 H, 2-H). HRMS m/z calculated for C₁₉H₂₀N₄OS [M+H]⁺, 353.1431; found, 353.1431. Elemental analysis calculated for C₁₉H₂₀N₄OS: C, 64.75; H, 5.72; N, 15.90; S, 9.10. Found: C, 64.48; H, 5.87; N, 15.55; S, 9.13.

6-((3-methoxyphenyl)thio)-5-methyl-7-(pent-4-yn-1-yl)-7H-pyrrolo[2,3-d]pyrimidin-4-amine (131)

After column chromatography (0 – 1% methanol in chloroform), **131** was afforded as a yellow solid (95 mg, 27% over two steps). R_f 0.40 (CH₃OH/CHCl₃, 1:10); m.p. 130.2 – 133.0 °C. ¹HNMR (400 MHz, DMSO-*d*₆): δ 1.71 – 1.74 (t, 2 H, CH₂), 2.07 – 2.10 (m, 2 H, CH₂), 2.41 (s, 3 H, 5-CH₃), 2.73 (s, 1 H, CH), 3.90 (s, 3 H, OCH₃), 4.09 – 4.13 (t, 2 H, CH₂), 6.29 – 6.31 (d, 1 H, phenyl, $J = 7.6$), 6.79 – 6.83 (m, 1 H, phenyl), 6.86 (s, 2 H, 4-NH₂, D₂O exchanged), 7.03 – 7.05 (d, 1 H, phenyl, $J = 7.72$), 7.13 – 7.15 (t, 1 H, phenyl), 8.10 (s, 1 H, 2-H). HRMS m/z calculated for C₁₉H₂₀N₄OS [M+H]⁺, 353.1431; found, 353.1438. Elemental analysis calculated for C₁₉H₂₀N₄OS·0.3776CH₃COCH₃: C, 64.59; H, 5.99; N, 14.97; S, 8.57. Found: C, 64.70; H, 5.95; N, 14.98; S, 8.48.

6-((4-methoxyphenyl)thio)-5-methyl-7-(pent-4-yn-1-yl)-7H-pyrrolo[2,3-d]pyrimidine-2,4-diamin (132)

After column chromatography (0 – 2% methanol in chloroform), **132** was afforded as a white solid (149 mg, 40% over two steps). R_f 0.40 (CH₃OH/CHCl₃, 1:10); m.p. 147.2 – 149.1 °C. ¹HNMR (300 MHz, DMSO-*d*₆): δ 1.65 (s, 2 H, CH₂), 2.06 (s, 3 H, 5-CH₃), 2.42 (s, 2 H, CH₂), 2.76 (s, 1 H, CH), 3.69 (s, 3 H, OCH₃), 3.94 (s, 2 H, CH₂), 5.76 (s, 2 H, 4-NH₂, D₂O exchanged), 6.36 (s, 2 H, 2-NH₂, D₂O exchanged), 6.86 – 6.88 (d, 2 H, phenyl, $J = 6.75$), 6.99 – 7.01 (d, 2 H, phenyl, $J = 6.84$). HRMS m/z calculated for C₁₉H₂₁N₅OS [M+H]⁺, 368.1540; found, 368.1545. Elemental analysis calculated for C₁₉H₂₁N₅OS·0.2287H₂O: C, 61.41; H, 5.82; N, 18.85; S, 8.63. Found: C, 61.39; H, 5.61; N, 18.84; S, 8.67.

6-((3,4-dimethoxyphenyl)thio)-5-methyl-7-(pent-4-yn-1-yl)-7H-pyrrolo[2,3-*d*]pyrimidine-2,4-diamine (133)

After column chromatography (0 – 2% methanol in chloroform), **133** was afforded as a white solid (135 mg, 34% over two steps). R_f 0.45 (CH₃OH/CHCl₃, 1:10); m.p. 162.5 – 187.5 °C. ¹HNMR (400 MHz, DMSO-*d*₆): δ 1.65 (t, 2 H, CH₂), 2.09 (s, 3 H, 5-CH₃), 2.42 (t, 2 H, CH₂), 2.79 (s, 1 H, CH), 3.38 (s, 3 H, OCH₃), 3.69 (s, 3 H, OCH₃), 3.94 – 3.98 (s, 2 H, CH₂), 5.75 (s, 2 H, 4-NH₂, D₂O exchanged), 6.32 (s, 2 H, 2-NH₂, D₂O exchanged), 6.45 – 6.48 (dd, 1 H, phenyl), 6.74 – 6.75 (d, 1 H, phenyl, $J = 2.12$), 6.86 – 6.89 (d, 1 H, phenyl, $J = 8.52$). HRMS m/z calculated for C₂₀H₂₃N₅O₂S [M+H]⁺, 398.1645; found, 398.1653. Elemental analysis calculated for C₂₀H₂₃N₅O₂S: C, 60.43; H, 5.83; N, 17.62; S, 8.07. Found: C, 60.28; H, 5.82; N, 17.54; S, 8.00.

5-methyl-7-(pent-4-yn-1-yl)-6-((3,4,5-trimethoxyphenyl)thio)-7H-pyrrolo[2,3-*d*]pyrimidine-2,4-diamine (134)

After column chromatography (0 – 1% methanol in chloroform), **134** was afforded as a white solid (128 mg, 30% over two steps). R_f 0.45 (CH₃OH/CHCl₃, 1:10); m.p. 146.5 – 149.5 °C. ¹HNMR (300 MHz, DMSO-*d*₆): δ 1.17 – 1.22 (m, 2 H, CH₂), 1.68 (m, 2 H, CH₂), 2.07 (m, 3 H, 5-CH₃), 2.42 (s, 2 H, CH₂), 2.74 (s, 1 H, CH), 3.06 – 3.84 (m, 9 H, OCH₃), 3.98 (s, 2 H, CH₂), 5.79 (s, 2 H, 4-NH₂, D₂O exchanged), 6.30 (s, 2 H, 2-NH₂, D₂O exchanged), 6.40 (s, 2 H, phenyl). HRMS m/z calculated for C₂₁H₂₅N₅O₃S [M+H]⁺, 428.1751; found, 428.1763. Elemental analysis calculated for C₂₁H₂₅N₅O₃S·0.4339 CH₃COCH₃: C, 59.17; H, 6.15; N, 15.47; S, 7.08. Found: C, 59.38; H, 6.18; N, 15.48; S, 8.16.

6-((2,3-dihydrobenzo[*b*][1,4]dioxin-6-yl)thio)-7-(3-(isopropylamino)propyl)-5-methyl-7*H*-pyrrolo[2,3-*d*]pyrimidin-4-amine (135)

After column chromatography (0 – 2% methanol in chloroform), **135** was afforded as a white solid (124 mg, 30% over two steps). R_f 0.50 (CH₃OH/CHCl₃, 1:10); m.p. 178.5 – 182.2 °C. ¹HNMR (400 MHz, DMSO-*d*₆): δ 0.86 – 0.87 (d, 6 H, CH₃, J = 6.16), 1.64 (t, 2 H, CH₂), 2.30 (t, 2 H, CH₂), 2.48 (s, 3 H, 5-CH₃), 2.49 (s, 1 H, CH₂), 4.01 (t, 1 H, CH), 4.17 (m, 5 H, OCH₂ and NH), 6.45 (s, 1 H, phenyl), 6.46 – 6.47 (d, 1 H, phenyl, J = 2.2), 6.78 – 6.80 (d, 1 H, phenyl, J = 8.44), 6.81 (s, 2 H, 4-NH₂, D₂O exchanged), 8.06 (s, 1 H, 2-H). HRMS m/z calculated for C₂₁H₂₇N₅O₂S [M+H]⁺, 414.1958; found, 414.1975. Elemental analysis calculated for C₂₁H₂₇N₅O₂S·0.1107CH₃(CH₂)₄CH₃·1.3465H₂O: C, 58.17; H, 7.04; N, 15.66; S, 7.17. Found: C, 58.19; H, 6.67; N, 15.47; S, 7.15.

General procedure for the synthesis of target compounds 136 – 143

To a microwave vial was added pyrrolo[2,3-*d*]pyrimidine **172** (266 mg, 1 mmol), cesium carbonate (326 mg, 1 mmol) and corresponding alkylating reagent (1 mmol). DMF (1 mL) was added to the mixture before the vial was sealed and placed in a microwave reactor. The reaction was irradiated at 80 °C for three hours. At the end of the reaction, the solvent was removed under vacuum and the residues were suspended in water (5 mL). The suspension was extracted by ethyl acetate (2 × 15 mL). After the organic layer was evaporated, the residue was dissolved in methanol (5 mL) and was added 1 N sodium hydroxide solution. The mixture was refluxed for three hours. Methanol was removed by vacuum and the remaining water suspension was extracted with ethyl acetate (2 × 20 mL). The organic layer was evaporated and purified through

column chromatography to afford the final compounds.

7-Benzyl-4-chloro-6-methyl-7*H*-pyrrolo[2,3-*d*]pyrimidin-2-amine (136)

After column chromatography (0 – 20% ethyl acetate in hexane), **136** was obtained as a pale yellow powder (228 mg, 84%). R_f 0.75 (ethyl acetate/hexane 1:1); m.p. 144.1 – 145.6 °C. $^1\text{H NMR}$ (500 MHz, $\text{DMSO-}d_6$): δ 2.21 (s, 3 H, 6- CH_3), 5.29 (s, 1 H, CH_2), 6.13 (s, 1 H, 5-H), 6.55 (s, 2 H, 2- NH_2 , D_2O exchanged), 7.05 – 7.06 (d, 1 H, phenyl, $J = 7.2$), 7.24 – 7.33 (m, 4 H, phenyl). HRMS m/z calculated for $\text{C}_{14}\text{H}_{13}\text{ClN}$ $[\text{M}+\text{H}]^+$, 273.0902; found, 273.0887. Elemental analysis calculated for $\text{C}_{14}\text{H}_{13}\text{ClN}_4 \cdot 0.0736 \text{CH}_3(\text{CH}_2)_4\text{CH}_3$: C, 62.15; H, 5.07; N, 20.08; Cl, 12.70. Found: C, 62.19; H, 4.96; N, 20.05; Cl, 12.71.

4-chloro-7-((4-methoxy-3,5-dimethylpyridin-2-yl)methyl)-6-methyl-7*H*-pyrrolo[2,3-*d*]pyrimidin-2-amine (137)

After column chromatography (0 – 20% ethyl acetate in hexane), **137** was obtained as a yellow powder (265 mg, 80%). R_f 0.50 ($\text{CH}_3\text{OH}/\text{CHCl}_3$, 1:10); m.p. 184.3 – 186.7 °C. $^1\text{H NMR}$ (500 MHz, $\text{DMSO-}d_6$): δ 2.15 (s, 6 H, pyridyl- CH_3), 2.29 (s, 3 H, 6- CH_3), 3.74 (s, 3 H, OCH_3), 5.30 (s, 1 H, CH_2), 6.08 (s, 1 H, 5-H), 6.40 (s, 2 H, 2- NH_2 , D_2O exchanged), 7.99 (s, 1 H, pyridyl). HRMS m/z calculated for $\text{C}_{16}\text{H}_{18}\text{ClN}_5\text{O}$ $[\text{M}+\text{H}]^+$, 332.1273; found, 332.1273. Elemental analysis calculated for $\text{C}_{16}\text{H}_{18}\text{ClN}_5\text{O} \cdot 0.0914 \text{CH}_3(\text{CH}_2)_4\text{CH}_3$: C, 58.51; H, 5.72; N, 20.62; Cl, 10.44. Found: C, 58.41; H, 5.63; N, 20.44; Cl, 10.44.

4-chloro-6-methyl-7-((6-methylpyridin-2-yl)methyl)-7H-pyrrolo[2,3-*d*]pyrimidin-2-amine (138)

After column chromatography (0 – 30% ethyl acetate in hexane), **138** was obtained as a white powder (201 mg, 70%). R_f 0.45 (CH₃OH/CHCl₃, 1:10); m.p. 176.0 – 179.8 °C. ¹HNMR (500 MHz, CDCl₃): δ 2.30 (s, 3 H, 6-CH₃), 2.66 (s, 3 H, pyridyl-CH₃), 4.87 (s, 1 H, CH₂), 5.49 (s, 1 H, 5-H), 6.22 (s, 2 H, 2-NH₂, D₂O exchanged), 6.57 (m, 1 H, pyridyl), 7.13 – 7.14 (m, 1 H, pyridyl), 7.57 (m, 1 H, pyridyl). HRMS m/z calculated for C₁₄H₁₄ClN₅ [M+H]⁺, 288.1010; found, 288.0993. Elemental analysis calculated for C₁₄H₁₄ClN₅·0.0339CHCl₃·0.0818CH₃(CH₂)₄CH₃: C, 58.38; H, 5.12; N, 23.43; Cl, 13.07. Found: C, 58.43; H, 4.92; N, 23.39; Cl, 13.08.

4-chloro-7-((3,4-dimethoxy pyridin-2-yl)methyl)-6-methyl-7H-pyrrolo[2,3-*d*]pyrimidin-2-amine (139)

After column chromatography (0 – 30% ethyl acetate in hexane), **139** was obtained as a pale yellow powder (250 mg, 75%). R_f 0.60 (CH₃OH/CHCl₃, 1:10); m.p. 183.3 – 186.5 °C. ¹HNMR (400 MHz, DMSO-*d*₆): δ 2.21 (s, 3 H, 6-CH₃), 3.85 (s, 3 H, OCH₃), 3.89 (s, 3 H, OCH₃), 5.36 (s, 1 H, CH₂), 6.07 (s, 1 H, 5-H), 6.42 (s, 2 H, 2-NH₂, D₂O exchanged), 7.03 – 7.05 (d, 1 H, pyridyl, $J = 5.56$), 8.00 – 8.01 (d, 1 H, pyridyl, $J = 5.52$). HRMS m/z calculated for C₁₅H₁₆ClN₅O₂ [M+H]⁺, 334.1065; found, 334.1050. Elemental analysis calculated for C₁₅H₁₆ClN₅O₂·0.3245CH₃COCH₃: C, 54.41; H, 5.13; N, 19.86; Cl, 10.05. Found: C, 54.41; H, 4.93; N, 19.65; Cl, 10.35.

4-chloro-7-((6-chloropyridin-3-yl)methyl)-6-methyl-7H-pyrrolo[2,3-d]pyrimidin-2-amine (140)

After column chromatography (0 – 20% ethyl acetate in hexane), **140** was obtained as a yellow powder (252 mg, 82%). R_f 0.60 (CH₃OH/CHCl₃, 1:10); m.p. 165.3 – 168.9 °C. ¹HNMR (500 MHz, DMSO-*d*₆): δ 2.25 (s, 3 H, 6-CH₃), 5.31 (s, 1 H, CH₂), 6.14 (s, 1 H, 5-H), 6.61 (s, 2 H, 2-NH₂, D₂O exchanged), 7.46 – 7.50 (m, 2 H, pyridyl). 8.29 (s, 1 H, pyridyl). HRMS m/z calculated for C₁₃H₁₁Cl₂N₅ [M+H]⁺, 308.0464; found, 308.0463. Elemental analysis calculated for C₁₃H₁₁Cl₂N₅·0.0306CHCl₃·0.1268CH₃(CH₂)₄CH₃: C, 51.32; H, 4.00; N, 21.70; Cl, 22.98. Found: C, 51.26; H, 3.68; N, 21.53; Cl, 22.87.

4-chloro-6-methyl-7-(pyridin-2-ylmethyl)-7H-pyrrolo[2,3-d]pyrimidin-2-amine (141)

After column chromatography (0 – 20% ethyl acetate in hexane), **141** was obtained as a pale yellow powder (213 mg, 78%). R_f 0.60 (CH₃OH/CHCl₃, 1:10); m.p. 176.6 – 178.1 °C. ¹HNMR (500 MHz, CDCl₃): δ 2.30 (s, 3 H, 6-CH₃), 5.47 (s, 1 H, CH₂), 6.22 (s, 1 H, 5-H), 6.88 – 6.90 (s, 2 H, 2-NH₂, D₂O exchanged), 7.27 (m, 2 H, pyridyl), 7.66 – 7.67 (m, 1 H, pyridyl), 8.60 (m, 1 H, pyridyl). HRMS m/z calculated for C₁₃H₁₂ClN₅ [M+H]⁺, 274.0854; found, 274.0839. Elemental analysis calculated for C₁₃H₁₂ClN₅·0.1135CH₃(CH₂)₄CH₃: C, 57.96; H, 4.83; N, 24.70; Cl, 12.51. Found: C, 57.88; H, 4.70; N, 24.63; Cl, 12.36.

General procedure for the synthesis of target compounds 144 – 149

To the 4-chloro analogs (0.5 mmol of **136** – **141**) in a bomb vessel was added

ammonia in methanol (7 N). The vessel was immediately sealed and heated in an oil bath to 145 °C. The reaction temperature was maintain at 145 °C for 12 hours before cool to room temperature. The methanol was evaporated and the residue was purified through column chromatography to afford the target compounds.

7-benzyl-6-methyl-7*H*-pyrrolo[2,3-*d*]pyrimidine-2,4-diamine (144)

After column chromatography (0 – 20% ethyl acetate in hexane), **144** was obtained as a pale yellow powder (92 mg, 73%). R_f 0.30 (ethyl acetate/hexane 1:1); m.p. 176.2 – 178.0 °C. $^1\text{H NMR}$ (500 MHz, $\text{DMSO-}d_6$): δ 2.11 (s, 3 H, 6- CH_3), 5.18 (s, 1 H, CH_2), 5.46 (s, 2 H, 4- NH_2 D_2O exchanged), 6.11 (s, 1 H, 5-H), 6.40 (s, 2 H, 2- NH_2 , D_2O exchanged), 7.02 – 7.03 (d, 1 H, phenyl, $J = 7.25$), 7.22 – 7.30 (m, 4 H, phenyl). HRMS m/z calculated for $\text{C}_{14}\text{H}_{15}\text{N}_5$ $[\text{M}+\text{H}]^+$, 254.1400; found, 254.1399. Elemental analysis calculated for $\text{C}_{14}\text{H}_{15}\text{N}_5 \cdot 0.1186\text{CH}_3\text{CO}_2\text{C}_2\text{H}_5$: C, 65.91; H, 6.09; N, 26.55. Found: C, 65.64; H, 6.04; N, 26.66.

7-((4-methoxy-3,5-dimethylpyridin-2-yl)methyl)-6-methyl-7*H*-pyrrolo[2,3-*d*]pyrimidine-2,4-diamine (145)

After column chromatography (0 – 2% methanol in chloroform), **145** was obtained as a white powder (121.68 mg, 78%). R_f 0.10 ($\text{CH}_3\text{OH}/\text{CHCl}_3$, 1:10); m.p. deg. 151.4 °C. $^1\text{H NMR}$ (500 MHz, $\text{DMSO-}d_6$): δ 2.16 (s, 6 H, pyridyl- CH_3), 2.24 (s, 3 H, 6- CH_3), 3.72 (s, 3 H, OCH_3), 5.20 (s, 1 H, CH_2), 6.05 (s, 1 H, 5-H), 5.40 (s, 2 H, 4- NH_2 , D_2O exchanged), 6.38 (s, 2 H, 2- NH_2 , D_2O exchanged), 8.02 (s, 1 H, pyridyl). HRMS m/z calculated for $\text{C}_{16}\text{H}_{20}\text{N}_6\text{O}$ $[\text{M}+\text{H}]^+$, 313.1771; found, 313.1769. Elemental analysis

calculated for $C_{16}H_{20}N_6O \cdot 0.6671CH_3OH \cdot 0.2004CHCl_3$: C, 56.64; H, 6.44; N, 23.50.

Found: C, 56.64; H, 6.45; N, 23.50.

6-methyl-7-((6-methylpyridin-2-yl)methyl)-7H-pyrrolo[2,3-*d*]pyrimidine-2,4-diamine (146)

After column chromatography (0 – 30% ethyl acetate in hexane), **146** was obtained as a white powder (87 mg, 65%). R_f 0.30 ($CH_3OH/CHCl_3$, 1:10); m.p. 170.3 – 173.6 °C. 1H NMR (500 MHz, $DMSO-d_6$): δ 2.14 (s, 3 H, 6- CH_3), 2.46 (s, 3 H, pyridyl- CH_3), 5.18 (s, 1 H, CH_2), 5.42 (s, 2 H, 4- NH_2 , D_2O exchanged), 6.14 (s, 1 H, 5-H), 6.37 (s, 2 H, 2- NH_2 , D_2O exchanged), 6.57 (m, 1 H, pyridyl), 7.13 – 7.14 (m, 1 H, pyridyl), 7.57 (m, 1 H, pyridyl). HRMS m/z calculated for $C_{14}H_{16}N_6$ $[M+H]^+$, 269.1509; found, 269.1506. Elemental analysis calculated for $C_{14}H_{16}N_6 \cdot 1.1858H_2O$: C, 58.05; H, 6.39; N, 29.01. Found: C, 58.13; H, 6.43; N, 28.85.

7-((3,4-dimethoxypyridin-2-yl)methyl)-6-methyl-7H-pyrrolo[2,3-*d*]pyrimidine-2,4-diamine (147)

After column chromatography (0 – 30% ethyl acetate in hexane), **147** was obtained as a pale yellow powder (111 mg, 71%). R_f 0.15 ($CH_3OH/CHCl_3$, 1:10); m.p. 215.7 – 218.5 °C. 1H NMR (500 MHz, $DMSO-d_6$): δ 2.12 (s, 3 H, 6- CH_3), 3.83 (s, 3 H, OCH_3), 3.88 (s, 3 H, OCH_3), 5.25 (s, 1 H, CH_2), 5.30 (s, 2 H, 4- NH_2 , D_2O exchanged), 6.03 (s, 1 H, 5-H), 6.29 (s, 2 H, 2- NH_2 , D_2O exchanged), 7.01 – 7.02 (d, 1 H, pyridyl, $J = 5.48$), 8.00 – 8.02 (d, 1 H, pyridyl, $J = 5.52$). HRMS m/z calculated for $C_{15}H_{18}N_6O_2$ $[M+H]^+$,

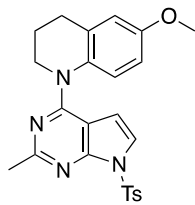
315.1564; found, 315.1566. Elemental analysis calculated for $C_{15}H_{18}N_6O_2 \cdot 0.4996H_2O$: C, 55.72; H, 5.92; N, 25.99. Found: C, 55.69; H, 6.07; N, 26.08.

7-((6-chloropyridin-3-yl)methyl)-6-methyl-7H-pyrrolo[2,3-d]pyrimidine-2,4-diamine (148)

After column chromatography (0 – 20% ethyl acetate in hexane), **148** was obtained as a yellow powder (89 mg, 62%). R_f 0.30 ($CH_3OH/CHCl_3$, 1:10); m.p. 168.1 – 170.4 °C. 1H NMR (500 MHz, $DMSO-d_6$): δ 2.15 (s, 3 H, 6- CH_3), 5.20 (s, 1 H, CH_2), 5.51 (s, 2 H, 4- NH_2 , D_2O exchanged), 6.11 (s, 1 H, 5-H), 6.44 (s, 2 H, 2- NH_2 , D_2O exchanged), 7.46 (d, 2 H, pyridyl, $J = 1.32$). 8.22 (s, 1 H, pyridyl). Elemental analysis calculated for $C_{13}H_{13}ClN_6 \cdot 0.1487CH_3COCH_3$: C, 54.31; H, 4.71; N, 28.26; Cl, 11.92. Found: C, 54.07; H, 4.73; N, 28.31; Cl, 11.65.

6-methyl-7-(pyridin-2-ylmethyl)-7H-pyrrolo[2,3-d]pyrimidine-2,4-diamine (149)

After column chromatography (0 – 30% ethyl acetate in hexane), **141** was obtained as a pale yellow powder (107 mg, 85%). R_f 0.20 ($CH_3OH/CHCl_3$, 1:10); m.p. 186.8 – 189.5 °C. 1H NMR (500 MHz, $DMSO-d_6$): δ 2.14 (s, 3 H, 6- CH_3), 5.24 (s, 1 H, CH_2), 5.45 (s, 2 H, 4- NH_2 , D_2O exchanged), 6.13 (s, 1 H, 5-H), 6.41 (s, 2 H, 2- NH_2 , D_2O exchanged), 6.68 – 6.70 (d, 1 H, pyridyl, $J = 7.8$), 7.26 (m, 1 H, pyridyl), 7.69 (m, 1 H, pyridyl), 8.51 – 8.52 (d, 1 H, pyridyl, $J = 4.25$). HRMS m/z calculated for $C_{13}H_{14}N_6$ $[M+H]^+$, 255.1353; found, 255.1350. Elemental analysis calculated for $C_{13}H_{14}N_6 \cdot 0.5153 C_2H_5OH$: C, 60.61; H, 6.20; N, 30.23. Found: C, 60.33; H, 5.89; N, 30.23.



6-methoxy-1-(2-methyl-7-tosyl-7H-pyrrolo[2,3-d]pyrimidin-4-yl)-1,2,3,4-tetrahydroquinoline (150)

To the stirred solution of **110** (147 mg, 0.5 mmol) in dichloromethane (5 mL) was added sodium hydroxide (80 mg, 2 mmol) and tetrabutylammonium hydrogensulfate (33.9 mg, 0.1 mmol). After the solution turned clear, tosyl chloride (190 mg, 1 mmol) was added and the reaction mixture was stirred at room temperature for six hours. At the end of the reaction, the organic layer was collected and washed with water (2 × 5 mL). The solvent was evaporated under vacuum and the mixture was purified through flash chromatography (0 – 20% ethyl acetate in hexane) before **151** was obtained as a pale yellow solid (179 mg, 80%). R_f 0.75 (ethyl acetate/hexane, 1:1); m.p. 123.9 – 126.1 °C. $^1\text{H NMR}$ (500 MHz, DMSO- d_6): δ 1.82 (q, 2 H, CH_2), 2.37 (s, 3 H, tosyl- CH_3), 2.47 (s, 3 H, 2- CH_3), 2.72 (t, 2 H, CH_2), 3.76 (s, 3 H, OCH_3), 3.99 (t, 2 H, NCH_2), 5.59 – 5.60 (d, 1 H, 5-H, $J = 4.05$), 6.71 – 6.73 (d, 1 H, phenyl, $J = 8.85$), 6.85 – 6.86 (d, 1 H, 6-H, $J = 3.05$), 7.02 – 7.04 (d, 1 H, phenyl, $J = 8.75$), 7.40 – 7.41 (d, 1 H, phenyl, $J = 4.05$), 7.44 – 7.46 (d, 2 H, tosyl, $J = 8.15$). 8.02 – 8.03 (d, 2 H, tosyl, $J = 8.35$). HRMS m/z calculated for $\text{C}_{24}\text{H}_{24}\text{N}_4\text{O}_3\text{S}$ $[\text{M}+\text{H}]^+$, 449.1642; found, 449.1645. Elemental analysis calculated for $\text{C}_{24}\text{H}_{24}\text{N}_4\text{O}_3\text{S}$: C, 64.27; H, 5.39; N, 12.49; S, 7.15. Found: C, 64.12; H, 5.48; N, 12.47; S, 7.28.

VI. Summary

For the projects in this dissertation, over one hundred and twenty new compounds have been synthesized and characterized. Among them, fifty-six compounds have been submitted for biological evaluation as microtubule-binding agents or HSP90 inhibitors. These compounds are listed below.

Compounds have been evaluated as microtubule-binding agents:

- 1) *N*-(4-methoxyphenyl)-2-methyl-7*H*-pyrrolo[2,3-*d*]pyrimidin-4-amine (**90**)
- 2) *N*-(4-methoxyphenyl)-*N*,2-dimethyl-7*H*-pyrrolo[2,3-*d*]pyrimidin-4-amine (**91**)
- 3) *N*-(4-methoxyphenyl)-*N*,2-dimethyl-7*H*-pyrrolo[2,3-*d*]pyrimidin-4-amine hydrochloride (**91·HCl**)
- 4) *N*-(3-methoxyphenyl)-*N*,2-dimethyl-7*H*-pyrrolo[2,3-*d*]pyrimidin-4-amine (**92**)
- 5) *N*-(3-methoxyphenyl)-2-methyl-7*H*-pyrrolo[2,3-*d*]pyrimidin-4-amine (**93**)
- 6) *N*-(2-methoxyphenyl)-*N*,2-dimethyl-7*H*-pyrrolo[2,3-*d*]pyrimidin-4-amine (**94**)
- 7) *N*-(2-methoxyphenyl)-2-methyl-7*H*-pyrrolo[2,3-*d*]pyrimidin-4-amine (**95**)
- 8) *N*,2-dimethyl-*N*-(*p*-tolyl)-7*H*-pyrrolo[2,3-*d*]pyrimidin-4-amine (**96**)
- 9) *N*-(4-chlorophenyl)-*N*,2-dimethyl-7*H*-pyrrolo[2,3-*d*]pyrimidin-4-amine (**97**)
- 10) *N*-(3,4-dichlorophenyl)-*N*,2-dimethyl-7*H*-pyrrolo[2,3-*d*]pyrimidin-4-amine (**98**)
- 11) 4-(methyl(2-methyl-7*H*-pyrrolo[2,3-*d*]pyrimidin-4-yl)amino)phenol (**99**)
- 12) *N*,2-dimethyl-*N*-(naphthalen-2-yl)-7*H*-pyrrolo[2,3-*d*]pyrimidin-4-amine (**100**)
- 13) 2-methyl-*N*-(naphthalen-2-yl)-7*H*-pyrrolo[2,3-*d*]pyrimidin-4-amine (**101**)
- 14) *N*⁴-(4-methoxyphenyl)-*N*⁴-methyl-7*H*-pyrrolo[2,3-*d*]pyrimidine-2,4-diamine (**102**)
- 15) *N*⁴-(4-methoxyphenyl)-7*H*-pyrrolo[2,3-*d*]pyrimidine-2,4-diamine (**103**)

- 16) N^4 -(4-methoxyphenyl)- N^4 ,6-dimethyl-7*H*-pyrrolo[2,3-*d*]pyrimidine-2,4-diamine (104)
- 17) N^4 -(3-methoxyphenyl)- N^4 ,6-dimethyl-7*H*-pyrrolo[2,3-*d*]pyrimidine-2,4-diamine (105)
- 18) N^4 -(2-methoxyphenyl)- N^4 ,6-dimethyl-7*H*-pyrrolo[2,3-*d*]pyrimidine-2,4-diamine (106)
- 19) N^4 ,6-dimethyl- N^4 -(*p*-tolyl)-7*H*-pyrrolo[2,3-*d*]pyrimidine-2,4-diamine (107)
- 20) N^4 -(4-chlorophenyl)- N^4 ,6-dimethyl-7*H*-pyrrolo[2,3-*d*]pyrimidine-2,4-diamine (108)
- 21) N^4 -(3,4-dichlorophenyl)- N^4 ,6-dimethyl-7*H*-pyrrolo[2,3-*d*]pyrimidine-2,4-diamine (109)
- 22) 6-methoxy-1-(2-methyl-7*H*-pyrrolo[2,3-*d*]pyrimidin-4-yl)-1,2,3,4-tetrahydro-quinoline (110)
- 23) 4-(6-methoxy-3,4-dihydroquinolin-1(2*H*)-yl)-7*H*-pyrrolo[2,3-*d*]pyrimidin-2-amine (111)
- 24) 4-(6-methoxy-3,4-dihydroquinolin-1(2*H*)-yl)-6-methyl-7*H*-pyrrolo[2,3-*d*]pyrimidin-2-amine (112)
- 25) 6-methoxy-1-(7*H*-pyrrolo[2,3-*d*]pyrimidin-4-yl)-1,2,3,4-tetrahydroquinoline (113)
- 26) *N*-(4-methoxyphenyl)-*N*,2,7-trimethyl-7*H*-pyrrolo[2,3-*d*]pyrimidin-4-amine (114)
- 27) *N*-(4-methoxyphenyl)-*N*,2,7-trimethyl-7*H*-pyrrolo[2,3-*d*]pyrimidin-4-amine hydrochloride salt (114·HCl)
- 28) 7-benzyl-*N*-(4-methoxyphenyl)-*N*,2-dimethyl-7*H*-pyrrolo[2,3-*d*]pyrimidin-4-amine (115)
- 29) *N*-(4-methoxyphenyl)-*N*,2-dimethyl-7-tosyl-7*H*-pyrrolo[2,3-*d*]pyrimidin-4-amine (116)
- 30) *N*-(4-methoxyphenyl)-*N*,2-dimethyl-6,7-dihydro-5*H*-pyrrolo[2,3-*d*]pyrimidin-4-amine (117)
- 31) N^4 -(4-methoxyphenyl)- N^4 -methyl-6,7-dihydro-5*H*-pyrrolo[2,3-*d*]pyrimidine-2,4-diamine (118)
- 32) (±)-4-(1-(4-methoxyphenyl)ethyl)-2-methyl-7*H*-pyrrolo[2,3-*d*]pyrimidine (119)
- 33) *N*-(4-methoxyphenyl)-*N*-methyl-1*H*-pyrrolo[3,2-*c*]pyridin-4-amine (120)
- 34) *N*-(4-methoxyphenyl)-*N*-methyl-1*H*-pyrrolo[2,3-*b*]pyridin-4-amine (121)
- 35) *N*-(4-methoxyphenyl)-*N*-methyl-1*H*-imidazo[4,5-*c*]pyridin-4-amine (122)
- 36) *N*-(4-methoxyphenyl)-*N*-methyl-1*H*-indol-4-amine (123)

- 37) *N*-(4-methoxyphenyl)-*N*-methylpyrido[3,4-*b*]pyrazin-5-amine (124)
- 38) 6-methoxy-1-(2-methyl-7-tosyl-7*H*-pyrrolo[2,3-*d*]pyrimidin-4-yl)-1,2,3,4-tetrahydroquinoline (150)

Compounds have been evaluated as HSP90 inhibitors:

- 39) 6-((2-methoxyphenyl)thio)-5-methyl-7-(pent-4-yn-1-yl)-7*H*-pyrrolo[2,3-*d*]pyrimidin-4-amine (130)
- 40) 6-((3-methoxyphenyl)thio)-5-methyl-7-(pent-4-yn-1-yl)-7*H*-pyrrolo[2,3-*d*]pyrimidin-4-amine (131)
- 41) 6-((4-methoxyphenyl)thio)-5-methyl-7-(pent-4-yn-1-yl)-7*H*-pyrrolo[2,3-*d*]pyrimidine-2,4-diamine (132)
- 42) 6-((3,4-dimethoxyphenyl)thio)-5-methyl-7-(pent-4-yn-1-yl)-7*H*-pyrrolo[2,3-*d*]pyrimidine-2,4-diamine (133)
- 43) 5-methyl-7-(pent-4-yn-1-yl)-6-((3,4,5-trimethoxyphenyl)thio)-7*H*-pyrrolo[2,3-*d*]pyrimidine-2,4-diamine (134)
- 44) 6-((2,3-dihydrobenzo[*b*][1,4]dioxin-6-yl)thio)-7-(3-(isopropylamino)propyl)-5-methyl-7*H*-pyrrolo[2,3-*d*]pyrimidin-4-amine (135)
- 45) 7-benzyl-4-chloro-6-methyl-7*H*-pyrrolo[2,3-*d*]pyrimidin-2-amine (136)
- 46) 4-chloro-7-((4-methoxy-3,5-dimethylpyridin-2-yl)methyl)-6-methyl-7*H*-pyrrolo[2,3-*d*]pyrimidin-2-amine (137)
- 47) 4-chloro-6-methyl-7-((6-methylpyridin-2-yl)methyl)-7*H*-pyrrolo[2,3-*d*]pyrimidin-2-amine (138)
- 48) 4-chloro-7-((3,4-dimethoxypyridin-2-yl)methyl)-6-methyl-7*H*-pyrrolo[2,3-*d*]pyrimidin-2-amine (139)

- 49) 4-chloro-7-((6-chloropyridin-3-yl)methyl)-6-methyl-7*H*-pyrrolo[2,3-*d*]pyrimidin-2-amine
(140)
- 50) 4-chloro-6-methyl-7-(pyridin-2-ylmethyl)-7*H*-pyrrolo[2,3-*d*]pyrimidin-2-amine (141)
- 51) 7-benzyl-6-methyl-7*H*-pyrrolo[2,3-*d*]pyrimidine-2,4-diamine (144)
- 52) 7-((4-methoxy-3,5-dimethylpyridin-2-yl)methyl)-6-methyl-7*H*-pyrrolo[2,3-*d*]pyrimidine-2,4-diamine (145)
- 53) 6-methyl-7-((6-methylpyridin-2-yl)methyl)-7*H*-pyrrolo[2,3-*d*]pyrimidine-2,4-diamine
(146)
- 54) 7-((3,4-dimethoxypyridin-2-yl)methyl)-6-methyl-7*H*-pyrrolo[2,3-*d*]pyrimidine-2,4-diamine (147)
- 55) 7-((6-chloropyridin-3-yl)methyl)-6-methyl-7*H*-pyrrolo[2,3-*d*]pyrimidine-2,4-diamine
(148)
- 56) 6-methyl-7-(pyridin-2-ylmethyl)-7*H*-pyrrolo[2,3-*d*]pyrimidine-2,4-diamine (149)

During the course of this dissertation work, the influence of the conformation on reactivity of certain heterocyclic scaffold was studied. The information gleaned from these studies has led to an optimized synthesis of substituted 5,6-dihydropyrrolo[2,3-*d*]pyrimidines. An advantageous method of removing the tosyl from aromatic amines was identified at the same time. In addition, a novel, previously unknown method of removing anisyl diphenylmethyl protection on the amine by the use hydrazine was discovered.

The biological evaluations of the synthesized compounds are currently in progress. The results of some analogs evaluated have confirmed the hypothesis proposed at the beginning of the project. Further, the 4-tetrahydroquinoline-substituted pyrrolo[2,3-*d*]pyrimidines and 5,6-dihydropyrrolo[2,3-*d*]pyrimidines are consistently more active than the lead compound. The complete findings and discussion will be published in due course.

BIBLIOGRAPHY

1. Jordan, M. A.; Wilson, L. Microtubules as a target for anticancer drugs. *Nature Rev. Cancer* **2004**, 4, 253-65.
2. Dumontet, C.; Jordan, M. A. Microtubule-binding agents: a dynamic field of cancer therapeutics. *Nature Rev. Drug Discovery* **2010**, 9, 790-803.
3. Li, H.; DeRosier, D. J.; Nicholson, W. V.; Nogales, E.; Downing, K. H. Microtubule structure at 8 Å resolution. *Structure* **2002**, 10, 1317-28.
4. Wang, H. W.; Nogales, E. Nucleotide-dependent bending flexibility of tubulin regulates microtubule assembly. *Nature* **2005**, 435, 911-5.
5. Elie-Caille, C.; Severin, F.; Helenius, J.; Howard, J.; Muller, D. J.; Hyman, A. A. Straight GDP-tubulin protofilaments form in the presence of taxol. *Curr. Biol.* **2007**, 17, 1765-70.
6. Chretien, D.; Jainosi, I.; Taveau, J. C.; Flyvbjerg, H. Microtubule's conformational cap. *Cell Struct. Funct.* **1999**, 24, 299-303.
7. Janosi, I. M.; Chretien, D.; Flyvbjerg, H. Structural microtubule cap: stability, catastrophe, rescue, and third state. *Biophys. J* **2002**, 83, 1317-30.
8. Etienne-Manneville, S. From signaling pathways to microtubule dynamics: the key players. *Curr. Opinion in Cell Biol.* **2010**, 22, 104-11.
9. Kavallaris, M. Microtubules and resistance to tubulin-binding agents. *Nature Rev. Cancer* **2010**, 10, 194-204.
10. Wilson, L.; Jordan, M. A.; Morse, A.; Margolis, R. L. Interaction of vinblastine with steady-state microtubules in vitro. *J. Mol. Biol.* **1982**, 159, 125-49.

11. Bai, R. L.; Pettit, G. R.; Hamel, E. Binding of dolastatin 10 to tubulin at a distinct site for peptide antimitotic agents near the exchangeable nucleotide and vinca alkaloid sites. *J Biol. Chem.* **1990**, 265, 17141-9.
12. Jordan, M. A.; Wilson, L. Kinetic analysis of tubulin exchange at microtubule ends at low vinblastine concentrations. *Biochemistry* **1990**, 29, 2730-9.
13. Na, G. C.; Timasheff, S. N. Stoichiometry of the vinblastine-induced self-association of calf brain tubulin. *Biochemistry* **1980**, 19, 1347-54.
14. Jordan, M. A.; Thrower, D.; Wilson, L. Mechanism of inhibition of cell proliferation by Vinca alkaloids. *Cancer Research* **1991**, 51, 2212-22.
15. Wani, M. C.; Taylor, H. L.; Wall, M. E.; Coggon, P.; McPhail, A. T. Plant antitumor agents. VI. The isolation and structure of taxol, a novel antileukemic and antitumor agent from *Taxus brevifolia*. *J Am. Chem. Soc.* **1971**, 93, 2325-7.
16. Schiff, P. B.; Fant, J.; Horwitz, S. B. Promotion of microtubule assembly in vitro by taxol. *Nature* **1979**, 277, 665-7.
17. Horwitz, S. B. How to make taxol from scratch. *Nature* **1994**, 367, 593-4.
18. Nogales, E.; Wolf, S. G.; Khan, I. A.; Luduena, R. F.; Downing, K. H. Structure of tubulin at 6.5 Å and location of the taxol-binding site. *Nature* **1995**, 375, 424-7.
19. Nogales, E. Structural insight into microtubule function. *Annu. Rev. Biophys. Biomol. Struct.* **2001**, 30, 397-420.
20. Derry, W. B.; Wilson, L.; Jordan, M. A. Substoichiometric binding of taxol suppresses microtubule dynamics. *Biochemistry* **1995**, 34, 2203-11.
21. Yvon, A. M.; Wadsworth, P.; Jordan, M. A. Taxol suppresses dynamics of individual microtubules in living human tumor cells. *Mol. Biol. Cell* **1999**, 10, 947-59.

22. Jordan, M. A.; Toso, R. J.; Thrower, D.; Wilson, L. Mechanism of mitotic block and inhibition of cell proliferation by taxol at low concentrations. *Proc. Natl. Acad. Sci.* **1993**, 90, 9552-6.
23. Bollag, D. M.; McQueney, P. A.; Zhu, J.; Hensens, O.; Koupal, L.; Liesch, J.; Goetz, M.; Lazarides, E.; Woods, C. M. Epothilones, a new class of microtubule-stabilizing agents with a taxol-like mechanism of action. *Cancer Research* **1995**, 55, 2325-33.
24. Nettles, J. H.; Li, H.; Cornett, B.; Krahn, J. M.; Snyder, J. P.; Downing, K. H. The binding mode of epothilone A on alpha,beta-tubulin by electron crystallography. *Science* **2004**, 305, 866-9.
25. Thomas, E. S.; Gomez, H. L.; Li, R. K.; Chung, H. C.; Fein, L. E.; Chan, V. F.; Jassem, J.; Pivot, X. B.; Klimovsky, J. V.; de Mendoza, F. H.; Xu, B.; Campone, M.; Lerzo, G. L.; Peck, R. A.; Mukhopadhyay, P.; Vahdat, L. T.; Roche, H. H. Ixabepilone plus capecitabine for metastatic breast cancer progressing after anthracycline and taxane treatment. *J Clin. Oncol.* **2007**, 25, 5210-7.
26. Vansteenkiste, J.; Lara, P. N., Jr.; Le Chevalier, T.; Breton, J. L.; Bonomi, P.; Sandler, A. B.; Socinski, M. A.; Delbaldo, C.; McHenry, B.; Lebwohl, D.; Peck, R.; Edelman, M. J. Phase II clinical trial of the epothilone B analog, ixabepilone, in patients with non small-cell lung cancer whose tumors have failed first-line platinum-based chemotherapy. *J Clin. Oncol.* **2007**, 25, 3448-55.
27. Dumontet, C.; Jordan, M. A.; Lee, F. F. Ixabepilone: targeting betaIII-tubulin expression in taxane-resistant malignancies. *Mol. Cancer Ther.* **2009**, 8, 17-25.
28. Graham, W.; Roberts, J. B. Intravenous colchicine in the management of gouty arthritis. *Ann. Rheum. Dis.* **1953**, 12, 16-9.

29. Hastie, S. B. Interactions of colchicine with tubulin. *Pharmacol. Ther.* **1991**, 51, 377-401.
30. Skoufias, D. A.; Wilson, L. Mechanism of inhibition of microtubule polymerization by colchicine: inhibitory potencies of unliganded colchicine and tubulin-colchicine complexes. *Biochemistry* **1992**, 31, 738-46.
31. Carmeliet, P.; Jain, R. K. Molecular mechanisms and clinical applications of angiogenesis. *Nature* **2011**, 473, 298-307.
32. Kanthou, C.; Tozer, G. M. The tumor vascular targeting agent combretastatin A-4-phosphate induces reorganization of the actin cytoskeleton and early membrane blebbing in human endothelial cells. *Blood* **2002**, 99, 2060-9.
33. Tozer, G. M.; Prise, V. E.; Wilson, J.; Cemazar, M.; Shan, S.; Dewhirst, M. W.; Barber, P. R.; Vojnovic, B.; Chaplin, D. J. Mechanisms associated with tumor vascular shut-down induced by combretastatin A-4 phosphate: intravital microscopy and measurement of vascular permeability. *Cancer Research* **2001**, 61, 6413-22.
34. Griggs, J.; Metcalfe, J. C.; Hesketh, R. Targeting tumour vasculature: the development of combretastatin A4. *Lancet Oncol.* **2001**, 2, 82-7.
35. Tozer, G. M.; Kanthou, C.; Parkins, C. S.; Hill, S. A. The biology of the combretastatins as tumour vascular targeting agents. *Int. J Exp. Pathol.* **2002**, 83, 21-38.
36. Prise, V. E.; Honess, D. J.; Stratford, M. R.; Wilson, J.; Tozer, G. M. The vascular response of tumor and normal tissues in the rat to the vascular targeting agent, combretastatin A-4-phosphate, at clinically relevant doses. *Int. J Oncol.* **2002**, 21, 717-26.

37. Davis, P. D.; Dougherty, G. J.; Blakey, D. C.; Galbraith, S. M.; Tozer, G. M.; Holder, A. L.; Naylor, M. A.; Nolan, J.; Stratford, M. R.; Chaplin, D. J.; Hill, S. A. ZD6126: a novel vascular-targeting agent that causes selective destruction of tumor vasculature. *Cancer Research* **2002**, *62*, 7247-53.
38. Panda, D.; Miller, H. P.; Islam, K.; Wilson, L. Stabilization of microtubule dynamics by estramustine by binding to a novel site in tubulin: a possible mechanistic basis for its antitumor action. *Proc. Natl. Acad. Sci.* **1997**, *94*, 10560-4.
39. Mooberry, S. L.; Tien, G.; Hernandez, A. H.; Plubrukarn, A.; Davidson, B. S. Laulimalide and isolaulimalide, new paclitaxel-like microtubule-stabilizing agents. *Cancer Research* **1999**, *59*, 653-60.
40. Landen, J. W.; Hau, V.; Wang, M.; Davis, T.; Ciliax, B.; Wainer, B. H.; Van Meir, E. G.; Glass, J. D.; Joshi, H. C.; Archer, D. R. Noscipine crosses the blood-brain barrier and inhibits glioblastoma growth. *Clin. Cancer Res.* **2004**, *10*, 5187-201.
41. Li, J.; Risinger, A. L.; Peng, J.; Chen, Z.; Hu, L.; Mooberry, S. L. Potent taccalonolides, AF and AJ, inform significant structure-activity relationships and tubulin as the binding site of these microtubule stabilizers. *J Am. Chem. Soc.* **2011**, *133*, 19064-7.
42. Hudes, G. R.; Greenberg, R.; Krigel, R. L.; Fox, S.; Scher, R.; Litwin, S.; Watts, P.; Speicher, L.; Tew, K.; Comis, R. Phase II study of estramustine and vinblastine, two microtubule inhibitors, in hormone-refractory prostate cancer. *J Clin. Oncol.* **1992**, *10*, 1754-61.

43. Hudes, G. R.; Nathan, F. E.; Khater, C.; Greenberg, R.; Gomella, L.; Stern, C.; McAleer, C. Paclitaxel plus estramustine in metastatic hormone-refractory prostate cancer. *Seminars in Oncology* **1995**, *22*, 41-5.
44. Honore, S.; Kamath, K.; Braguer, D.; Horwitz, S. B.; Wilson, L.; Briand, C.; Jordan, M. A. Synergistic suppression of microtubule dynamics by discodermolide and paclitaxel in non-small cell lung carcinoma cells. *Cancer Research* **2004**, *64*, 4957-64.
45. D'Agostino, G.; del Campo, J.; Mellado, B.; Izquierdo, M. A.; Minarik, T.; Cirri, L.; Marini, L.; Perez-Gracia, J. L.; Scambia, G. A multicenter phase II study of the cryptophycin analog LY355703 in patients with platinum-resistant ovarian cancer. *Int. J Gynecol. Cancer* **2006**, *16*, 71-6.
46. Argyriou, A. A.; Koltzenburg, M.; Polychronopoulos, P.; Papapetropoulos, S.; Kalofonos, H. P. Peripheral nerve damage associated with administration of taxanes in patients with cancer. *Crit. Rev. Oncol. Hematol.* **2008**, *66*, 218-28.
47. Gidding, C. E.; Kellie, S. J.; Kamps, W. A.; de Graaf, S. S. Vincristine revisited. *Crit. Rev. Oncol. Hematol.* **1999**, *29*, 267-87.
48. Markman, M. Managing taxane toxicities. *Support Care Cancer* **2003**, *11*, 144-7.
49. Cunningham, C.; Appleman, L. J.; Kirvan-Visovatti, M.; Ryan, D. P.; Regan, E.; Vukelja, S.; Bonate, P. L.; Ruvuna, F.; Fram, R. J.; Jekunen, A.; Weitman, S.; Hammond, L. A.; Eder, J. P., Jr. Phase I and pharmacokinetic study of the dolastatin-15 analogue tasidotin (ILX651) administered intravenously on days 1, 3, and 5 every 3 weeks in patients with advanced solid tumors. *Clin. Cancer Res.* **2005**, *11*, 7825-33.

50. Aghajanian, C.; Burris, H. A., 3rd; Jones, S.; Spriggs, D. R.; Cohen, M. B.; Peck, R.; Sabbatini, P.; Hensley, M. L.; Greco, F. A.; Dupont, J.; O'Connor, O. A. Phase I study of the novel epothilone analog ixabepilone (BMS-247550) in patients with advanced solid tumors and lymphomas. *J Clin. Oncol.* **2007**, *25*, 1082-8.
51. Zatloukal, P.; Gervais, R.; Vansteenkiste, J.; Bosquee, L.; Sessa, C.; Brain, E.; Dansin, E.; Urban, T.; Dohollou, N.; Besenval, M.; Quoix, E. Randomized multicenter phase II study of larotaxel (XRP9881) in combination with cisplatin or gemcitabine as first-line chemotherapy in nonirradiable stage IIIB or stage IV non-small cell lung cancer. *J Thorac. Oncol.* **2008**, *3*, 894-901.
52. Bock, C.; Lengauer, T. Managing drug resistance in cancer: lessons from HIV therapy. *Nature reviews. Cancer* **2012**, *12*, 494-501.
53. Fojo, A. T.; Menefee, M. Microtubule targeting agents: basic mechanisms of multidrug resistance (MDR). *Seminars in Oncology* **2005**, *32*, S3-8.
54. Gangjee, A.; Zhao, Y.; Lin, L.; Raghavan, S.; Roberts, E. G.; Risinger, A. L.; Hamel, E.; Mooberry, S. L. Synthesis and discovery of water-soluble microtubule targeting agents that bind to the colchicine site on tubulin and circumvent Pgp mediated resistance. *J Med. Chem.* **2010**, *53*, 8116-28.
55. Lhomme, C.; Joly, F.; Walker, J. L.; Lissoni, A. A.; Nicoletto, M. O.; Manikhas, G. M.; Baekelandt, M. M.; Gordon, A. N.; Fracasso, P. M.; Mietlowski, W. L.; Jones, G. J.; Dugan, M. H. Phase III study of valsopodar (PSC 833) combined with paclitaxel and carboplatin compared with paclitaxel and carboplatin alone in patients with stage IV or suboptimally debulked stage III epithelial ovarian cancer or primary peritoneal cancer. *J Clin. Oncol.* **2008**, *26*, 2674-82.

56. Kuttesch, J. F.; Parham, D. M.; Luo, X.; Meyer, W. H.; Bowman, L.; Shapiro, D. N.; Pappo, A. S.; Crist, W. M.; Beck, W. T.; Houghton, P. J. P-glycoprotein expression at diagnosis may not be a primary mechanism of therapeutic failure in childhood rhabdomyosarcoma. *J Clin. Oncol.* **1996**, *14*, 886-900.
57. Zhang, C. C.; Yang, J. M.; Bash-Babula, J.; White, E.; Murphy, M.; Levine, A. J.; Hait, W. N. DNA damage increases sensitivity to vinca alkaloids and decreases sensitivity to taxanes through p53-dependent repression of microtubule-associated protein 4. *Cancer Research* **1999**, *59*, 3663-70.
58. Kavallaris, M.; Tait, A. S.; Walsh, B. J.; He, L.; Horwitz, S. B.; Norris, M. D.; Haber, M. Multiple microtubule alterations are associated with Vinca alkaloid resistance in human leukemia cells. *Cancer Research* **2001**, *61*, 5803-9.
59. Don, S.; Verrills, N. M.; Liaw, T. Y.; Liu, M. L.; Norris, M. D.; Haber, M.; Kavallaris, M. Neuronal-associated microtubule proteins class III beta-tubulin and MAP2c in neuroblastoma: role in resistance to microtubule-targeted drugs. *Mol. Cancer Ther.* **2004**, *3*, 1137-46.
60. Seve, P.; Dumontet, C. Is class III beta-tubulin a predictive factor in patients receiving tubulin-binding agents? *Lancet Oncol.* **2008**, *9*, 168-75.
61. Gangjee, A.; Zhao, Y.; Hamel, E.; Westbrook, C.; Mooberry, S. L. Synthesis and biological activities of (R)- and (S)-N-(4-Methoxyphenyl)-N,2,6-trimethyl-6,7-dihydro-5H-cyclopenta[d]pyrimidin-4-a minium chloride as potent cytotoxic antitubulin agents. *J Med. Chem.* **2011**, *54*, 6151-5.
62. Freedman, H.; Huzil, J. T.; Luchko, T.; Luduena, R. F.; Tuszynski, J. A. Identification and characterization of an intermediate taxol binding site within

microtubule nanopores and a mechanism for tubulin isotype binding selectivity. *J Chem. Infor. Mod.* **2009**, 49, 424-36.

63. Gan, P. P.; Pasquier, E.; Kavallaris, M. Class III beta-tubulin mediates sensitivity to chemotherapeutic drugs in non small cell lung cancer. *Cancer Research* **2007**, 67, 9356-63.
64. Cicchillitti, L.; Penci, R.; Di Michele, M.; Filippetti, F.; Rotilio, D.; Donati, M. B.; Scambia, G.; Ferlini, C. Proteomic characterization of cytoskeletal and mitochondrial class III beta-tubulin. *Mol. Cancer Ther.* **2008**, 7, 2070-9.
65. Raspaglio, G.; Filippetti, F.; Prislei, S.; Penci, R.; De Maria, I.; Cicchillitti, L.; Mozzetti, S.; Scambia, G.; Ferlini, C. Hypoxia induces class III beta-tubulin gene expression by HIF-1alpha binding to its 3' flanking region. *Gene* **2008**, 409, 100-8.
66. Katsetos, C. D.; Draberova, E.; Legido, A.; Dumontet, C.; Draber, P. Tubulin targets in the pathobiology and therapy of glioblastoma multiforme. I. Class III beta-tubulin. *J Cell Physiol.* **2009**, 221, 505-13.
67. Trepel, J.; Mollapour, M.; Giaccone, G.; Neckers, L. Targeting the dynamic HSP90 complex in cancer. *Nature Reviews. Cancer* **2010**, 10, 537-49.
68. Whitesell, L.; Lindquist, S. L. HSP90 and the chaperoning of cancer. *Nature Reviews. Cancer* **2005**, 5, 761-72.
69. Buchner, J. Hsp90 & Co. - a holding for folding. *Trends Biochem. Sci.* **1999**, 24, 136-41.
70. Nathan, D. F.; Vos, M. H.; Lindquist, S. In vivo functions of the *Saccharomyces cerevisiae* Hsp90 chaperone. *Proc. Natl. Acad. Sci.* **1997**, 94, 12949-56.

71. Zhao, R.; Davey, M.; Hsu, Y. C.; Kaplanek, P.; Tong, A.; Parsons, A. B.; Krogan, N.; Cagney, G.; Mai, D.; Greenblatt, J.; Boone, C.; Emili, A.; Houry, W. A. Navigating the chaperone network: an integrative map of physical and genetic interactions mediated by the hsp90 chaperone. *Cell* **2005**, 120, 715-27.
72. Jameel, A.; Skilton, R. A.; Campbell, T. A.; Chander, S. K.; Coombes, R. C.; Luqmani, Y. A. Clinical and biological significance of HSP89 alpha in human breast cancer. *Int. J Cancer* **1992**, 50, 409-15.
73. Yufu, Y.; Nishimura, J.; Nawata, H. High constitutive expression of heat shock protein 90 alpha in human acute leukemia cells. *Leuk. Res.* **1992**, 16, 597-605.
74. Ciocca, D. R.; Clark, G. M.; Tandon, A. K.; Fuqua, S. A.; Welch, W. J.; McGuire, W. L. Heat shock protein hsp70 in patients with axillary lymph node-negative breast cancer: prognostic implications. *J Natl. Cancer Inst.* **1993**, 85, 570-4.
75. Chant, I. D.; Rose, P. E.; Morris, A. G. Analysis of heat-shock protein expression in myeloid leukaemia cells by flow cytometry. *Br. J Haematol.* **1995**, 90, 163-8.
76. Kaur, J.; Ralhan, R. Differential expression of 70-kDa heat shock-protein in human oral tumorigenesis. *Int. J Cancer* **1995**, 63, 774-9.
77. Ralhan, R.; Kaur, J. Differential expression of Mr 70,000 heat shock protein in normal, premalignant, and malignant human uterine cervix. *Clin. Cancer Res.* **1995**, 1, 1217-22.
78. Yano, M.; Naito, Z.; Tanaka, S.; Asano, G. Expression and roles of heat shock proteins in human breast cancer. *Jpn. J Cancer Res.* **1996**, 87, 908-15.

79. Santarosa, M.; Favaro, D.; Quaia, M.; Galligioni, E. Expression of heat shock protein 72 in renal cell carcinoma: possible role and prognostic implications in cancer patients. *Eur. J Cancer* **1997**, *33*, 873-7.
80. Conroy, S. E.; Sasieni, P. D.; Fentiman, I.; Latchman, D. S. Autoantibodies to the 90kDa heat shock protein and poor survival in breast cancer patients. *Eur. J Cancer* **1998**, *34*, 942-3.
81. Ali, M. M.; Roe, S. M.; Vaughan, C. K.; Meyer, P.; Panaretou, B.; Piper, P. W.; Prodromou, C.; Pearl, L. H. Crystal structure of an Hsp90-nucleotide-p23/Sba1 closed chaperone complex. *Nature* **2006**, *440*, 1013-7.
82. Prodromou, C.; Panaretou, B.; Chohan, S.; Siligardi, G.; O'Brien, R.; Ladbury, J. E.; Roe, S. M.; Piper, P. W.; Pearl, L. H. The ATPase cycle of Hsp90 drives a molecular 'clamp' via transient dimerization of the N-terminal domains. *The EMBO Journal* **2000**, *19*, 4383-92.
83. Shiau, A. K.; Harris, S. F.; Southworth, D. R.; Agard, D. A. Structural Analysis of E. coli hsp90 reveals dramatic nucleotide-dependent conformational rearrangements. *Cell* **2006**, *127*, 329-40.
84. Street, T. O.; Lavery, L. A.; Agard, D. A. Substrate binding drives large-scale conformational changes in the Hsp90 molecular chaperone. *Mol. Cell* **2011**, *42*, 96-105.
85. Soroka, J.; Wandinger, S. K.; Mausbacher, N.; Schreiber, T.; Richter, K.; Daub, H.; Buchner, J. Conformational switching of the molecular chaperone Hsp90 via regulated phosphorylation. *Mol. Cell* **2012**, *45*, 517-28.

86. Gorre, M. E.; Ellwood-Yen, K.; Chiosis, G.; Rosen, N.; Sawyers, C. L. BCR-ABL point mutants isolated from patients with imatinib mesylate-resistant chronic myeloid leukemia remain sensitive to inhibitors of the BCR-ABL chaperone heat shock protein 90. *Blood* **2002**, 100, 3041-4.
87. Sawai, A.; Chandarlapaty, S.; Greulich, H.; Gonen, M.; Ye, Q.; Arteaga, C. L.; Sellers, W.; Rosen, N.; Solit, D. B. Inhibition of Hsp90 down-regulates mutant epidermal growth factor receptor (EGFR) expression and sensitizes EGFR mutant tumors to paclitaxel. *Cancer Research* **2008**, 68, 589-96.
88. Kamal, A.; Thao, L.; Sensintaffar, J.; Zhang, L.; Boehm, M. F.; Fritz, L. C.; Burrows, F. J. A high-affinity conformation of Hsp90 confers tumour selectivity on Hsp90 inhibitors. *Nature* **2003**, 425, 407-10.
89. Vilenchik, M.; Solit, D.; Basso, A.; Huezo, H.; Lucas, B.; He, H.; Rosen, N.; Spampinato, C.; Modrich, P.; Chiosis, G. Targeting wide-range oncogenic transformation via PU24FC1, a specific inhibitor of tumor Hsp90. *Chem. Biol.* **2004**, 11, 787-97.
90. Eiseman, J. L.; Lan, J.; Lagattuta, T. F.; Hamburger, D. R.; Joseph, E.; Covey, J. M.; Egorin, M. J. Pharmacokinetics and pharmacodynamics of 17-demethoxy 17-[[2-dimethylamino)ethyl]amino]geldanamycin (17DMAG, NSC 707545) in C.B-17 SCID mice bearing MDA-MB-231 human breast cancer xenografts. *Cancer Chemother. Pharmacol.* **2005**, 55, 21-32.
91. Biamonte, M. A.; Van de Water, R.; Arndt, J. W.; Scannevin, R. H.; Perret, D.; Lee, W. C. Heat shock protein 90: inhibitors in clinical trials. *J Med. Chem.* **2010**, 53, 3-17.

92. Shi, J.; Van de Water, R.; Hong, K.; Lamer, R. B.; Weichert, K. W.; Sandoval, C. M.; Kasibhatla, S. R.; Boehm, M. F.; Chao, J.; Lundgren, K.; Timple, N.; Lough, R.; Ibanez, G.; Boykin, C.; Burrows, F. J.; Kehry, M. R.; Yun, T. J.; Harning, E. K.; Ambrose, C.; Thompson, J.; Bixler, S. A.; Dunah, A.; Snodgrass-Belt, P.; Arndt, J.; Enyedy, I. J.; Li, P.; Hong, V. S.; McKenzie, A.; Biamonte, M. A. EC144 is a potent inhibitor of the heat shock protein 90. *J Med. Chem.* **2012**, *55*, 7786-95.
93. Schnur, R. C.; Corman, M. L.; Gallaschun, R. J.; Cooper, B. A.; Dee, M. F.; Doty, J. L.; Muzzi, M. L.; DiOrio, C. I.; Barbacci, E. G.; Miller, P. E.; et al. erbB-2 oncogene inhibition by geldanamycin derivatives: synthesis, mechanism of action, and structure-activity relationships. *J Med. Chem.* **1995**, *38*, 3813-20.
94. Ge, J.; Normant, E.; Porter, J. R.; Ali, J. A.; Dembski, M. S.; Gao, Y.; Georges, A. T.; Grenier, L.; Pak, R. H.; Patterson, J.; Sydor, J. R.; Tibbitts, T. T.; Tong, J. K.; Adams, J.; Palombella, V. J. Design, synthesis, and biological evaluation of hydroquinone derivatives of 17-amino-17-demethoxygeldanamycin as potent, water-soluble inhibitors of Hsp90. *J Med. Chem.* **2006**, *49*, 4606-15.
95. Brough, P. A.; Aherne, W.; Barril, X.; Borgognoni, J.; Boxall, K.; Cansfield, J. E.; Cheung, K. M.; Collins, I.; Davies, N. G.; Drysdale, M. J.; Dymock, B.; Eccles, S. A.; Finch, H.; Fink, A.; Hayes, A.; Howes, R.; Hubbard, R. E.; James, K.; Jordan, A. M.; Lockie, A.; Martins, V.; Massey, A.; Matthews, T. P.; McDonald, E.; Northfield, C. J.; Pearl, L. H.; Prodromou, C.; Ray, S.; Raynaud, F. I.; Roughley, S. D.; Sharp, S. Y.; Surgenor, A.; Walmsley, D. L.; Webb, P.; Wood, M.; Workman, P.; Wright, L. 4,5-diarylisoxazole Hsp90 chaperone inhibitors: potential therapeutic agents for the treatment of cancer. *J Med. Chem.* **2008**, *51*, 196-218.

96. Nakashima, T.; Ishii, T.; Tagaya, H.; Seike, T.; Nakagawa, H.; Kanda, Y.; Akinaga, S.; Soga, S.; Shiotsu, Y. New molecular and biological mechanism of antitumor activities of KW-2478, a novel nonansamycin heat shock protein 90 inhibitor, in multiple myeloma cells. *Clin. Cancer Res.* **2010**, *16*, 2792-802.
97. Woodhead, A. J.; Angove, H.; Carr, M. G.; Chessari, G.; Congreve, M.; Coyle, J. E.; Cosme, J.; Graham, B.; Day, P. J.; Downham, R.; Fazal, L.; Feltell, R.; Figueroa, E.; Frederickson, M.; Lewis, J.; McMenamin, R.; Murray, C. W.; O'Brien, M. A.; Parra, L.; Patel, S.; Phillips, T.; Rees, D. C.; Rich, S.; Smith, D. M.; Trewartha, G.; Vinkovic, M.; Williams, B.; Woolford, A. J. Discovery of (2,4-dihydroxy-5-isopropylphenyl)-[5-(4-methylpiperazin-1-ylmethyl)-1,3-dihydrois oindol-2-yl]methanone (AT13387), a novel inhibitor of the molecular chaperone Hsp90 by fragment based drug design. *J Med. Chem.* **2010**, *53*, 5956-69.
98. Ying, W.; Du, Z.; Sun, L.; Foley, K. P.; Proia, D. A.; Blackman, R. K.; Zhou, D.; Inoue, T.; Tatsuta, N.; Sang, J.; Ye, S.; Acquaviva, J.; Ogawa, L. S.; Wada, Y.; Barsoum, J.; Koya, K. Ganetespib, a unique triazolone-containing Hsp90 inhibitor, exhibits potent antitumor activity and a superior safety profile for cancer therapy. *Mol. Cancer Ther.* **2012**, *11*, 475-84.
99. Caldas-Lopes, E.; Cerchietti, L.; Ahn, J. H.; Clement, C. C.; Robles, A. I.; Rodina, A.; Moulick, K.; Taldone, T.; Gozman, A.; Guo, Y.; Wu, N.; de Stanchina, E.; White, J.; Gross, S. S.; Ma, Y.; Varticovski, L.; Melnick, A.; Chiosis, G. Hsp90 inhibitor PU-H71, a multimodal inhibitor of malignancy, induces complete responses in triple-negative breast cancer models. *Proc. Natl. Acad. Sci.* **2009**, *106*, 8368-73.

100. Bussenius, J.; Blazey, C. M.; Aay, N.; Anand, N. K.; Arcalas, A.; Baik, T.; Bowles, O. J.; Buhr, C. A.; Costanzo, S.; Curtis, J. K.; DeFina, S. C.; Dubenko, L.; Heuer, T. S.; Huang, P.; Jaeger, C.; Joshi, A.; Kennedy, A. R.; Kim, A. I.; Lara, K.; Lee, J.; Li, J.; Lougheed, J. C.; Ma, S.; Malek, S.; Manalo, J. C.; Martini, J. F.; McGrath, G.; Nicoll, M.; Nuss, J. M.; Pack, M.; Peto, C. J.; Tsang, T. H.; Wang, L.; Womble, S. W.; Yakes, M.; Zhang, W.; Rice, K. D. Discovery of XL888: a novel tropane-derived small molecule inhibitor of HSP90. *Bioorg. Med. Chem. Lett.* **2012**, *22*, 5396-404.
101. Kasibhatla, S. R.; Hong, K.; Biamonte, M. A.; Busch, D. J.; Karjian, P. L.; Sensintaffar, J. L.; Kamal, A.; Lough, R. E.; Brekken, J.; Lundgren, K.; Grecko, R.; Timony, G. A.; Ran, Y.; Mansfield, R.; Fritz, L. C.; Ulm, E.; Burrows, F. J.; Boehm, M. F. Rationally designed high-affinity 2-amino-6-halopurine heat shock protein 90 inhibitors that exhibit potent antitumor activity. *J Med. Chem.* **2007**, *50*, 2767-78.
102. Bao, R.; Lai, C. J.; Qu, H.; Wang, D.; Yin, L.; Zifcak, B.; Atoyian, R.; Wang, J.; Samson, M.; Forrester, J.; DellaRocca, S.; Xu, G. X.; Tao, X.; Zhai, H. X.; Cai, X.; Qian, C. CUDC-305, a novel synthetic HSP90 inhibitor with unique pharmacologic properties for cancer therapy. *Clin. Cancer Res.* **2009**, *15*, 4046-57.
103. Kim, S. H.; Bajji, A.; Tangallapally, R.; Markovitz, B.; Trovato, R.; Shenderovich, M.; Baichwal, V.; Bartel, P.; Cimbor, D.; McKinnon, R.; Robinson, R.; Papac, D.; Wettstein, D.; Carlson, R.; Yager, K. M. Discovery of (2S)-1-[4-(2-{6-amino-8-[(6-bromo-1,3-benzodioxol-5-yl)sulfanyl]-9H-purin-9-yl}ethyl)piperidin-1-yl]-2-hydroxypropan-1-one (MPC-3100), a purine-based Hsp90 inhibitor. *J Med. Chem.* **2012**, *55*, 7480-501.

104. Fadden, P.; Huang, K. H.; Veal, J. M.; Steed, P. M.; Barabasz, A. F.; Foley, B.; Hu, M.; Partridge, J. M.; Rice, J.; Scott, A.; Dubois, L. G.; Freed, T. A.; Silinski, M. A.; Barta, T. E.; Hughes, P. F.; Ommen, A.; Ma, W.; Smith, E. D.; Spangenberg, A. W.; Eaves, J.; Hanson, G. J.; Hinkley, L.; Jenks, M.; Lewis, M.; Otto, J.; Pronk, G. J.; Verleysen, K.; Haystead, T. A.; Hall, S. E. Application of chemoproteomics to drug discovery: identification of a clinical candidate targeting hsp90. *Chem. Biol.* **2010**, *17*, 686-94.
105. Menezes, D. L.; Taverna, P.; Jensen, M. R.; Abrams, T.; Stuart, D.; Yu, G. K.; Duhl, D.; Machajewski, T.; Sellers, W. R.; Pryer, N. K.; Gao, Z. The novel oral Hsp90 inhibitor NVP-HSP990 exhibits potent and broad-spectrum antitumor activities in vitro and in vivo. *Mol. Cancer Ther.* **2012**, *11*, 730-9.
106. Roe, S. M.; Prodromou, C.; O'Brien, R.; Ladbury, J. E.; Piper, P. W.; Pearl, L. H. Structural basis for inhibition of the Hsp90 molecular chaperone by the antitumor antibiotics radicicol and geldanamycin. *J Med. Chem.* **1999**, *42*, 260-6.
107. Xu, W.; Marcu, M.; Yuan, X.; Mimnaugh, E.; Patterson, C.; Neckers, L. Chaperone-dependent E3 ubiquitin ligase CHIP mediates a degradative pathway for c-ErbB2/Neu. *Proc. Natl. Acad. Sci.* **2002**, *99*, 12847-52.
108. Modi, S.; Stopeck, A.; Linden, H.; Solit, D.; Chandarlapaty, S.; Rosen, N.; D'Andrea, G.; Dickler, M.; Moynahan, M. E.; Sugarman, S.; Ma, W.; Patil, S.; Norton, L.; Hannah, A. L.; Hudis, C. HSP90 inhibition is effective in breast cancer: a phase II trial of tanespimycin (17-AAG) plus trastuzumab in patients with HER2-positive metastatic breast cancer progressing on trastuzumab. *Clin. Cancer Res.* **2011**, *17*, 5132-9.

109. Sequist, L. V.; Gettinger, S.; Senzer, N. N.; Martins, R. G.; Janne, P. A.; Lilenbaum, R.; Gray, J. E.; Iafrate, A. J.; Katayama, R.; Hafeez, N.; Sweeney, J.; Walker, J. R.; Fritz, C.; Ross, R. W.; Grayzel, D.; Engelman, J. A.; Borger, D. R.; Paez, G.; Natale, R. Activity of IPI-504, a novel heat-shock protein 90 inhibitor, in patients with molecularly defined non-small-cell lung cancer. *J Clin. Oncol.* **2010**, *28*, 4953-60.
110. Richardson, P. G.; Mitsiades, C. S.; Laubach, J. P.; Lonial, S.; Chanan-Khan, A. A.; Anderson, K. C. Inhibition of heat shock protein 90 (HSP90) as a therapeutic strategy for the treatment of myeloma and other cancers. *Br. J Haematol.* **2011**, *152*, 367-79.
111. Richardson, P. G.; Chanan-Khan, A. A.; Lonial, S.; Krishnan, A. Y.; Carroll, M. P.; Alsina, M.; Albitar, M.; Berman, D.; Messina, M.; Anderson, K. C. Tanespimycin and bortezomib combination treatment in patients with relapsed or relapsed and refractory multiple myeloma: results of a phase 1/2 study. *Br. J Haematol.* **2011**, *153*, 729-40.
112. Amarnath, V.; Madhav, R. A Survey of Methods for the Preparation of Pyrrolopyrimidines. *Synthesis* **1974**, 1974, 837-59.
113. Fletcher, T. M.; Cathers, B. E.; Ravikumar, K. S.; Mamiya, B. M.; Kerwin, S. M. Inhibition of human telomerase by 7-deaza-2'-deoxyguanosine nucleoside triphosphate analogs: potent inhibition by 6-thio-7-deaza-2'-deoxyguanosine 5'-triphosphate. *Bioorganic. Chem.* **2001**, *29*, 36-55.
114. Gangjee, A.; Yu, J.; Kisliuk, R. L. 2-Amino-4-oxo-6-substituted-pyrrolo[2,3-d]pyrimidines as potential inhibitors of thymidylate synthase. *J Heterocycl. Chem.* **2002**, *39*, 833-40.

115. Klepper, F.; Jahn, E. M.; Hickmann, V.; Carell, T. Synthesis of the transfer-RNA nucleoside queuosine by using a chiral allyl azide intermediate. *Angew. Chem. Int. Ed.* **2007**, *46*, 2325-7.
116. Lockman, J. W.; Murphy, B. R.; Zigar, D. F.; Judd, W. R.; Slattum, P. M.; Gao, Z. H.; Ostanin, K.; Green, J.; McKinnon, R.; Terry-Lorenzo, R. T.; Fleischer, T. C.; Boniface, J. J.; Shenderovich, M.; Willardsen, J. A. Analogues of 4-[(7-Bromo-2-methyl-4-oxo-3H-quinazolin-6-yl)methylprop-2-ynylamino]-N-(3-pyridylmethyl)benzamide (CB-30865) as potent inhibitors of nicotinamide phosphoribosyltransferase (Nampt). *J Med. Chem.* **2010**, *53*, 8734-46.
117. Wang, L.; Cherian, C.; Desmoulin, S. K.; Polin, L.; Deng, Y.; Wu, J.; Hou, Z.; White, K.; Kushner, J.; Matherly, L. H.; Gangjee, A. Synthesis and antitumor activity of a novel series of 6-substituted pyrrolo[2,3-d]pyrimidine thienoyl antifolate inhibitors of purine biosynthesis with selectivity for high affinity folate receptors and the proton-coupled folate transporter over the reduced folate carrier for cellular entry. *J Med. Chem.* **2010**, *53*, 1306-18.
118. Gangjee, A.; Lin, X.; Kisliuk, R. L.; McGuire, J. J. Synthesis of N-{4-[(2,4-diamino-5-methyl-4,7-dihydro-3H-pyrrolo[2,3-d]pyrimidin-6-yl)thio]benzoyl}-L-glutamic acid and N-{4-[(2-amino-4-oxo-5-methyl-4,7-dihydro-3H-pyrrolo[2,3-d]pyrimidin-6-yl)thio]benzoyl}-L-glutamic acid as dual inhibitors of dihydrofolate reductase and thymidylate synthase and as potential antitumor agents. *J Med. Chem.* **2005**, *48*, 7215-22.
119. Chen, Z.; Venkatesan, A. M.; Dehnhardt, C. M.; Ayril-Kaloustian, S.; Brooijmans, N.; Mallon, R.; Feldberg, L.; Hollander, I.; Lucas, J.; Yu, K.; Kong, F.; Mansour, T.

- S. Synthesis and SAR of novel 4-morpholinopyrrolopyrimidine derivatives as potent phosphatidylinositol 3-kinase inhibitors. *J Med. Chem.* **2010**, 53, 3169-82.
120. Shah, K.; Vincent, F.; Cuento, M. A. Modulators of GTPases and modulator-resistant enzymes and their uses in drug design and target validation. WO2004024082A2, 2004.
121. Xie, H.; Zeng, L.; Zeng, S.; Lu, X.; Zhang, G.; Zhao, X.; Cheng, N.; Tu, Z.; Li, Z.; Xu, H.; Yang, L.; Zhang, X.; Huang, M.; Zhao, J.; Hu, W. Novel pyrrolopyrimidine analogues as potent dipeptidyl peptidase IV inhibitors based on pharmacokinetic property-driven optimization. *Eur. J Med. Chem.* **2012**, 52, 205-12.
122. Chao, Q.; Hadd, M. J.; Holladay, M. W.; Rowbottom, M. Preparation of azolopyridine and azolopyrimidine compounds for treating JAK kinase mediated diseases. WO2012030924A1, 2012.
123. Yoneda, F.; Higuchi, M.; Senga, K.; Kanahori, M.; Nishigaki, S. Synthesis and properties of some pyrrolo[2,3-d]pyrimidine derivatives. *Chem. Pharm. Bull.* **1973**, 21, 473-7.
124. West, R. A.; Beauchamp, L. 2-Alkyl(aryl)- and 2,7-dimethyl-4-substituted aminopyrrolo[2,3-d]pyrimidines. *J. Org. Chem.* **1961**, 26, 3809-12.
125. Reigan, P.; Gbaj, A.; Chinje, E.; Stratford, I. J.; Douglas, K. T.; Freeman, S. Synthesis and enzymatic evaluation of xanthine oxidase-activated prodrugs based on inhibitors of thymidine phosphorylase. *Bioorg. Med. Chem. Lett.* **2004**, 14, 5247-50.
126. Castelhana, A. L.; McKibben, B.; Witter, D. J. Preparation of aminopyrrolopyrimidines as adenosine A1 receptor antagonists. US6878716B1, 2005.

127. Minakawa, N.; Kawano, Y.; Murata, S.; Inoue, N.; Matsuda, A.
Oligodeoxynucleotides containing 3-bromo-3-deazaadenine and 7-bromo-7-deazaadenine 2'-deoxynucleosides as chemical probes to investigate DNA-protein interactions. *Chembiochem* **2008**, 9, 464-70.
128. Rodriguez, A. L.; Koradin, C.; Dohle, W.; Knochel, P. Versatile Indole Synthesis by a 5-endo-dig Cyclization Mediated by Potassium or Cesium Bases We thank the DFG (Leibniz-Programm) and the Fonds der Chemischen Industrie for generous financial support. A.L.R. and C. K. thank the Humboldt-Foundation and the BASF AG, respectively, for fellowships. W.D. was supported by the BMBF program (03 D 0056 2). We thank Dr. J. Henkelmann (BASF AG) for helpful discussions and the BASF AG for the generous gift of chemicals. *Angew. Chem. Int. Ed.* **2000**, 39, 2488-90.
129. Taylor, E. C.; Patel, H. H.; Jun, J.-G. A One-Step Ring Transformation/Ring Annulation Approach to Pyrrolo[2,3-d]pyrimidines. A New Synthesis of the Potent Dihydrofolate Reductase Inhibitor TNP-351. *J. Org. Chem.* **1995**, 60, 6684-7.
130. Taylor, E. C.; Hendess, R. W. Synthesis of Pyrrolo(2,3-D)Pyrimidines. The Aglycone of Toyocamycin. *J Am. Chem. Soc.* **1965**, 87, 1995-2003.
131. Gangjee, A.; Yu, J.; Kisliuk, R. L.; Haile, W. H.; Sobrero, G.; McGuire, J. J. Design, synthesis, and biological activities of classical N-[4-[2-(2-amino-4-ethylpyrrolo[2,3-d]pyrimidin-5-yl)ethyl]benzoyl]-l-glutamic acid and its 6-methyl derivative as potential dual inhibitors of thymidylate synthase and dihydrofolate reductase and as potential antitumor agents. *J Med. Chem.* **2003**, 46, 591-600.

132. Mitchell, I. S.; Spencer, K. L.; Stengel, P.; Han, Y.; Kallan, N. C.; Munson, M.; Vigers, G. P. A.; Blake, J.; Piscopio, A.; Josey, J.; Miller, S.; Xiao, D.; Xu, R.; Rao, C.; Wang, B.; Bernacki, A. L. AKT protein kinase inhibitors for use in treatment of hyperproliferative diseases. WO2005051304A2, 2005.
133. Taylor, E. C.; Young, W. B.; Spanka, C. Synthesis of N-{4-[2-(2-Amino-5,6-dihydro-4(3H)-oxo-7H-pyrrolo[2,3-d]pyrimidin-6-yl)ethyl]benzoyl}-L-glutamic Acid: A Ring-Contracted Analog of 5,10-Dideaza-5,6,7,8-tetrahydrofolic Acid. *J. Org. Chem.* **1996**, 61, 1261-6.
134. Secrist, J. A.; Liu, P. S. Studies directed toward a total synthesis of nucleoside Q. Annulation of 2,6-diaminopyrimidin-4-one with .alpha.-halo carbonyls to form pyrrolo[2,3-d]pyrimidines and furo[2,3-d]pyrimidines. *J. Org. Chem.* **1978**, 43, 3937-41.
135. Gangjee, A. Bicyclic compounds having antimitotic and/or antitumor activity and methods of use thereof. WO2010006025A1, 2010.
136. Gewalt, K. Heterocyclen aus CH-aciden Nitrilen, IX. Über die Reaction von α -Hydroxy-ketonen mit Malodinitril (Heterocycles from CH-acidic nitriles. IX. Reaction of α -hydroxy ketones with malononitrile). *Chem. Ber.* **1966**, 99, 1002-7.
137. Takamuro, I.; Sekine, Y.; Tsuboi, Y.; Nogi, K.; Taniguchi, H. Preparation of pyrazolopyrimidines as a small conductance potassium channel (SK channel) blocking agents. WO2004064721A2, 2004.
138. Bronson, J.; Dhar, M.; Ewing, W.; Lonberg, N. Chapter 26 - To Market, To Market—2010. In *Annual Reports in Medicinal Chemistry*, John, E. M., Ed. Academic Press: 2011; Vol. Volume 46, pp 433-502.

139. Towle, M. J.; Salvato, K. A.; Budrow, J.; Wels, B. F.; Kuznetsov, G.; Aalfs, K. K.; Welsh, S.; Zheng, W.; Seletsky, B. M.; Palme, M. H.; Habgood, G. J.; Singer, L. A.; Dipietro, L. V.; Wang, Y.; Chen, J. J.; Quincy, D. A.; Davis, A.; Yoshimatsu, K.; Kishi, Y.; Yu, M. J.; Littlefield, B. A. In vitro and in vivo anticancer activities of synthetic macrocyclic ketone analogues of halichondrin B. *Cancer Research* **2001**, 61, 1013-21.
140. Fahy, J.; Duflos, A.; Ribet, J.-P.; Jacquesy, J.-C.; Berrier, C.; Jouannetaud, M.-P.; Zunino, F. Vinca Alkaloids in Superacidic Media: A Method for Creating a New Family of Antitumor Derivatives. *J Am. Chem. Soc.* **1997**, 119, 8576-77.
141. Kruczynski, A.; Barret, J.-M.; Etiévant, C.; Colpaert, F.; Fahy, J.; Hill, B. T. Antimitotic and tubulin-interacting properties of vinflunine, a novel fluorinated Vinca alkaloid. *Biochem. Pharmacol.* **1998**, 55, 635-648.
142. Ling, V. Multidrug resistance: molecular mechanisms and clinical relevance. *Cancer Chemother. Pharmacol.* **1997**, 40 Suppl, S3-8.
143. Leonard, G. D.; Fojo, T.; Bates, S. E. The role of ABC transporters in clinical practice. *Oncologist* **2003**, 8, 411-24.
144. Chiou, J. F.; Liang, J. A.; Hsu, W. H.; Wang, J. J.; Ho, S. T.; Kao, A. Comparing the relationship of Taxol-based chemotherapy response with P-glycoprotein and lung resistance-related protein expression in non-small cell lung cancer. *Lung* **2003**, 181, 267-73.
145. Yeh, J. J.; Hsu, W. H.; Wang, J. J.; Ho, S. T.; Kao, A. Predicting chemotherapy response to paclitaxel-based therapy in advanced non-small-cell lung cancer with P-glycoprotein expression. *Respiration* **2003**, 70, 32-5.

146. Safety and Effectiveness of Combretastatin A-4 Phosphate Combined With Chemotherapy in Advanced Solid Tumors.
<http://www.clinicaltrials.gov/ct2/show/NCT00113438?term=combretastatin&rank=1>
147. Gelderblom, H.; Verweij, J.; Nooter, K.; Sparreboom, A. Cremophor EL: the drawbacks and advantages of vehicle selection for drug formulation. *Eur. J Cancer* **2001**, *37*, 1590-8.
148. Bai, R. L.; Paull, K. D.; Herald, C. L.; Malspeis, L.; Pettit, G. R.; Hamel, E. Halichondrin B and homohalichondrin B, marine natural products binding in the vinca domain of tubulin. Discovery of tubulin-based mechanism of action by analysis of differential cytotoxicity data. *J Biol. Chem.* **1991**, *266*, 15882-9.
149. Paull, K. D.; Lin, C. M.; Malspeis, L.; Hamel, E. Identification of novel antimetabolic agents acting at the tubulin level by computer-assisted evaluation of differential cytotoxicity data. *Cancer Research* **1992**, *52*, 3892-900.
150. Trott, O.; Olson, A. J. AutoDock Vina: improving the speed and accuracy of docking with a new scoring function, efficient optimization, and multithreading. *J Comput. Chem.* **2010**, *31*, 455-61.
151. Bursulaya, B. D.; Totrov, M.; Abagyan, R.; Brooks, C. L., 3rd. Comparative study of several algorithms for flexible ligand docking. *J Comput. Aided Mol. Des.* **2003**, *17*, 755-63.
152. Llauger, L.; He, H.; Kim, J.; Aguirre, J.; Rosen, N.; Peters, U.; Davies, P.; Chiosis, G. Evaluation of 8-arylsulfanyl, 8-arylsulfoxyl, and 8-arylsulfonyl adenine derivatives as inhibitors of the heat shock protein 90. *J Med. Chem.* **2005**, *48*, 2892-905.

153. He, H.; Zatorska, D.; Kim, J.; Aguirre, J.; Llauger, L.; She, Y.; Wu, N.; Immormino, R. M.; Gewirth, D. T.; Chiosis, G. Identification of potent water soluble purine-scaffold inhibitors of the heat shock protein 90. *J Med. Chem.* **2006**, 49, 381-90.
154. Immormino, R. M.; Kang, Y.; Chiosis, G.; Gewirth, D. T. Structural and quantum chemical studies of 8-aryl-sulfanyl adenine class Hsp90 inhibitors. *J Med. Chem.* **2006**, 49, 4953-60.
155. Gangjee, A.; Yang, J.; Ihnat, M. A.; Kamat, S. Antiangiogenic and antitumor agents. Design, synthesis, and evaluation of novel 2-amino-4-(3-bromoanilino)-6-benzylsubstituted pyrrolo[2,3-d]pyrimidines as inhibitors of receptor tyrosine kinases. *Bioorg. Med. Chem.* **2003**, 11, 5155-70.
156. Gangjee, A.; Namjoshi, O. A.; Yu, J.; Ihnat, M. A.; Thorpe, J. E.; Warnke, L. A. Design, synthesis and biological evaluation of substituted pyrrolo[2,3-d]pyrimidines as multiple receptor tyrosine kinase inhibitors and antiangiogenic agents. *Bioorg. Med. Chem.* **2008**, 16, 5514-28.
157. Gangjee, A.; Li, W.; Lin, L.; Zeng, Y.; Ihnat, M.; Warnke, L. A.; Green, D. W.; Cody, V.; Pace, J.; Queener, S. F. Design, synthesis, and X-ray crystal structures of 2,4-diaminofuro[2,3-d]pyrimidines as multireceptor tyrosine kinase and dihydrofolate reductase inhibitors. *Bioorg. Med. Chem.* **2009**, 17, 7324-36.
158. Gangjee, A.; Kurup, S.; Ihnat, M. A.; Thorpe, J. E.; Shenoy, S. S. Synthesis and biological activity of N(4)-phenylsubstituted-6-(2,4-dichloro phenylmethyl)-7H-pyrrolo[2,3-d]pyrimidine-2,4-diamines as vascular endothelial growth factor receptor-2 inhibitors and antiangiogenic and antitumor agents. *Bioorg. Med. Chem.* **2010**, 18, 3575-87.

159. Gangjee, A.; Namjoshi, O. A.; Ihnat, M. A.; Buchanan, A. The contribution of a 2-amino group on receptor tyrosine kinase inhibition and antiangiogenic activity in 4-anilinosubstituted pyrrolo[2,3-d]pyrimidines. *Bioorg. Med. Chem. Lett.* **2010**, *20*, 3177-81.
160. Gangjee, A.; Zaware, N.; Raghavan, S.; Ihnat, M.; Shenoy, S.; Kisliuk, R. L. Single agents with designed combination chemotherapy potential: synthesis and evaluation of substituted pyrimido[4,5-b]indoles as receptor tyrosine kinase and thymidylate synthase inhibitors and as antitumor agents. *J Med. Chem.* **2010**, *53*, 1563-78.
161. Gangjee, A.; Zhao, Y.; Raghavan, S.; Ihnat, M. A.; Disch, B. C. Design, synthesis and evaluation of 2-amino-4-m-bromoanilino-6-arylmethyl-7H-pyrrolo[2,3-d]pyrimidines as tyrosine kinase inhibitors and antiangiogenic agents. *Bioorg. Med. Chem.* **2010**, *18*, 5261-73.
162. Gangjee, A.; Kurup, S.; Ihnat, M. A.; Thorpe, J. E.; Disch, B. N(4)-Aryl-6-substitutedphenylmethyl-7H-pyrrolo[2,3-d]pyrimidine-2,4-diamines as receptor tyrosine kinase inhibitors. *Bioorg. Med. Chem.* **2012**, *20*, 910-4.
163. Gangjee, A.; Zaware, N.; Raghavan, S.; Yang, J.; Thorpe, J. E.; Ihnat, M. A. N(4)-(3-Bromophenyl)-7-(substituted benzyl) pyrrolo[2,3-d]pyrimidines as potent multiple receptor tyrosine kinase inhibitors: design, synthesis, and in vivo evaluation. *Bioorg. Med. Chem.* **2012**, *20*, 2444-54.
164. Wright, L.; Barril, X.; Dymock, B.; Sheridan, L.; Surgenor, A.; Beswick, M.; Drysdale, M.; Collier, A.; Massey, A.; Davies, N.; Fink, A.; Fromont, C.; Aherne, W.; Boxall, K.; Sharp, S.; Workman, P.; Hubbard, R. E. Structure-activity relationships in purine-based inhibitor binding to HSP90 isoforms. *Chem. Biol.* **2004**, *11*, 775-85.

165. Sun, N.; Wang, S.; Mo, W.; Hu, B.; Shen, Z.; Hu, X. A facile protocol for the synthesis of mono-N-methyl anilines via formimidate intermediates. *Tetrahedron* **2010**, *66*, 7142-48.
166. Kaboudin, B.; Khodamorady, M. Organic Reactions in Water: A Practical and Convenient Method for the N-Formylation of Amines in Water. *Synlett* **2010**, *2010*, 2905-07.
167. Gangjee, A.; Yu, J.; McGuire, J. J.; Cody, V.; Galitsky, N.; Kisliuk, R. L.; Queener, S. F. Design, synthesis, and X-ray crystal structure of a potent dual inhibitor of thymidylate synthase and dihydrofolate reductase as an antitumor agent. *J Med. Chem.* **2000**, *43*, 3837-51.
168. Laot, Y.; Petit, L.; Zard, S. Z. Unusual radical addition on a heteroaromatic nitrogen. A convenient access to new pyrimidine derivatives. *Chem. Commun. (Camb.)* **2010**, *46*, 5784-6.
169. Laot, Y.; Petit, L.; Zard, S. Z. Synthesis of fluoroazaindolines by an uncommon radical ipso substitution of a carbon-fluorine bond. *Org. Lett.* **2010**, *12*, 3426-9.
170. Gangjee, A.; Lin, X.; Queener, S. F. Design, synthesis, and biological evaluation of 2,4-diamino-5-methyl-6-substituted-pyrrolo[2,3-d]pyrimidines as dihydrofolate reductase inhibitors. *J Med. Chem.* **2004**, *47*, 3689-92.